EUR/SAM Corridor: 2015 Collision Risk Assessment

Code: NYVI-IDSA-INF-074-16-1.0
Prepared: 10/02/17
Page: 1/153

Approvals

Prepared by:	Reviewed by:	Approved by:
Visado en Internav	*Visado en Internav*	*Visado en Internav*
Gema Ana Paz Bernó **INECO**	Mª Mar Tabernero Serrano **Head of Department of Research and Definition of Air Navigation Advanced Systems**	Nicolás Martín Martín **Head of Navigation and Surveillance Division**

Change record

The Change record reflects, at least, the last three modifications made in the document.

Issue	Date	Affected pages	Changes
0.1	December 2016	All	Document creation
0.2	January 2017	All	Update using Eurocontrol 2016 data for Pz calculation
0.3	February 2017	All	Internal comments
1.0	February 2017	All	Final version

Distribution control sheet

Copy	Name	Post	Organization
1	Enrique Maurer	Systems Director	ENAIRE
2	Nicolás Martín Martín	Head of Navigation and Surveillance Division	ENAIRE
3	Mª Mar Tabernero	Head of Department of Research and Definition of Air Navigation Advanced Systems	ENAIRE
4		SATMA Group	

Index

Figure index

Table Index

Executive Summary

This report presents the 2015 collision risk assessment made for the EUR/SAM Corridor. It assesses the current and projected lateral and vertical collision risk in the Corridor, where RNP10 and RVSM are implemented, for flight levels between FL290 and FL410.

Two quantitative risk assessments, based on suitable versions of the Reich Collision Risk Model, have been carried out. The first assessment corresponds to the lateral collision risk whilst the second one concerns the vertical collision risk. The vertical collision risk assessment has been split into two parts. The first part considers the risk contribution of technical causes, whilst the second one considers the complete risk due to all causes, including operational ones.

The analysed scenario is the airspace where RNP10 and RVSM are implemented. The current route network structure is composed of four nearly parallel north-south routes, being the two easternmost bidirectional and the other two, unidirectional. Traffic on the DCT Area, placed to the west of the current UN-741, has not been considered in the analysis. Nevertheless, it is assumed that its contribution would not change the results dramatically.

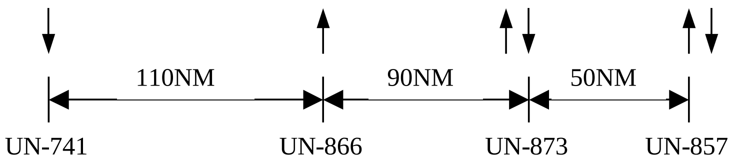

Current route network

As far as crossing traffic is concerned, the traffic on the published routes that crosses the Corridor in SAL, Dakar and Recife (UR-976/UA-602, UL-435 and UL-695/UL-375, respectively) and the traffic that crosses the Corridor using non published routes used by more than 4 aircraft per month, have been considered.

The internal software tool CRM, used in previous studies, has been updated and used to obtain the different parameters of the Reich Collision Risk Model in each one of the UIRs crossed by the Corridor.

The CRM program uses flight plan data obtained from Palestra, Enaire's database for the Canaries, and traffic data from the samples provided by SAL, Dakar and Atlantic-Recife. Real data from the Canaries has been available for the complete year 2015, while not all the data from the rest of the FIRs/UIRs has been available. The traffic samples used to perform this analysis are the ones from 1st July 2015 to 31st July 2015. This month has been selected as it was the one with the higher number of flights. The number of flights and the flight time for the complete year 2015, required for some of the calculations, have been extrapolated.

Besides, extrapolation of traffic data has been necessary in some cases in order to obtain the traffic distribution along the Corridor and on crossing routes. Therefore, trajectories and information at required waypoints (i.e., time and FL) have been assumed, considering the most logical routes and speeds. This may have an influence in the results, as several assumptions have been made due to the incompleteness and inconsistencies, in some cases, of the provided data.

Considering a number of parameters such as probabilities of lateral and vertical overlaps, lateral, vertical and crossing occupancies, average speed, average relative velocities and aircraft dimensions, the lateral, technical vertical and total vertical collision risks have been assessed and compared with the maximum Target Level of Safety (TLS) values allowed, $TLS = 5 \cdot 10^{-9}$, $TLS = 2.5 \cdot 10^{-9}$ and $TLS = 5 \cdot 10^{-9}$, respectively.

The risk has been evaluated in 6 different locations along the Corridor and an estimation of the collision risk for the next 10 years has been calculated, assuming a traffic growth rate of 5.2% per year.

The results obtained are very similar in all the locations and the risk associated to the Corridor is the largest of all the values obtained.

Assuming that the traffic levels of July 2015 are representative of the whole year, the calculated lateral collision risk is $2.0662 * 10^{-9}$, whilst the lateral collision risk estimated for 2025 with an annual traffic growth rate of 5.2% is $3.4303 * 10^{-9}$. These values do not take into account traffic on the DCT Area routes. Nevertheless, since traffic on this route represents approximately 4% of the traffic in the Corridor, it is considered that the collision risk derived from this route will not make the collision risk go above the TLS and, as a consequence, the system is considered to be laterally safe in the period under consideration.

As far as the technical vertical risk is concerned, the value of the collision risk for 2015 (assuming traffic levels of July 2015 representative of the whole year), is estimated to be $0.3108 * 10^{-9}$ and the technical vertical collision risk estimated for 2025 with an annual traffic growth rate of 5.2%, $0.5160 * 10^{-9}$. Both values are below the TLS.

Regarding the vertical risk due to large height deviations, it has been calculated using the LHD notifications reported by the four involved States. The contribution of these deviations to the total vertical risk in the Corridor is $5.3335 * 10^{-7}$, which greatly exceeds the TLS.

In previous safety assessments, [Ref. 3], [Ref. 5] and [Ref.7], it was remarked that all the deviations received had been due to coordination errors between ATC units and not related to RVSM operations. In the same way, it was also explained that none of those reports received indicated that there had existed any traffic in conflict. This is also the case of this study.

Given that coordination errors continue to be the main cause of occurrence of LHD, the use of adequate corrective actions to reduce this type of errors should be applied as soon as possible in order to reduce the risk levels. .

1. Introduction

This report presents the 2015 collision risk assessment made for the EUR/SAM Corridor. It assesses the current and projected lateral and vertical collision risk in the Corridor, where RNP10 and RVSM are implemented, with real data of traffic between FL290 and FL410 collected from 1st July 2015 to 31st July 2015 and with the number of flights and the flight time required for some of the calculations extrapolated for the complete year 2015.

For this study, the program CRM has been updated and used to obtain the different parameters of the Reich Collision Risk Model in each one of the UIRs crossed by the Corridor. Taking these values into account and the traffic forecast for the future, it has been possible to estimate the collision risk for the following years.

2. Airspace description

As it has already been said, the airspace analysed in this report is the EUR/SAM Corridor, where RNP10 and RVSM are implemented. This Corridor lies in the South Atlantic airspace between the Canary Islands and Brazil.

The analysed scenario is the current tracks system. Figure 1 shows the existing route network together with the horizontal boundaries of the area to be considered in the risk assessment.

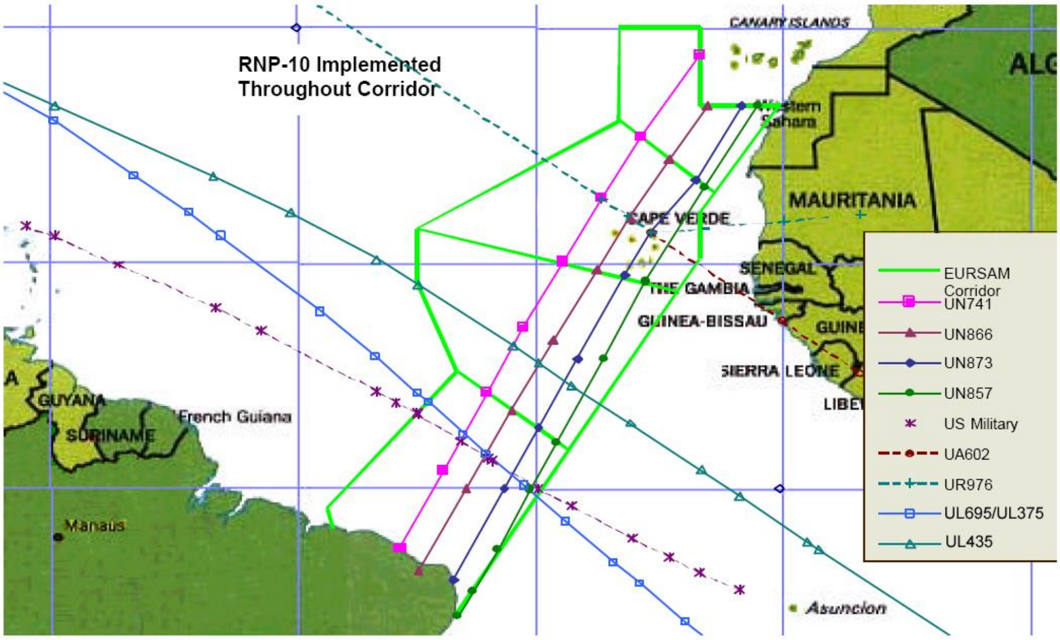

Figure 1.
Existing route network.

The existing route network is composed of four nearly parallel north-south routes situated within the Canaries UIR, SAL Oceanic UIR/UTA, Dakar Oceanic UIR and Recife FIR.

The denomination of the routes is, from west to east, UN-741, UN-866, UN-873 and UN-857, and their magnetic direction is around 45°-50° for northbound traffic and 225°-230° for southbound traffic.

Minimum lateral separation between routes is 110 NM for routes UN-741/UN-866, 90 NM for routes UN-866/UN-873 and 50NM for routes UN-873/UN-857.

Routes UN-741 and UN-866 are unidirectional, with traffic in odd and even flight levels, (Southbound traffic on route UN-741 and Northbound traffic on route UN-866). On the other hand, routes UN-873 and UN-857 are bidirectional. The flight level allocation scheme in these last two routes is the following:

- Southbound flight levels: FL300, FL320, FL340, FL360, FL380 and FL400.
- Northbound flight levels: FL290, FL310, FL330, FL350, FL370, FL390 and FL410.

The following figure shows a detailed image of the tracks system, with all the fixes or Waypoint Position Reporting Points that define it:

EUR/SAM Corridor: 2015 Collision Risk Assessment

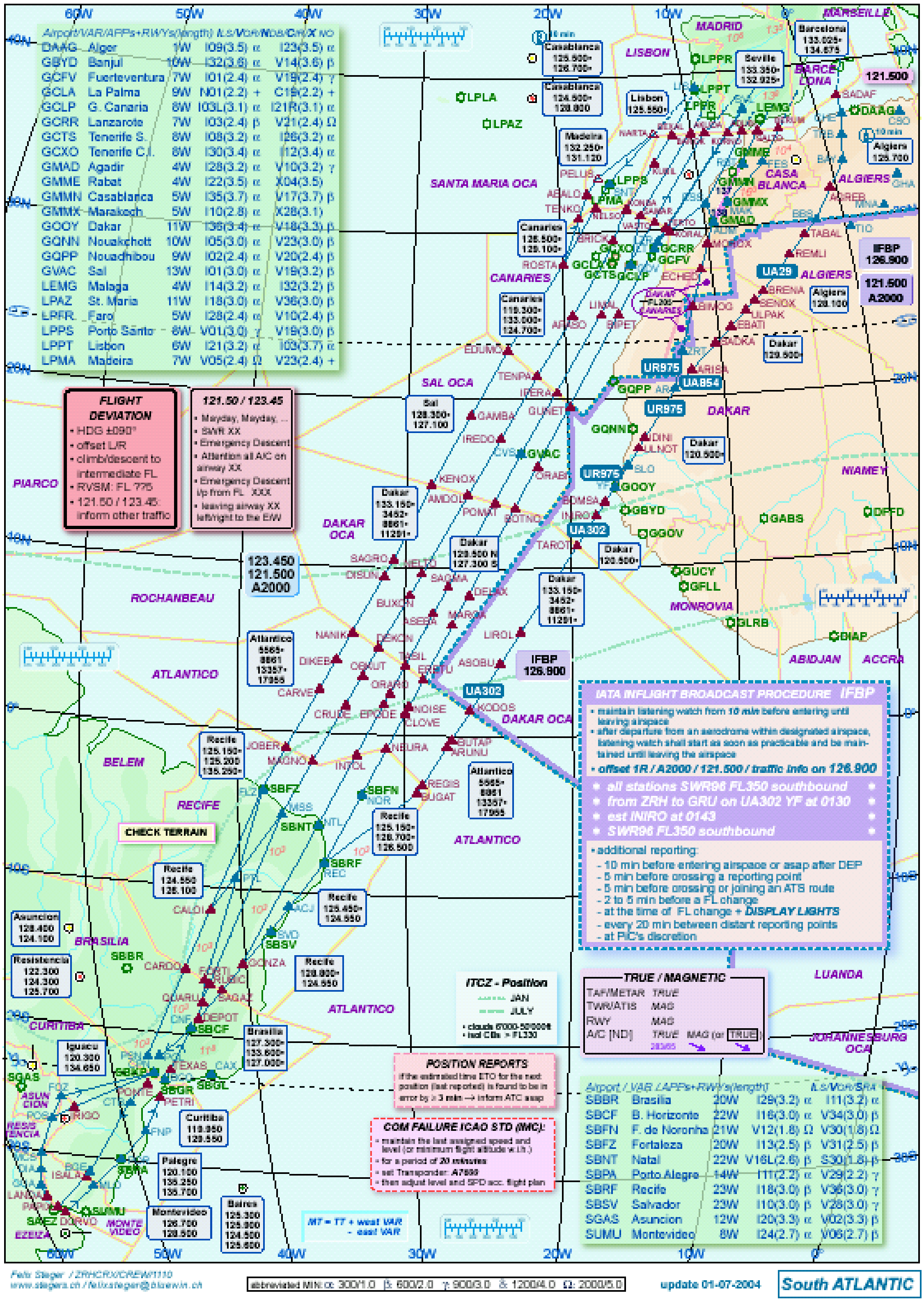

Figure 2.
EUR/SAM Corridor.

A scheme of the current route network is shown in Figure 3.

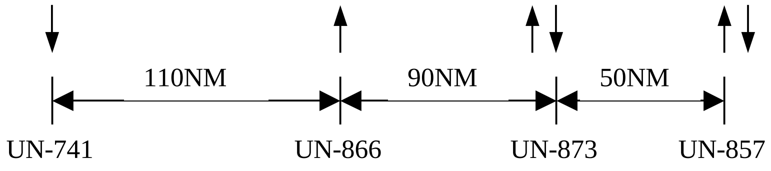

Figure 3.
Route network.

Besides these four routes, there is also traffic on the so-called DCT Area. This area is placed west of the current UN-741. This traffic is random and there is great dispersion in the trajectories. The main crossing points in this area are:

- Canaries-SAL:
  - GOBEG: 29°"N, 25°W
  - INSAD: 27°59'58"N, 25°W
  - IXIKU: 27°N, 24°59'58"W
  - KUXOV: 26°0'01"N, 24°59'59"W
  - LAPTU: 25°00'03"N, 24°59'59"W
  - XIGLU: 23°35'59"N, 24°24'W
- SAL-Dakar:
  - TARIM: 15°10'24"N, 29°32'30"W
  - XUVIT: 15°10'24"N, 30°41'36"W
  - BIKOM: 15°43'30"N, 31°48'18"W
  - NATAS: 16°20'24"N, 33°W
  - GARPO: 16°16'30"N, 34°10'W
  - TUTLO: 17°N, 37°30'W
- Dakar-Recife:
  - MOVGA: 7°40'N, 35°W

Besides, part of this traffic crosses other FIRs out of SATMA responsibility, as Santa Maria or Piarco FIRs.

An image of some of these routes along the Corridor, using Google Earth, can be seen in white in the following figures.

EUR/SAM Corridor: 2015 Collision Risk Assessment

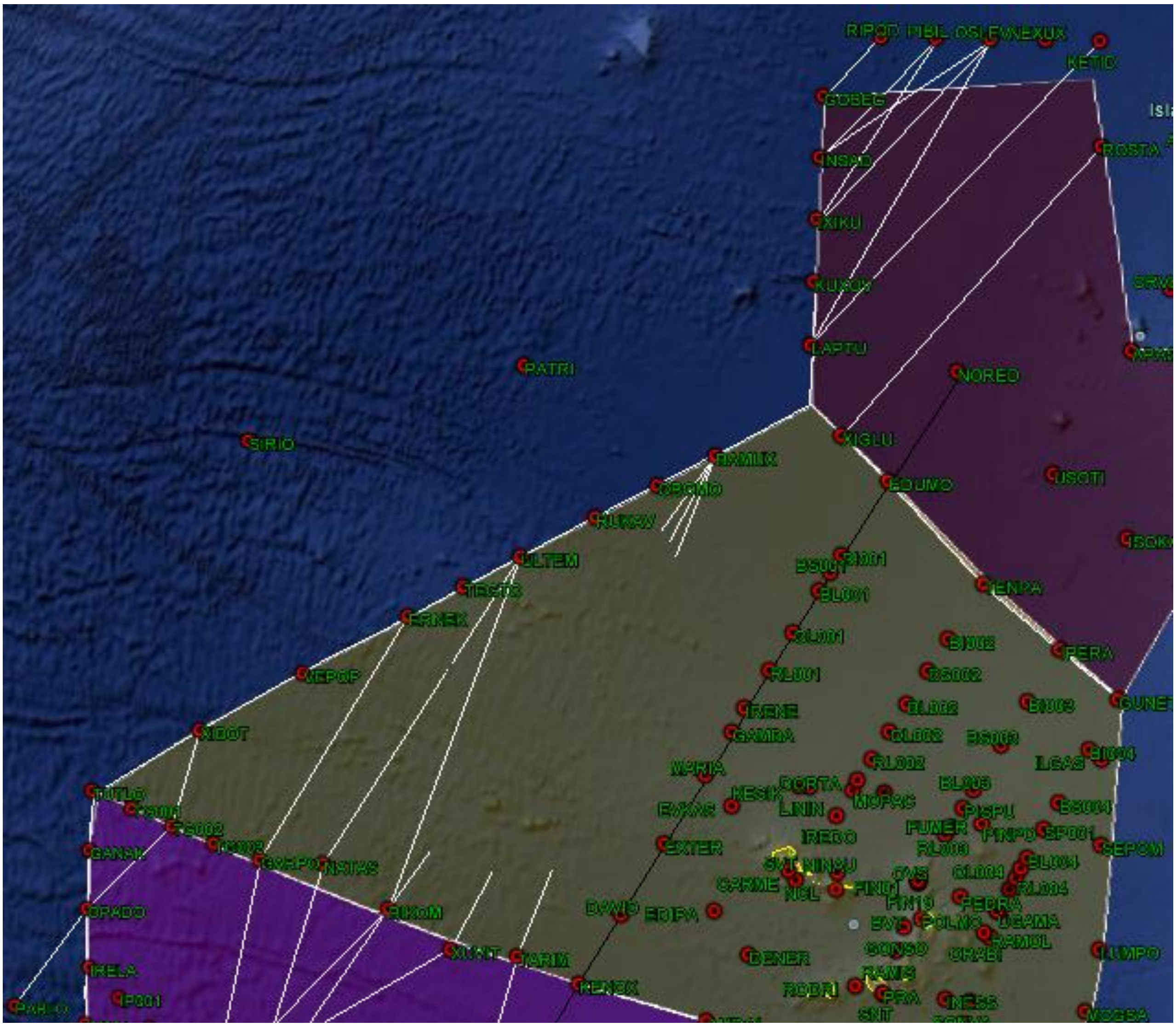

Figure 4.

Main DCT Area routes. Canaries-SAL.

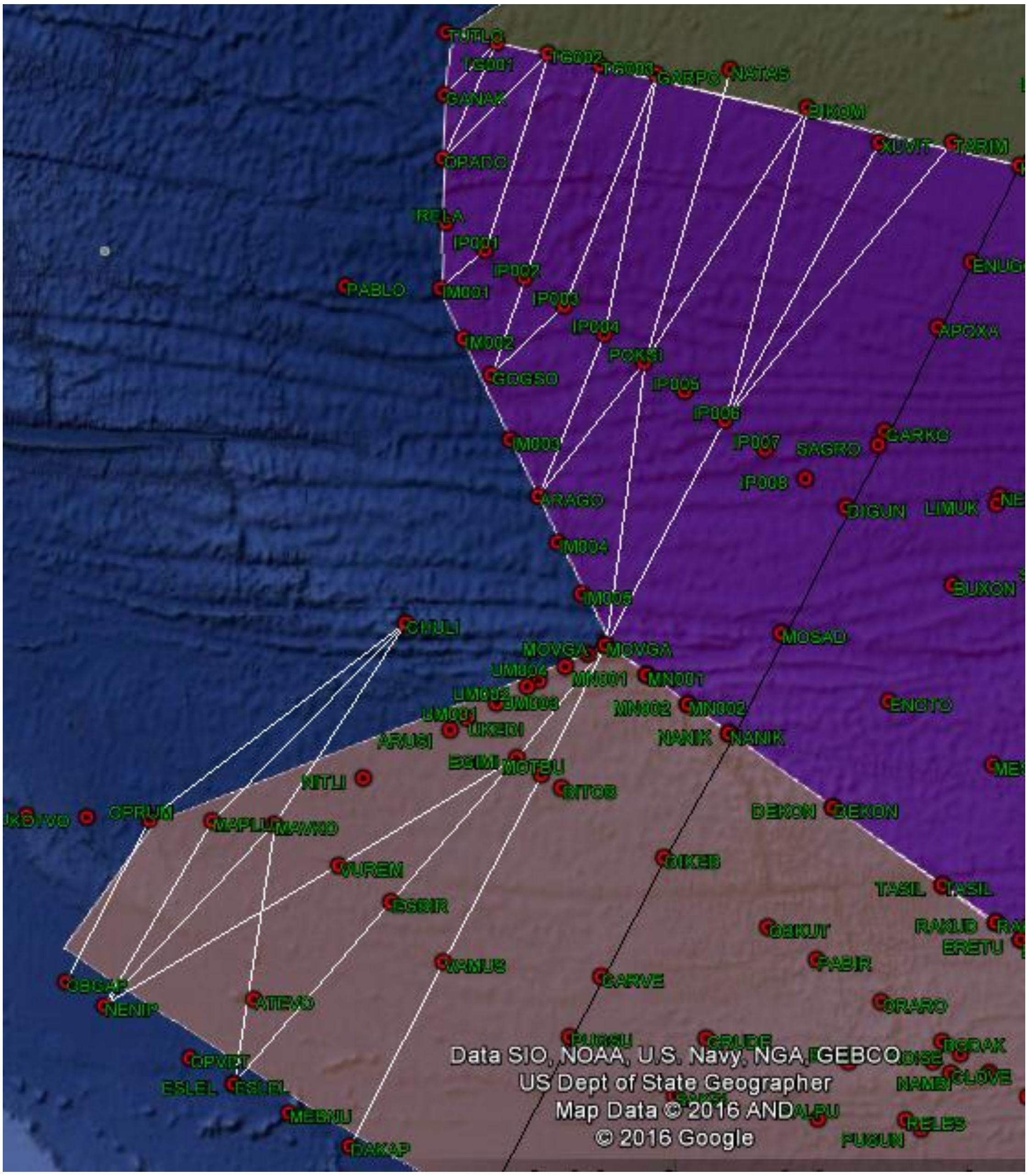

Figure 5.
Main DCT Area routes. Dakar-Recife.

As can be seen, there is great dispersion of the routes, so the analysis of this area is not straightforward. Due to their total low appearance (approximately 4% of the total flights in Canaries[1]), these routes have not been considered in this collision risk assessment. However, in the last years the traffic in this DCT area has been increasing, so it is possible that this assumption cannot be made in the future.

[1] *Data from Canaries has been used because information for the complete year 2015 is available.*

There is also some traffic crossing the Corridor in published routes in SAL UIR (UR-976/UA-602), in Dakar UIR (UL-435) and in Recife UIR (UL-695/UL-375). Apart from the published crossing routes, some crossing traffic in non-published routes has also been detected. Consequently, a number of crossing trajectories have been identified for the purpose of this assessment, besides the trajectories already considered in the previous studies. Given that not all the trajectories could be analysed, some hypotheses have been made:

- As it was introduced in the "Double Unidirectionality" Post-Implementation Collision Risk Assessment [Ref. 3], there is also traffic in the proximity of this route that has been cleared with a "Direct to" between LUMPO and ULTEM waypoints. The number of aircraft on these direct-to trajectories is comparable to the number of aircraft that fly exactly on route UR-976/UA-602. Therefore, this crossing traffic cannot be considered negligible. Next figure shows the direct route ULTEM-LUMPO in the way in which it has been extrapolated. Although there appears to be certain dispersion around the line that joins ULTEM and LUMPO, it will be considered that all those flights have flown over that line, since it is not possible to analyze each of them independently. This crossing trajectory will be referred to as ULTEM-LUMPO hereafter. Figure 6 shows in Google Earth both UR-976/UA-602 and the direct ULTEM-LUMPO route.

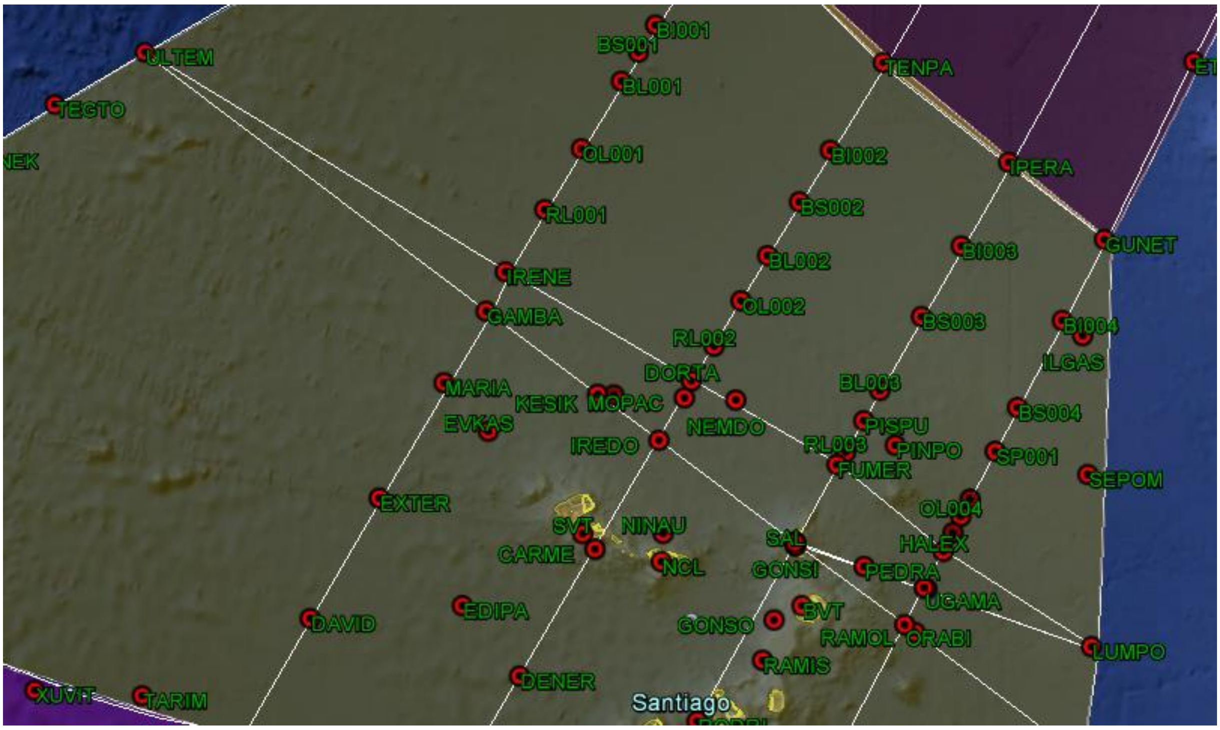

Figure 6.
UR976/UA602 and ULTEM-LUMPO routes in SAL Oceanic UIR

- Regarding the routes that cross the complete corridor, six trajectories have been detected: one in Canaries and four in SAL. All these routes were used more than four times during July 2015:
    - Canaries:
        - NORED-ETIBA
    - SAL:
        - BAMUX-LUMPO

- BAMUX-ILGAS
- ULTEM-ILGAS
- KENOX-MOGSA

Figure 7 shows in Google Earth these five routes.

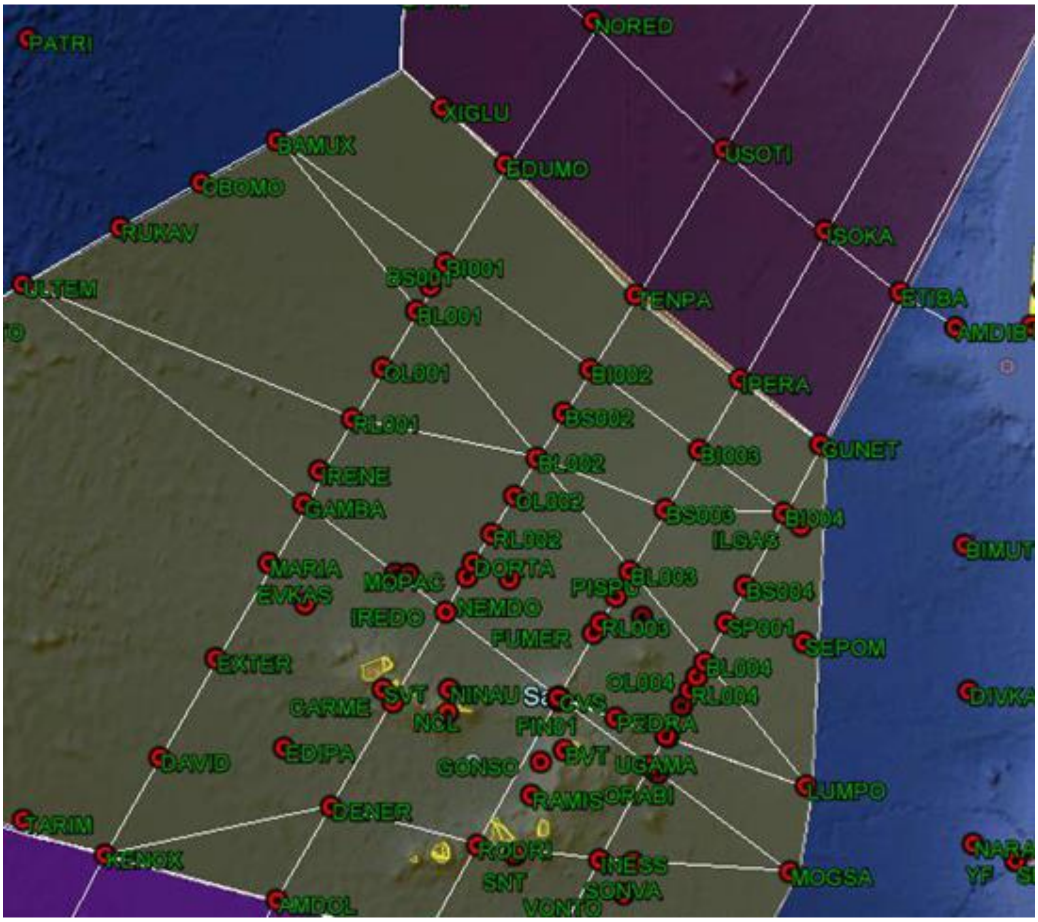

Figure 7.
UR-976/UA-602 and non published crossing routes in Canaries and SAL.

- Besides these crossing routes, other four routes (one in SAL and three in Dakar) were identified in previous risk assessments and had at least 1 flight during July 2015, so they have been maintained and included in this study. These trajectories are:
  - SAL:
    - ULTEM-SEPOM
    - BAMUX-SEPOM
  - Dakar:
    - ENUGO-APIGU
    - APOXA-GONSA
    - SAGRO-LIRAX

Figure 8 and Figure 9 show these trajectories drawn in Google Earth.

Figure 8.
UR-976/UA-602 and non published crossing routes in SAL.

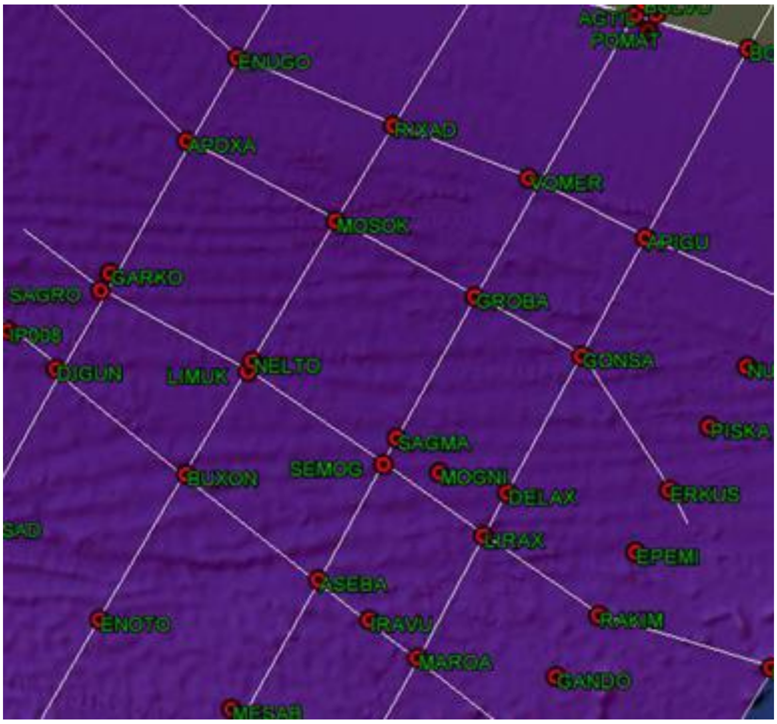

Figure 9.
UL-435 and non published crossing routes in Dakar.

In the analysis of these trajectories, many waypoints given by coordinates have been extrapolated and addressed with names created for simplification. Next table summarizes these created points:

Point	Latitude	Longitude
BI001	021 45 02N	024 20 40W
BI002	020 30 02N	022 32 27W
BI003	019 33 16N	021 13 08W
BI004	018 49 03N	020 12 16W
BL001	021 11 38N	024 41 46W
BL002	019 28 56N	023 11 54W
BL003	018 10 32N	022 04 53W
BL004	017 07 24N	021 11 36W
BS001	021 28 43N	024 31 13W
BS002	020 00 03N	022 52 01W
BS003	018 52 43N	021 38 38W
BS004	017 59 21N	020 41 30W
BULVO	014 02 28N	024 30 12W
CARME	016 40 49N	024 56 32W
DAVID	015 58 44N	027 48 28W
EXTER	017 08 57N	027 07 15W
IP006	010 58 30N	033 10 34W
IP007	010 32 07N	032 34 29W
IP008	010 05 40N	031 58 31W
MARIA	018 15 44N	026 28 41W
OL004	016 57 35N	021 17 31W
PISPU	017 53 20N	022 14 53W
RL002	018 36 53N	023 44 48W
RL003	017 35 29N	022 26 06W
RL004	016 48 25N	021 22 20W
SP001	017 34 30N	020 55 43W

Table 1.
Extrapolated points and their coordinates.

Besides these trajectories that cross the whole corridor, 20 more trajectories between points (real crossings o changes between routes) with at least 4 flights per month have been detected:

- EDUMO-BI002
- BL002-CVS
- NEMDO-BI003
- BL003-IREDO
- MARIA-IREDO
- SP001-SEPOM
- SVT-KENOX
- BOTNO-SNT
- EXTER-CARME

- BAMUX-KENOX
- CARME-KENOX
- ORABI-BULVO
- XUVIT-DIGUN
- TARIM-DIGUN
- SAGRO-BUXON
- SAGRO-MOSOK
- LIRAX-IRAVU
- IRAVU-MESAB
- IP006-NANIK
- IP007-NANIK
- IP008-NANIK
- IP008-MOSAD

All the analyzed trajectories are shown in Figure 10, Figure 11 and Figure 12:

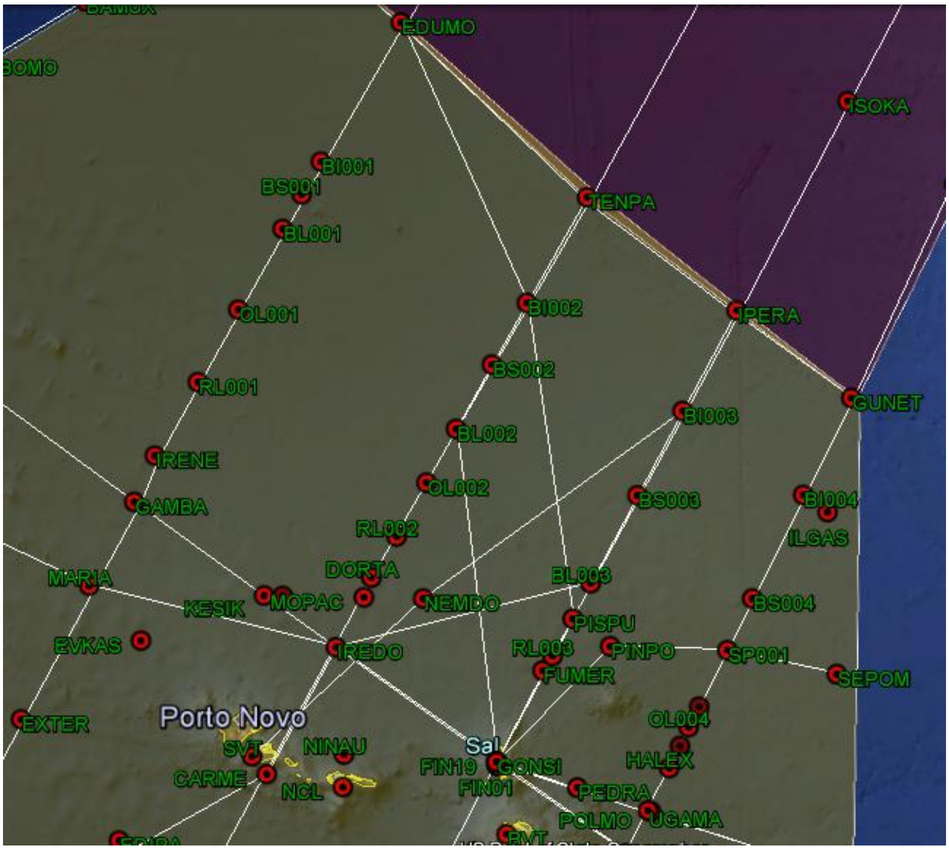

Figure 10.
Analysed crossing traffic in SAL in non-published routes (1).

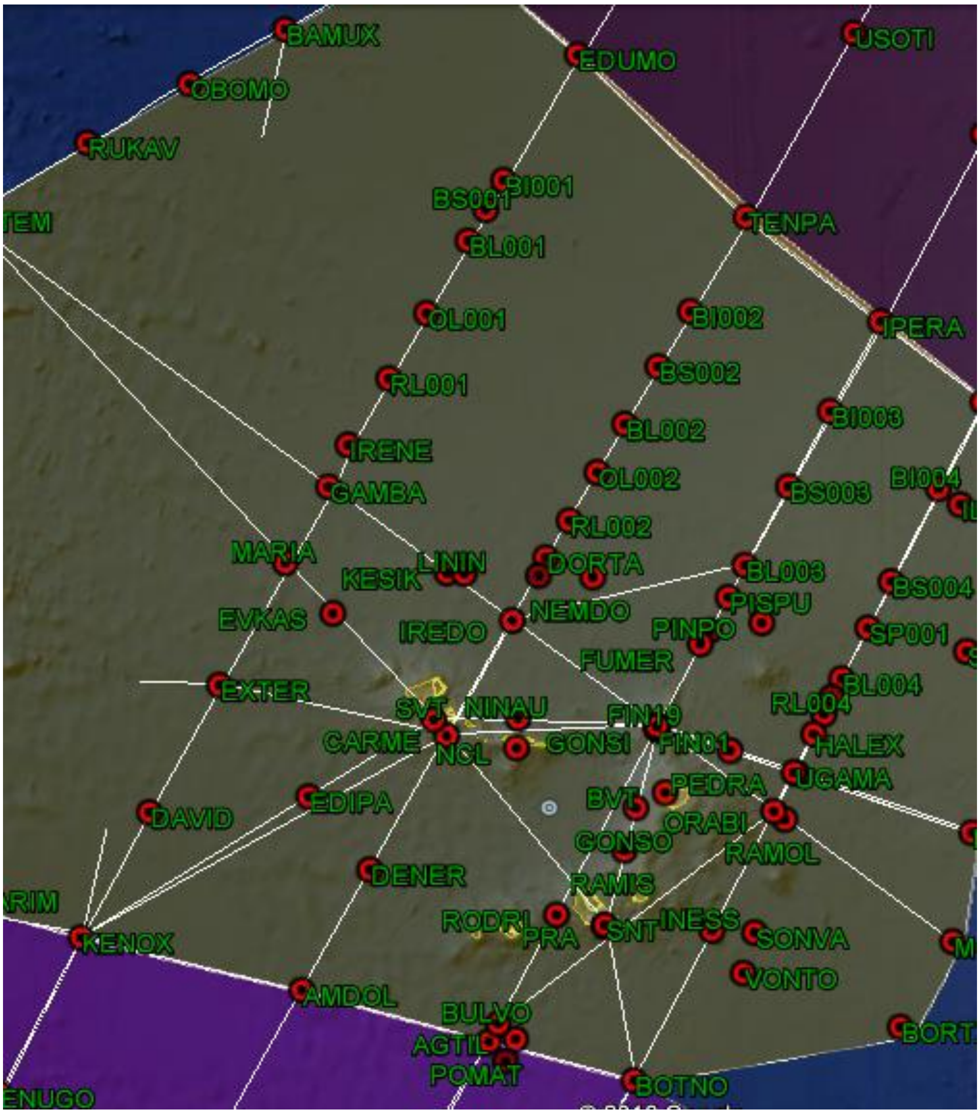

Figure 11.
Analysed crossing traffic in SAL in non-published routes (2).

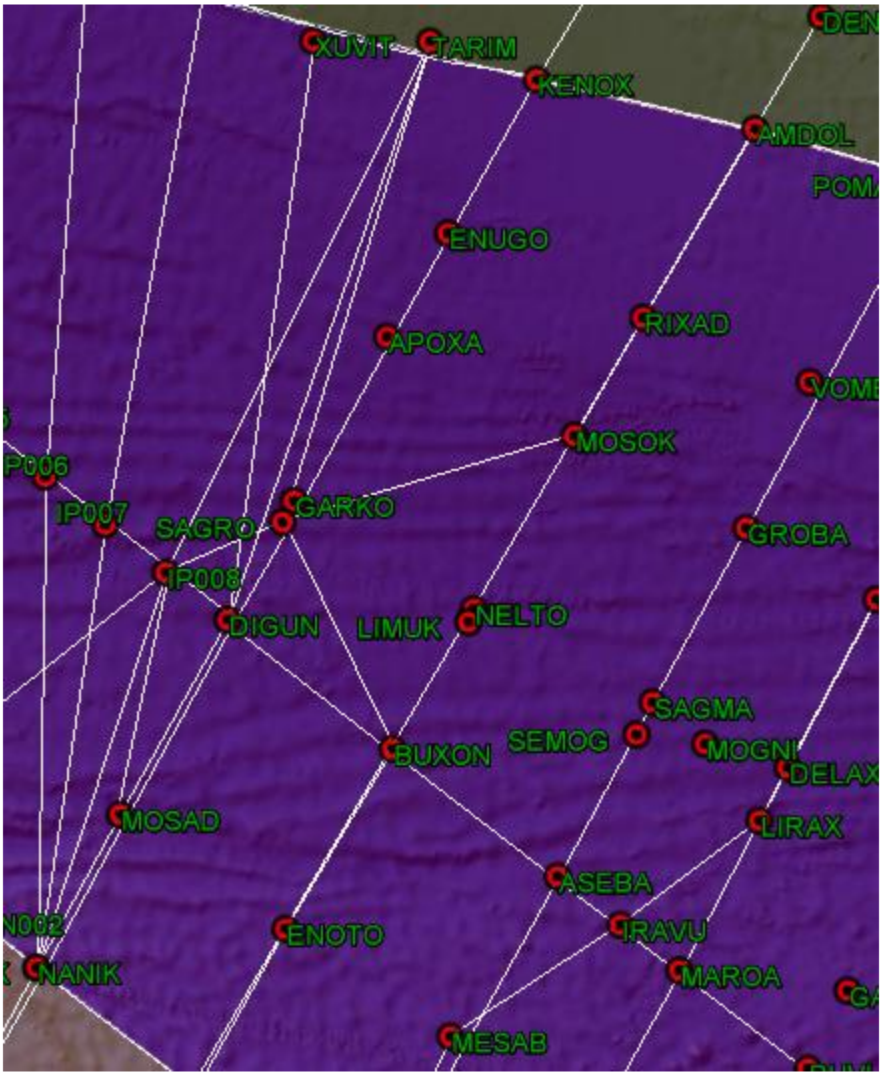

Figure 12.
Analyzed crossing traffic in Dakar in non-published routes.

Analysing these trajectories, only 4.05% of the traffic is not being considered in the Canaries UIR, 1.67% in SAL, 1.21% in Dakar and 0.76% in Recife. Therefore, these hypotheses seem reasonable, at least in a first approach, especially considering that these crossings or changes between routes only occur when there is not any traffic around.

2.1. ATS Services and Procedures

The airspace in the area of the South Atlantic EUR/SAM Corridor is subject to procedural control with pilot voice waypoint position reporting. While VHF voice communications are available in some areas of the Corridor, the primary means of communications is HF voice. Appropriately equipped aircraft can also use SATCOM and HF Data Link (HFDL) throughout the South Atlantic EUR/SAM Corridor.

There are two DME stations inside the RNP10 airspace, namely CVS, Almilcar Cabral, and NOR, Noronha. Their ranges are limited by the RF horizon to about 200 NM. There are also some DME stations to the north and south of the RNP10 airspace, in the Canary Islands and in Recife.

Although radar surveillance is not available for the parallel route system in the four FIR/UIRs, it is available in the adjacent Canaries TMA, on the coast of Brazil and in Cape Verde. Radar range is also limited by the RF horizon.

These radars do provide an opportunity to monitor the lateral and the vertical deviations of aircraft flying in the Corridor. However, information from these radars was not available for this study.

The system called SACCAN (ADS-CPDLC in the Canaries FIR/UIR) is also installed in the Canary Islands. The main purpose of SACCAN is to provide air traffic control services to FANS 1/A aircraft operating in the Canary airspace.

FANS 1/A equipped aircraft use the SITA and ARINC networks and can communicate with SACCAN by means of the Aeronautical Mobile Satellite Service (AMSS) provided by INMARSAT, or by VHF when within the range of any of the multiple SITA or ARINC VHF data link stations, like the ones of SITA located in the Canary Islands.

The technical coverage of SACCAN is the coverage provided by the constellation of geostationary satellites INMARSAT, i.e. global coverage (except for the poles). Nevertheless, operationally, the area of interest is the oceanic area of the Canaries FIR where there is not radar coverage.

SACCAN uses FANS-1/A technology. The system improves surveillance (with ADS) and communications (with CPDLC) of the FANS-1 or FANS-A equipped aircraft, when flying over the oceanic area of the Canaries FIR. The system is in operational state since 27th August 2009 ([Ref. 23]). In the same way, ADS-C and CPDLC are also in operational state in Atlantic FIR.

According to the AIRAC AIP SUPR 13/A/09GO of 30th July 2009, the operational implementation of ADS-C and CPDLC in Dakar Oceanic is also effective from 27th August 2009.

As far as SAL FIR is concerned, ADS-C and CPDLC are also in operational state since 2011.

This study does not consider the reduction of the collision risk that would be obtained with the use of ADS.

2.2. Data sources and software

For this study, flight progress data from the Canaries, SAL, Dakar and Atlantic ACCs, between FL290 and FL410, have been made available from 1st July 2015 to 31st July 2015. When data, such as the number of flights or flight time for the rest of 2015 has been necessary, it has been extrapolated using information from Canaries as a basis.

Data for the complete year 2015 from the Canaries are based on the flight progress information stored in Palestra, Enaire's database. It consists of initial flight plan data updated by the controllers with pilot position reports.

Occasionally, it may occur that controllers do not enter the information into the database system due to workload-derived constraints, even though they have undoubtedly updated their personal flight progress information. As a consequence, the altitude information obtained from Palestra is not always correct. In the same way, it is possible that typographical errors have been introduced while inputting the information or that some information has been omitted. Some of these errors have been detected and corrected by software.

In the collision risk assessment made by ARINC in 2001, [Ref. 2], which was the base for RNP10 implementation in the South Atlantic Corridor and for the introduction of the current route UN-873, it was mentioned that several errors regarding flight level were identified in the flight plans because a high proportion of flights did not match the vertical route structure.

This has been verified analysing some flight plans from Palestra, chosen by chance. The used software takes this into account and corrects altitudes assuming that:

- All aircraft conform to the vertical route structure.
- No aircraft entered or left the vertical route structure.
- The reported altitudes are close to the actual altitudes.
- The reported altitudes are less than the actual altitudes.

The analysed Palestra flight plans have been those which cover the time period from 1st January 2015 to 31st December 2015. They include reports for all waypoints in the Canaries UIR.

Besides data from Palestra, traffic samples from SAL, Dakar and Atlantic-Recife have also been available for this assessment. Particularly, data from SAL is available from July to December, data from Dakar for March, April and from July to December and data from Recife for all 2015. Data provided by States include information from all aircraft overflying the airspace on the four main routes of the Corridor.

Regarding crossing routes, SAL and Dakar provide traffic information from airways UR-976/UA-602 and UL-435, respectively. On the other hand, Recife provides crossing traffic data from route UL-375/UL-695.

As the data format from SAL, Dakar and Recife is different from each other and different from the one used by Palestra, a transformation of formats was necessary to unify the format to the one used by Palestra.

It must be said that, in the provided data, sometimes there was not information of all the needed waypoints and, in other cases, the information was incoherent. As a result, trajectories and information at required waypoints (i.e., time and FL) were assumed, considering the most logical routes and speeds for the extrapolation. This may have an influence on the results, as it will be explained later on.

As it has already been said, extrapolation has been necessary for the main routes of the Corridor, in order to obtain the traffic distribution along the Corridor. It has also been necessary to extrapolate crossing traffic on published routes when information of all the required waypoints was not available. Specially, for the ULTEM-LUMPO direct-to trajectory, it has been necessary to extrapolate all the flights of the crossing route and all the flights of the main routes to the points where the line ULTEM-LUMPO intersects each of the main routes. This approximation has also been done in the direct trajectories ULTEM-SEPOM, ULTEM-ILGAS, BAMUX-SEPOM, BAMUX-ILGAS, BAMUX-LUMPO, ENUGO-APIGU, APOXA-GONSA and SAGRO-LIRAX, using the intersection points described in Table 1.

Apart from traffic information, data on large height deviations have also been received, as it will be explained in 4.3.

2.2.1. Software

The software tool CRM, created by Enaire, has been used to obtain the different parameters of the lateral and vertical Reich Collision Risk Model in each one of the UIRs crossed by the Corridor, in the current route network.

The CRM program uses flight plan data obtained from Palestra, Enaire's database, for the Canaries and traffic data from the samples provided by SAL, Dakar and Atlantic-Recife. For this study, flight plan data from 1st July 2015 to 31st July 2015 for all the FIRs have been examined to determine the type of aircraft in the airspace, the average flight characteristics of the typical aircraft and the passing frequencies of these aircraft. Data for the complete year in Canaries has also been used as a basis to extrapolate some data of the rest of the UIRs when information of the complete year has been necessary (it is to be noted that lateral and vertical deviations of the whole 2015 have been considered). Taking these values into account and the traffic forecast for the future, it is possible to estimate the collision risk for the following years.

2.3. Aircraft population

The most common aircraft types, the number of flights per type and the proportion of these types over the total of flights detected during 2015 between FL290 and FL410 have been analysed.

Table 2 shows the values obtained for the Canaries UIR in 2015 together with the geometric dimensions of these aircraft types. Similar results have been obtained for the rest of UIRs.

Aircraft type	Count	% AC	Length (m)	Wingspan (m)	Height (m)
A332	5348	22.998%	63.70	60.03	16.74
B738	3234	13.907%	39.47	34.31	12.50
B77W	2081	8.949%	73.90	60.90	18.50
A343	1822	7.835%	63.70	60.30	16.74
A346	1677	7.212%	74.37	63.60	17.8
A320	1652	7.104%	37.57	34.10	11.76
B772	1428	6.141%	63.70	60.90	18.50
B752	1360	5.848%	47.32	38.05	13.60
B763	877	3.771%	47.60	54.90	15.90
B748	617	2.653%	76.30	65.45	19.50
B744	465	2.000%	70.70	64.40	19.40
A333	390	1.677%	63.70	60.03	16.74
A319	357	1.535%	33.84	34.10	11.76
B77L	244	1.049%	67.78	61.68	18.50
E190	217	0.933%	36.24	28.72	10.57
A321	178	0.765%	37.57	34.10	11.76
B737	148	0.636%	33.60	34.30	12.50
B734	135	0.581%	36.40	28.90	11.10
FA7X	101	0.434%	22.82	25.80	7.74
B788	100	0.430%	56.70	60.10	16.90
F900	74	0.318%	20.20	19.3	7.60
GLEX	52	0.224%	30.30	28.65	7.57
CL60	52	0.224%	20.86	19.35	6.28
MD11	48	0.206%	61.20	51.70	17.60
F2TH	46	0.198%	20.21	19.33	7.55
E135	44	0.189%	26.33	20.04	6.76
E35L	42	0.181%	26.33	21.17	6.76
C17	41	0.176%	53.00	51.80	16.80
GLF4	36	0.155%	26.90	23.79	7.64
GLF5	29	0.125%	29.42	28.50	7.87
A310	28	0.120%	46.40	43.89	15.80
B733	28	0.120%	33.40	28.90	11.10
CJR9	24	0.103%	36.20	23.30	7.50
B753	24	0.103%	54.47	38.05	13.56
LJ35	22	0.095%	14.71	11.97	3.71
IL76	19	0.082%	46.59	50.50	14.76
B762	19	0.082%	48.50	47.60	15.80
GALX	15	0.065%	18.99	17.71	6.52
H25B	14	0.060%	15.60	15.70	5.40
LJ60	13	0.056%	17.89	13.35	4.44

Aircraft type	Count	% AC	Length (m)	Wingspan (m)	Height (m)
B735	10	0.043%	31.01	28.88	11.10
A400	8	0.034%	42.40	45.10	14.70
FA50	7	0.030%	18.52	18.96	6.97
A124	7	0.030%	69.10	73.30	20.78
A345	7	0.030%	67.90	63.45	17.10
C680	6	0.026%	11.22	14.95	4.56
E145	6	0.026%	29.87	20.04	6.75
GL5T	6	0.026%	28.69	28.65	7.70
CRJ2	5	0.022%	26.80	21.21	6.30
CL30	5	0.022%	20.90	18.40	6.10
LJ55	5	0.022%	16.80	13.30	4.50
LJ45	5	0.022%	17.70	14.60	4.30
GLF6	4	0.017%	30.41	30.36	7.72
IL96	4	0.017%	69.10	73.30	20.78
C56X	3	0.013%	15.80	17.00	5.20
E170	3	0.013%	29.90	26.00	9.67
G280	3	0.013%	20.30	19.20	6.50
F100	3	0.013%	35.53	28.07	8.49
C5	3	0.013%	75.30	67.90	19.80
C650	3	0.013%	14.29	15.91	4.57
DC10	2	0.009%	55.20	50.40	17.90
B777	2	0.009%	67.78	61.68	18.50
LJ31	2	0.009%	14.83	13.35	3.75
A342	2	0.009%	59.39	60.30	16.74
M081	2	0.009%	45.10	32.90	9.00
ASTR	2	0.009%	16.94	16.05	5.54
LJ40	2	0.009%	16.93	14.56	4.31
C750	2	0.009%	22.05	19.38	5.84
D328	2	0.009%	21.11	20.98	7.24
J328	2	0.009%	20.90	20.90	7.20
K35E	2	0.009%	41.50	39.90	12.70
WW24	2	0.009%	15.90	13.70	4.80
A330	2	0.009%	63.60	60.30	16.70
B52	1	0.004%	48.03	56.40	12.40
C25C	1	0.004%	16.26	15.49	4.69
C30J	1	0.004%	29.80	40.40	11.84
E55P	1	0.004%	15.60	15.90	5.10
A359	1	0.004%	66.80	64.75	17.05
B789	1	0.004%	62.80	60.10	16.90
MD83	1	0.004%	45.10	32.80	9.05

Aircraft type	Count	% AC	Length (m)	Wingspan (m)	Height (m)
B773	1	0.004%	73.90	60.90	19.30
FA20	1	0.004%	17.15	16.32	5.32
T204	1	0.004%	46.00	42.00	13.90
B739	1	0.004%	42.10	34.30	12.60
C130	1	0.004%	29.79	28.26	8.38
B757	1	0.004%	49.70	38.05	13.50
GLF2	1	0.004%	24.36	20.98	7.47
PC12	1	0.004%	14.40	16.20	4.30
Unknown	7	0.030%	----	----	----

Table 2.
Aircraft population and number of flights per type during 2015 in the Canaries UIR.

The data sample in the Canaries UIR includes 23.254 flights of 89 different aircraft types. The population is dominated by large airframes such as A330-200, B777-300AR, A340-300, A340-600, B747-400, B777-200LR, B747-800 and A330-300. These 8 types make up about 60.5% of the total number of flights. The next 5 types, which also belong to the Airbus and Boeing families, make up another 32.2% and the rest 7.3% is distributed among the other 76 aircraft types.

2.4. Temporal distribution of flights

Several graphs, showing the temporal distribution of flights, will be displayed in this section. The first one, Figure 13, shows the distribution of the number of flights per day in EDUMO, TENPA, IPERA and GUNET from 1st January 2015 to 31st December 2015, differentiating between northbound (NB) and southbound (SB) traffic. Next, Figure 14 shows the distribution of the number of flights per day in the Canaries for the traffic sample selected in this study: from 1st July 2015 to 31st July 2015.

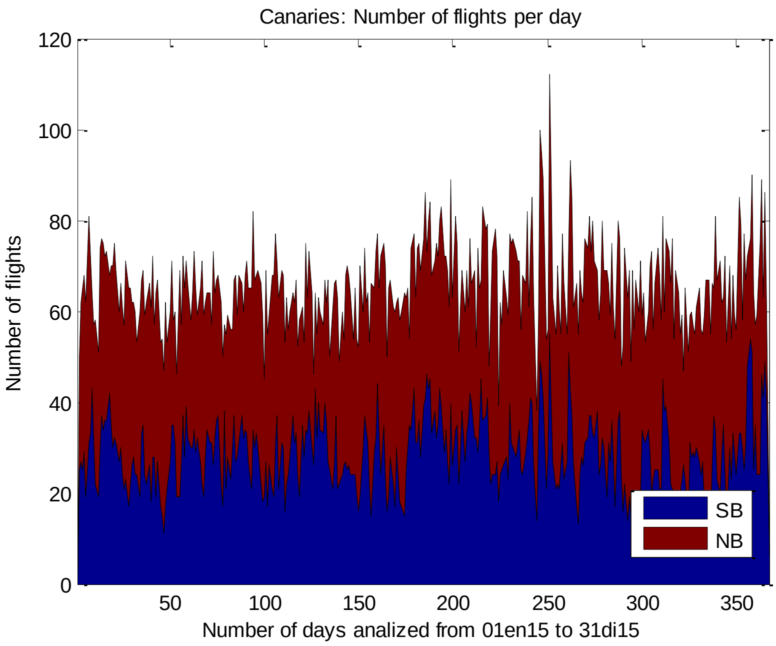

Figure 13.
Number of flights per day in the Canaries. Year 2015.

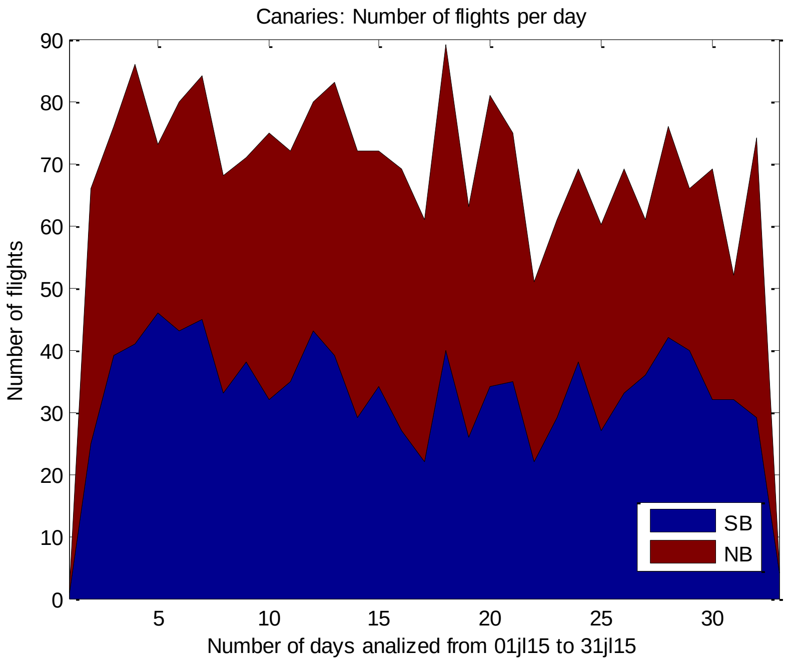

Figure 14.
Number of flights per day in the Canaries. July 2015.

The overall average traffic for 2015 is 63.36 flights per day with a standard deviation of 10.81 flights. In July, the average traffic was slightly higher, 65 flights per day, with a standard deviation of 18.47 flights. The highest peak of traffic was reached in September, when there were 112 flights in one day.

Figure 15 shows the distribution of the yearly traffic over the days of the week.

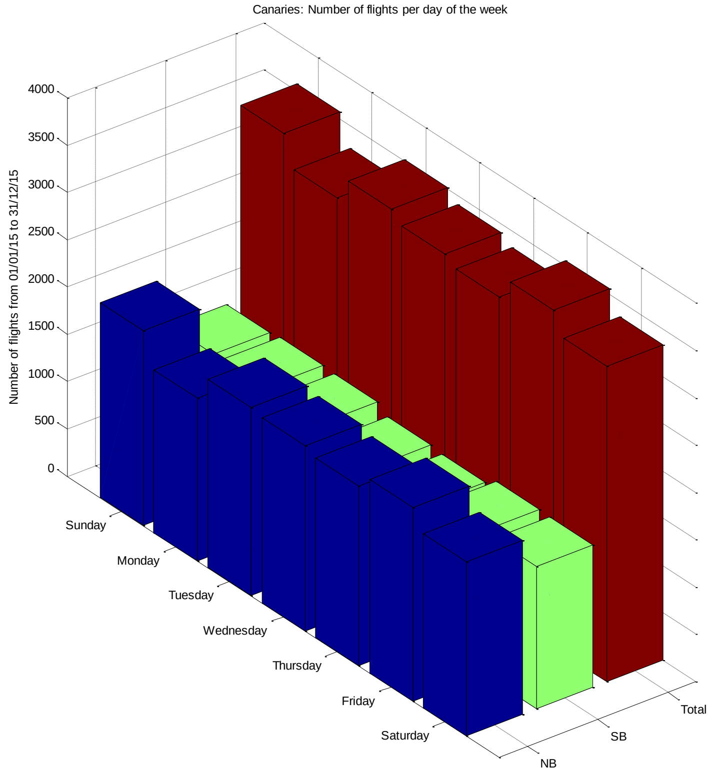

Figure 15.
Number of flights per day of the week in the Canaries. Year 2015.

The distributions of flights per half-hour are shown in the following figures. The first one shows the distribution of flights obtained with the time of waypoint crossing in EDUMO, TENPA, IPERA and GUNET (Canaries) during 2015. The second one shows the same distribution of flights, but during July, distributing the 2145 aircraft detected over the studied period according to the time of day at which they crossed those waypoints. The third one shows the distribution of flights obtained with the time of waypoint crossing in DIKEB, OBKUT, ORARO and NOISE (Recife). They also distinguish between northbound (NB) and southbound (SB) traffic.

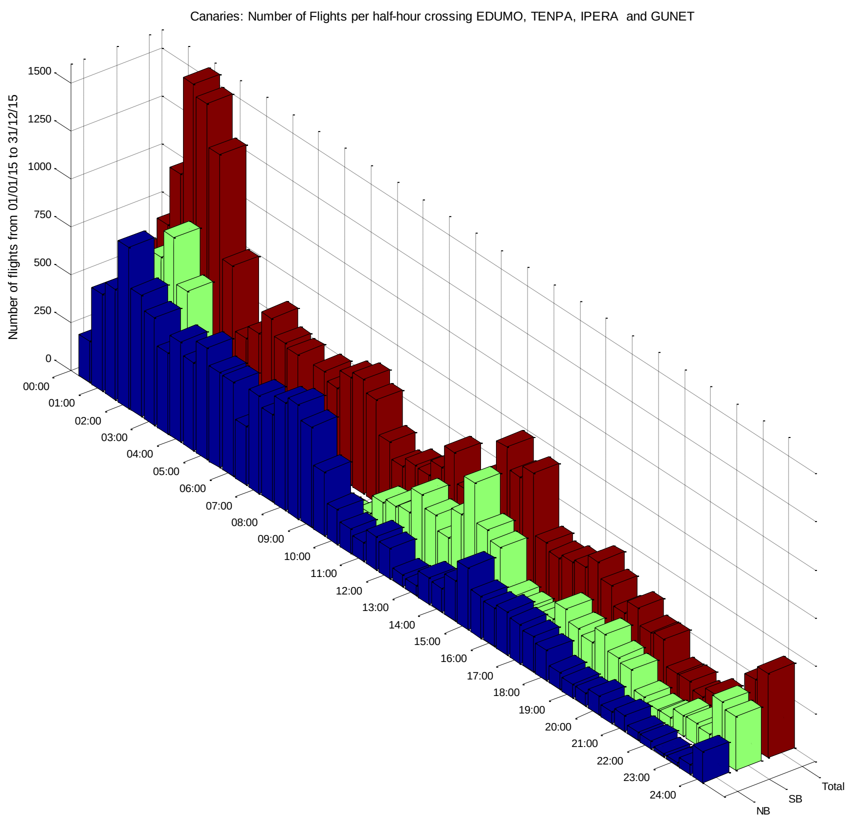

Figure 16.
Number of flights per half-hour crossing EDUMO, TENPA, IPERA and GUNET. Year 2015.

It can be seen that during 2015, in the Canaries, it is from 00:00h to 3:00h and from 11:00 to 17:00h when the highest concentration of southbound flights occurs, whilst most of the northbound aircraft concentrate from 00:00h to 10:00h.

Figure 17 shows the temporal distribution for Canaries during July 2015. Following, Figure 18 shows the temporal distribution of the 1.672 aircraft detected over this period in Recife, according to the time of day at which they crossed DIKEB, OBKUT, ORARO and NOISE waypoints.

In this figure, it can be seen that in Recife the highest traffic concentration occurs between 00:00h and 8:00h and, in a lower extent, from 15:00h to 24:00h.

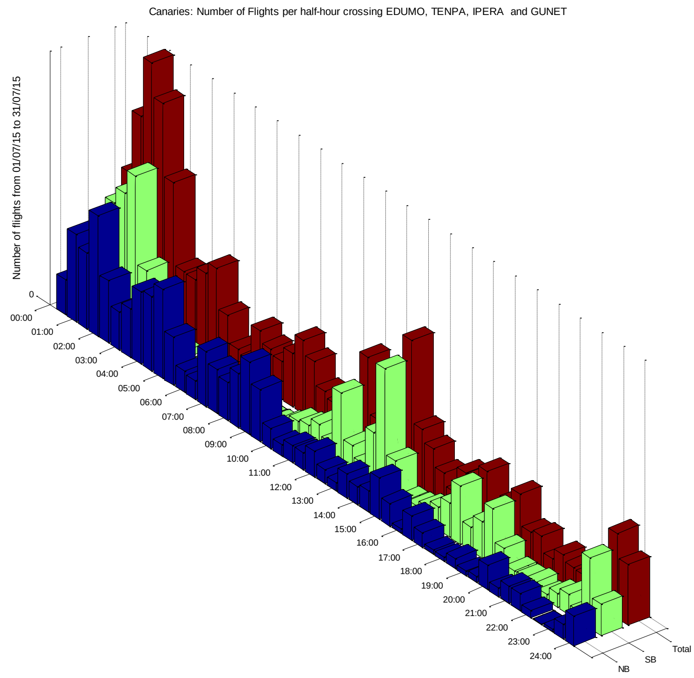

Figure 17.
Number of flights per half-hour crossing EDUMO, TENPA, IPERA and GUNET. July 2015.

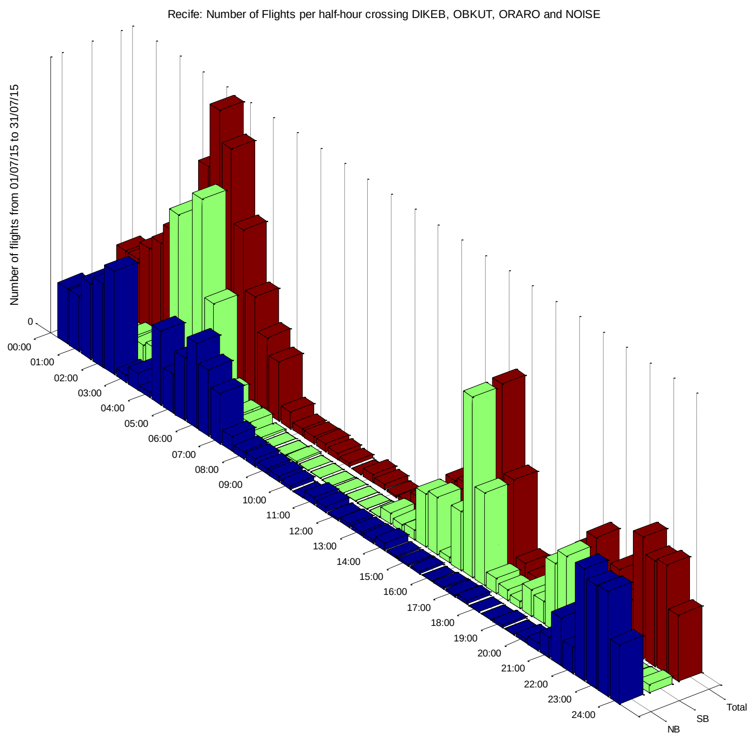

Figure 18.
Number of flights per half-hour crossing DIKEB, OBKUT, ORARO and NOISE. July 2015.

2.5. Traffic distribution per flight level

Traffic distribution per flight level during 2015 will be depicted in the graphics of this section. Figure 19 shows the total amount of traffic for the main routes in the Canaries, distributed by route and flight level. Figure 20 and Figure 21 are similar, but they only include the southbound and the northbound traffic, respectively.

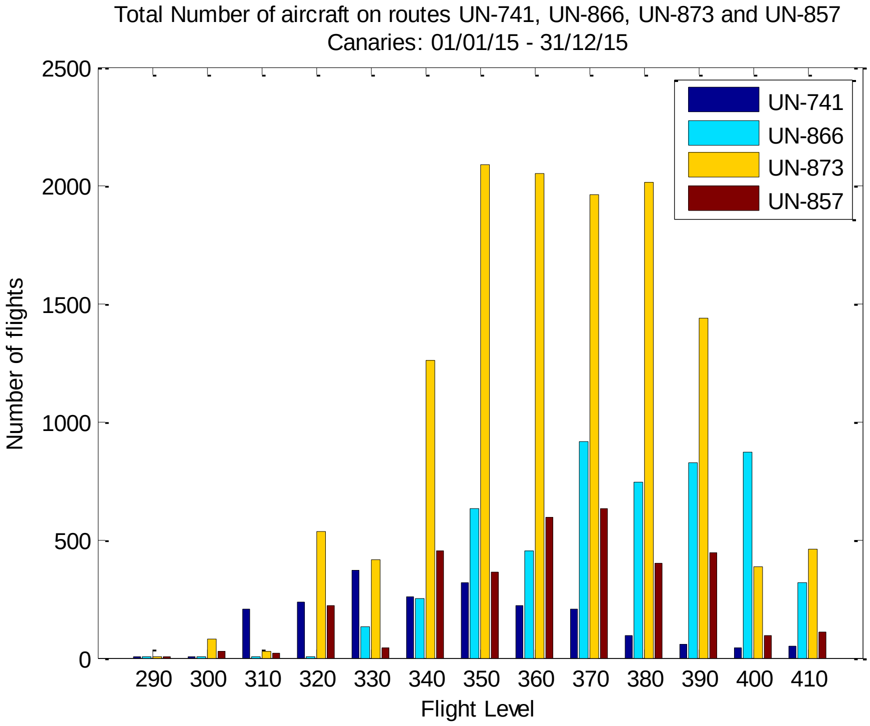

Figure 19.
Number of aircraft on routes UN-741, UN-866, UN-873 and UN-857 in the Canaries.

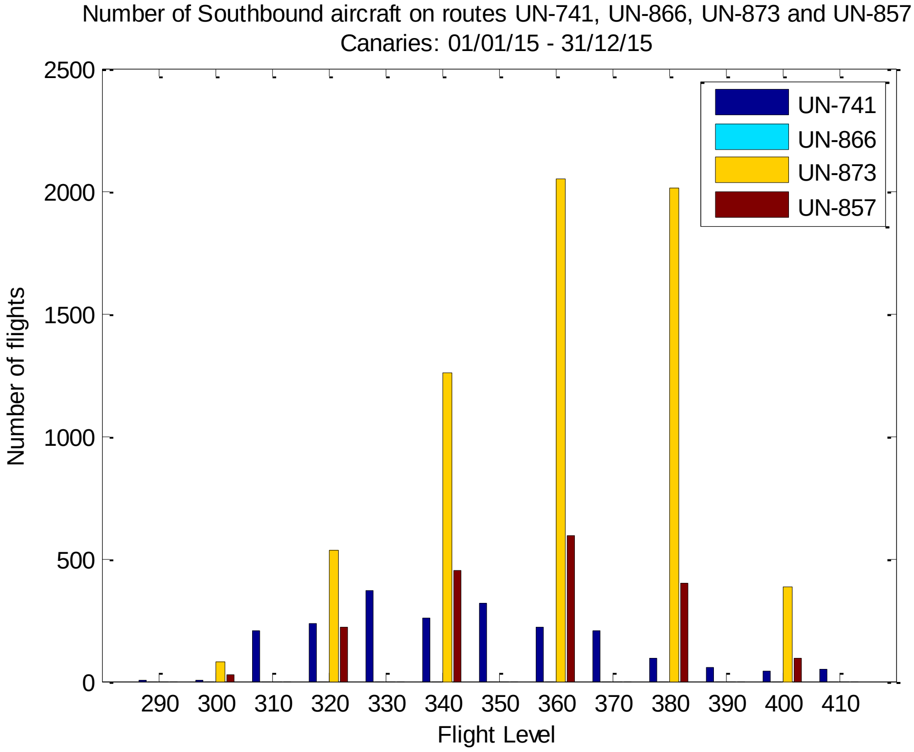

Figure 20.
Number of Southbound aircraft on routes UN-741, UN-866, UN-873 and UN-857 in the Canaries.

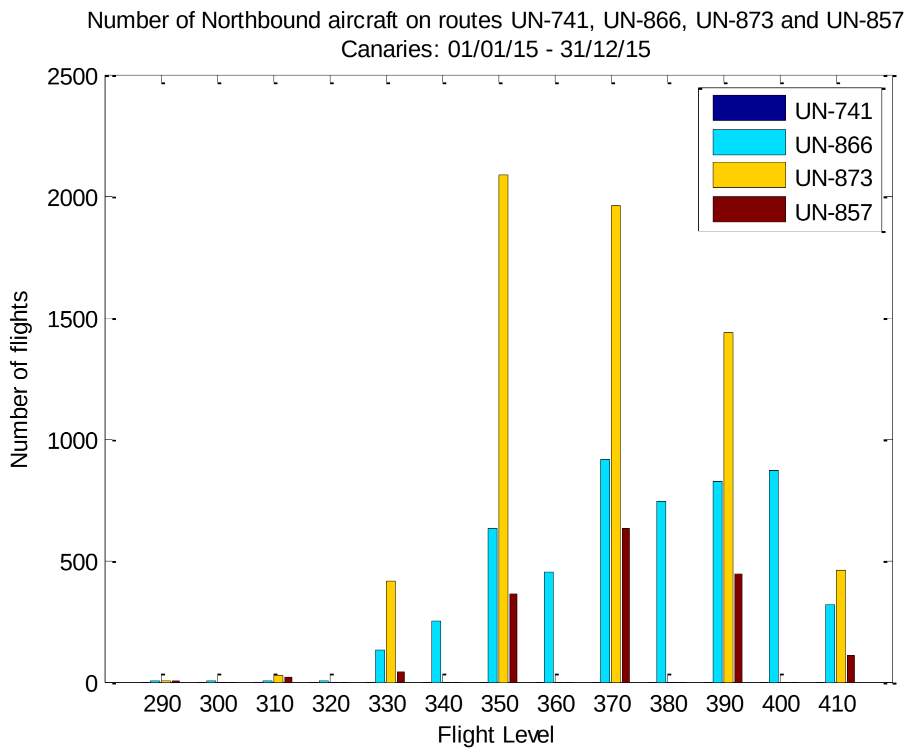

Figure 21.
Number of Northbound aircraft on routes UN-741, UN-866, UN-873 and UN-857 in the Canaries.

2.6. Locations for risk assessments

For the studied scenario, lateral and vertical collision risks are assessed. This assessment is made in six different locations along the Corridor, covering the four UIRs. These locations are shown in Figure 22:

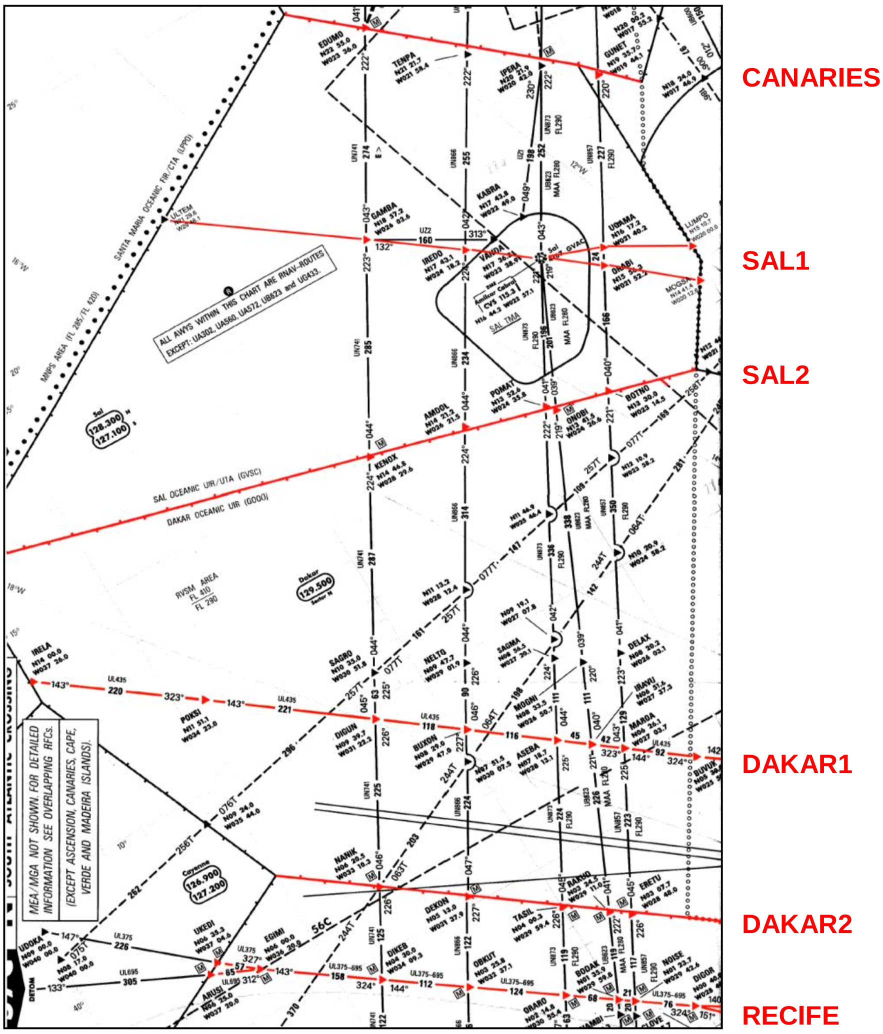

Figure 22.
Locations for risk assessments.

The locations are:

- Canaries: boundary between the Canaries UIR and the SAL OCEANIC UIR
- SAL1: Route UR-976/UA-602
- SAL2: Boundary between SAL OCEANIC UIR and DAKAR OCEANIC UIR
- DAKAR1: Route UL-435
- DAKAR2: Boundary between DAKAR OCEANIC UIR and ATLANTIC FIR
- RECIFE: Route UL-375/UL-695

Traffic data from 1st July 2015 to 31st July 2015 has been used to obtain collision risk in the six locations where the assessment has been done.

The risk associated to the Corridor will be the largest among the values obtained in all the locations.

3. Lateral collision risk assessment

3.1. Reich Collision risk model

As the four routes in the EUR/SAM Corridor are nearly parallel, it is possible to use the Reich Collision Risk Model to calculate lateral collision risk.

It models the lateral collision risk due to the loss of lateral separation between aircraft on adjacent parallel tracks flying at the same flight level.

The model reads as follows:

$$N_{ay} = P_y(S_y) \cdot P_z(0) \cdot \frac{\lambda_y}{S_x} \cdot \left\{ E_{y_{same}} \cdot \left[\frac{|\Delta \bar{v}|}{2 \cdot \lambda_x} + \frac{|\overline{\dot{y}}|}{2 \cdot \lambda_y} + \frac{|\overline{\dot{z}}|}{2 \cdot \lambda_z} \right] + E_{y_{opposite}} \cdot \left[\frac{2 \cdot |\bar{v}|}{2 \cdot \lambda_x} + \frac{|\overline{\dot{y}}|}{2 \cdot \lambda_y} + \frac{|\overline{\dot{z}}|}{2 \cdot \lambda_z} \right] \right\}$$

Equation 1.

Where:

- N_{ay} is the expected number of accidents (two per each aircraft collision) per flight hour due to the loss of lateral separation between aircraft flying on tracks with nominal spacing S_y.
- S_y is the minimum standard lateral separation.
- $P_y(S_y)$ is the probability of lateral overlap of aircraft nominally flying on laterally adjacent paths at the same flight level.
- $P_z(0)$ is the probability of vertical overlap of aircraft nominally flying at the same flight level.
- $E_{y\ same}$ is the same direction lateral occupancy, i.e. the average number of same direction aircraft flying on laterally adjacent tracks at the same flight level within segments of length $2 \cdot S_x$ centred on the typical aircraft.
- $E_{y\ opposite}$ is the opposite direction lateral occupancy, i.e. the average number of opposite direction aircraft flying on laterally adjacent tracks at the same flight level within segments of length $2 \cdot S_x$ centred on the typical aircraft.
- S_x is the length of the longitudinal window used in the calculation of occupancies.
- λ_x is the average length of an aircraft.
- λ_y is the average width of an aircraft.
- λ_z is the average height of an aircraft.
- $|\Delta \bar{v}|$ is the average relative along-track speed of two aircraft flying at the same flight level in the same direction.
- $|\bar{v}|$ is the average ground speed of an aircraft.

- $\overline{|\dot{y}|}$ is the average lateral cross-track speed between aircraft that have lost their lateral separation.
- $\overline{|\dot{z}|}$ is the average relative vertical speed of aircraft flying at the same flight level.

A collision, and consequently two accidents, can only occur if there is an overlap between two aircraft in all three dimensions simultaneously. Equation 1 gathers the product of the probabilities of losing separation in each one of the three dimensions.

As it has already been said, $P_z(0)$ is the probability of vertical overlap; $P_y(S_y)$, the probability of lateral overlap and the combinations $\frac{\lambda_y}{S_x} \cdot E_{y_{same}}$ and $\frac{\lambda_y}{S_x} \cdot E_{y_{opposite}}$ relate to the probability of longitudinal overlap of aircraft on adjacent parallel tracks and at the same altitude.

All the probabilities can be interpreted as proportions of flight time in the airspace during which overlap in the pertinent dimension occurs.

As the collision risk is expressed as the expected number of accidents per flight hour, the joint overlap probability must be converted into number of events involving joint overlap in the three dimensions, relating overlap probability with passing frequency[2]. This is achieved using the expressions within square brackets in Equation 1. Each of the terms within square brackets represents the reciprocal of the average duration of an overlap in one of the dimensions. For example, $|\Delta\bar{v}|/_{2 \cdot \lambda_x}$ is the reciprocal of the average duration of an overlap in the longitudinal direction for same direction traffic. In the same way, for opposite direction, the average relative speed is 2v and the average overlap time is $2 \cdot |\bar{v}|/_{2 \cdot \lambda_x}$.

The model is based on the following hypothesis:

- All tracks are parallel
- All collisions usually occur between aircraft on adjacent routes, although, if the probability of overlap is significantly large, they may also occur on non-adjacent routes.
- The entry times into the track system are uncorrelated.
- The lateral deviations of aircraft on adjacent tracks are uncorrelated.
- The lateral speed of an aircraft is not correlated with its lateral deviation.
- The aircraft are replaced by rectangular boxes.
- There is no corrective action by pilots or ATC when aircraft are about to collide.

The model also assumes that the nature of the events making up the lateral collision risk is completely random. This implies that any location within the system can be used to collect a representative data sample on the performance of the system.

In the following sections all the parameters that appear in Equation 1 will be analysed.

[2] *Passing frequency between two adjacent routes is the average number of events, per flight hour, in which two aircraft are in longitudinal overlap when travelling in the opposite or same direction at the same flight level.*

3.2. Average aircraft dimensions: $\lambda_x, \lambda_y, \lambda_z$

In previous Table 2, the dimensions of the aircraft types found in the Canaries UIR during the studied period were presented. Using this information, the average aircraft dimensions have been calculated with the dimensions of each aircraft type and the proportions of flights by type as weighting factors. These data are shown in Table 3.

Location	Value Length (λ_x)		Wingspan (λ_y)		Height (λ_z)	
	Value (ft)	Value (NM)	Value (ft)	Value (NM)	Value (ft)	Value (NM)
Canaries	187.52	0.0309	170.38	0.0280	51.20	0.0084
SAL1	214.71	0.0353	197.24	0.0325	56.58	0.0093
SAL2	214.71	0.0353	197.24	0.0325	56.58	0.0093
Dakar1	209.37	0.0345	191.90	0.0316	55.39	0.0091
Dakar2	209.26	0.0344	191.97	0.0316	55.42	0.0091
Recife	211.47	0.0348	193.50	0.0318	55.92	0.0092

Table 3.
Average aircraft dimensions.

3.3. Probability of vertical overlap: $P_z(0)$

The probability of vertical overlap of aircraft nominally flying at the same flight level of laterally adjacent flight paths is denoted by $P_z(0)$ and it is defined by:

$$P_z(0) = \int_{-\lambda_z}^{\lambda_z} f^{z_{12}}(z)dz$$

Equation 2.

where $f^{z_{12}}$ denotes the probability density of the vertical distance z_{12} between two aircraft with height deviations z_1 and z_2 nominally at the same flight level, i.e.

$$z_{12} = z_1 - z_2$$

Equation 3.

and

$$f^{z_{12}} = \int_{-\infty}^{\infty} f^{TVE}(z_1) f^{TVE}(z_1 - z)dz$$

Equation 4.

Equation 4 assumes that deviations of the two aircraft are independent and have the same probability density, $f^{TVE}(z_1)$. λ_z denotes the average aircraft height. Substitution of Equation 4 into Equation 2 gives:

$$P_z(0) = \int_{-\lambda_z}^{\lambda_z} \int_{-\infty}^{\infty} f^{TVE}(z_1) f^{TVE}(z_1 - z)dz_1 dz$$

Equation 5.

This expression can be approximated by:

$$P_z(0) \approx 2\lambda_z \int_{-\infty}^{\infty} f^{TVE}(z_1) f^{TVE}(z_1) dz_1$$

Equation 6.

Thus, the probability density $f^{TVE}(z_1)$ is needed to calculate $P_z(0)$.

In this collision risk assessment, the values for $P_z(0)$ and $P_z(1000)$ (see 4.2.6) have been calculated using the Eurocontrol RVSM Tool. In the case of Pz(0), the obtained result has been $P_z(0)$=0.3989.

3.4. Average ground speed: v

As data on cleared speeds have not been provided, speeds and relative velocities have been estimated by comparing waypoint report times. To do this, the CRM program compares the time of waypoint crossing in two waypoints of the track; it calculates the difference between them and multiplies the inverse of this value by the distance that separates those waypoints. The result of this operation is the speed of each aircraft. The average speed, v, is then obtained as the mean value of the speeds of all the aircraft that flew on the four routes during the considered period of time.

As it was previously mentioned, Palestra database contains several errors. Some errors have been detected in some waypoint crossing times, what leads to extremely high speeds, even impossible in some cases.

As an example, Figure 23 shows speeds of the southbound aircraft that flew in the Canaries UIR, in the studied period of time, on route UN-741 and on route UN-873.

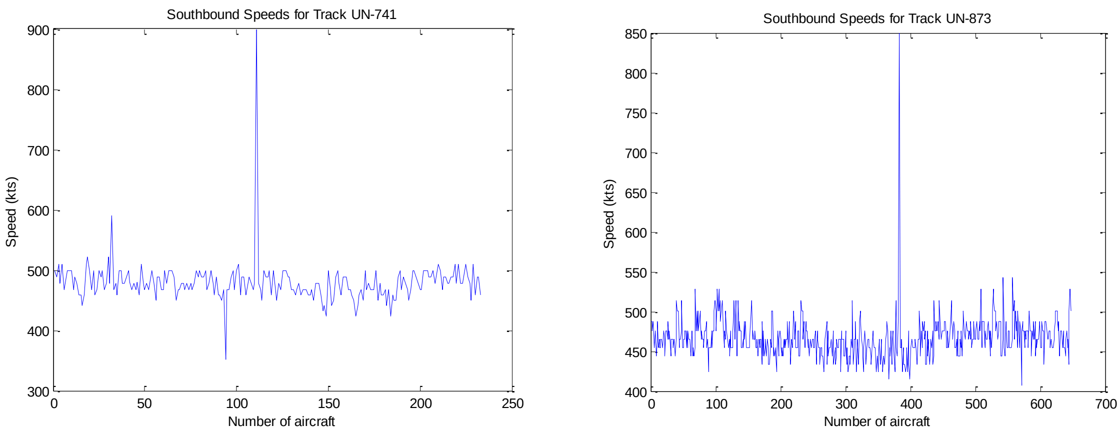

Figure 23.
Speeds obtained directly from Palestra.

For example, data from the flight plan, identified as the one corresponding to the highest peak for southbound speeds on route UN-741 is shown here:

Clase	Fijo	Cx	Cy	HoraETO	NivelPaso	TipoETO
1	DPLP03	01521570	0275831N	10-07-15,22:23:23	25	TDR
1	ECKOS	01520250	0280224N	10-07-15,22:24:28	60	TDR
1	23GDVE	01502090	0275455N	10-07-15,22:26:07	120	AUTOM.
1	26G134	01502570	0274831N	10-07-15,22:26:41	152	AUTOM.
1	26G178	01518060	0273949N	10-07-15,22:27:54	197	TDR
2	-	01602220	0274243N	10-07-15,22:33:49	286	TDR
2	-	01608290	0274504N	10-07-15,22:34:49	360	TDR
1	NORED	02228450	0243816N	10-07-15,23:34:40	360	AUTOM.
1	EDUMO	02335590	0225502N	10-07-15,23:43:00	360	MANUAL

According to the flight plan, the distance between NORED and EDUMO, separated 120 NM, has been flown in just 8'20", what leads to such a high speed (864 kts).

The CRM software tries to correct this problem limiting the maximum speed. This maximum speed has been fixed in 575 kts. This value is still too high, but it has been taken since it corrects those values that were excessively high and it considers possible anomalous cases in which, because of the characteristics of the aircraft and the existing wind, speeds higher than the habitual ones could be reached.

With this limitation, the speed of each aircraft that flew during the analysed period of time on each route in the Canaries UIR is shown in the following graphs:

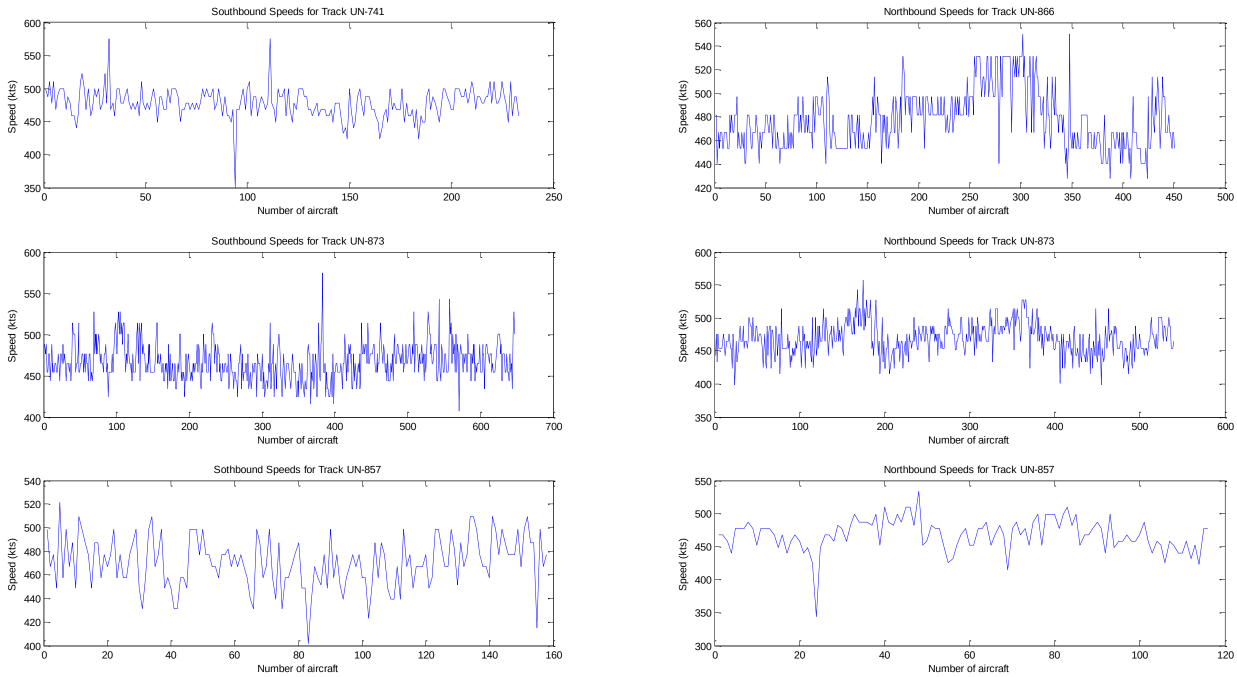

Figure 24.
Speeds limited to 575 kts in the current scenario in the Canaries.

Similar graphs can be obtained for the rest of locations.

From these speeds, the average ground speed obtained in the different locations is shown in Table 4:

Location	Average speeds		
	Southbound (kts)	Northbound (kts)	Average (kts)
Canaries	471.83	471.51	471.67
SAL1	459.51	461.52	460.51
SAL2	454.58	475.28	464.93
Dakar1	483.97	441.10	462.54
Dakar2	466.36	460.30	463.33
Recife	463.39	455.75	459.57

Table 4.
Average speeds.

3.5. Average relative longitudinal speed: Δv

Δv denotes the average relative longitudinal speed between aircraft flying in the same direction. As it has already been pointed out, in the case of aircraft flying in opposite directions, the average relative longitudinal speed is 2v.

The relative longitudinal speed has been obtained from the differences between the speeds of all the pairs of aircraft that constitute a proximate pair[3] in the same direction. The average relative speed is the mean value of all the calculated differences.

The results obtained for the current scenario can be seen in Table 5. The value considered in the collision risk assessment is the one shown in the last column of the table in order to be conservative and minimize the errors produced in the relative longitudinal speed calculation.

Location	Average relative longitudinal speeds			
	Southbound (kts)	Northbound (kts)	Average (kts)	Considered value (kts)
Canaries	16.7567	16.7481	16.7524	17
SAL1	41.2433	32.9611	37.1022	38
SAL2	34.2937	18.7771	26.5354	27
Dakar1	17.7274	56.3930	37.0602	38
Dakar2	35.5188	34.0082	34.7635	35
Recife	27.6643	27.5115	27.5879	28

Table 5.
Average relative longitudinal speeds.

[3] *Lateral proximate pair.- It is defined as an event in which one aircraft on one track passes another aircraft on an adjacent track at the same level and within a longitudinal distance 2Sx ($2T_0$ if it is expressed in time).*

3.6. Average relative lateral speed: $\bar{\dot{y}}$

$|\bar{\dot{y}}|$ is the average relative lateral cross-track speed between aircraft, flying on adjacent routes at the same flight level, that have lost their lateral separation.

The estimation of this parameter generally involves the extrapolation of radar data, speeds and lateral deviations, but such radar data were not available for the current report.

In the study made by ARINC ([Ref. 2]), this value was considered to be $|\bar{\dot{y}}| = 42\ kts$, which corresponds to a deviation angle of approximately 5° at an average ground speed of 475-480kts. Although, for example in the North Atlantic (NAT), the considered value was $|\bar{\dot{y}}| = 80\ kts$, ARINC thought that this value was too conservative for the SAT. Occurrence of waypoint insertion errors and other types of operational errors in the SAT is quite limited, because routes are defined by predetermined fixes, not being necessary to tell their coordinates, which can be misunderstood, but simply its name. ARINC took this into consideration to reduce the value of $|\bar{\dot{y}}|$.

In this study, the value considered has also been $|\bar{\dot{y}}| = 42\ kts$.

3.7. Average relative vertical speed: $\bar{\dot{z}}$

$|\bar{\dot{z}}|$ denotes the average modulus of the relative vertical speed between a pair of aircraft on the same flight level of adjacent tracks that has lost lateral separation. It is generally assumed that $|\bar{\dot{z}}|$ is independent of the size of the lateral separation between the aircraft and, for aircraft in level flight, it can also be considered that there is no dependency of $|\bar{\dot{z}}|$ with the vertical separation between the aircraft.

Data about $|\bar{\dot{z}}|$ are relatively scarce. Nevertheless, in the study made by ARINC ([Ref. 2]), it was mentioned that data from the NAT showed that $|\bar{\dot{z}}|$ was of the order of 1kt. From that, ARINC took $|\bar{\dot{z}}| = 1.5\ kts$, slightly more conservative. This value has also been considered in this case.

3.8. Lateral overlap probability: $P_y(S_y)$

The probability of lateral overlap of aircraft nominally flying on adjacent flight paths, separated by S_y, is denoted by $P_y(S_y)$ and it is defined by:

$$P_y(S_y) = \int_{-\lambda_y}^{\lambda_y} f^{y_{12}}(y)dy$$

Equation 7.

Where $f^{y_{12}}$ denotes the probability density of the lateral distance y_{12} between two aircraft with lateral deviations y_1 and y_2, nominally separated by S_y, i.e.

$$y_{12} = y_1 - y_2$$

Equation 8.

and

$$f^{y_{12}} = \int_{-\infty}^{\infty} f^y(y_1) f^y(S_y + y_1 - y) dy_1$$

Equation 9.

Equation 9 assumes that the lateral deviations of the two aircraft are independent and have the same probability density, $f^y(y_1)$. λ_y denotes the average aircraft width. Substitution of Equation 9 into Equation 7 gives:

$$P_y(S_y) = \int_{-\lambda_y}^{\lambda_y} \int_{-\infty}^{\infty} f^y(y_1) f^y(S_y + y_1 - y) dy_1 dy$$

Equation 10.

This expression can be approximated by:

$$P_y(S_y) \approx 2\lambda_y \int_{-\infty}^{\infty} f^y(y_1) f^y(S_y + y_1) dy_1$$

Equation 11.

The probability density function $f^y(y_1)$ depends on the nominal and non-nominal navigation capabilities of the aircraft. Nominal navigation performance takes into account typical lateral deviations that arise from ordinary navigational uncertainties when systems are working properly, whilst non-nominal performance represents atypical errors that occur infrequently and that would likely arise from pilot or controller mistakes, or from equipment malfunctions. These atypical errors play an important role in the collision risk, since they may cause large deviations.

The different types of lateral navigation errors are classified as follows according to [Ref. 9]:

Type of error	Description
A	Committed by aircraft not certified for operation in the RNP airspace
B	ATC system loop error
C1	Equipment control error including inadvertent waypoint error
C2	Waypoint insertion error due to the correct entry of incorrect position
D	Other with failure notified to ATC in time for action
E	Other with failure notified to ATC too late for action
F	Other with failure notified/receive by ATC
G	Lateral deviations due to weather when unable to obtain prior ATC clearance

Table 6.
Lateral navigation error types.

If data of the occurrence of each of these types of errors were available, it would be possible to model the probability density function of the lateral deviations associated to each individual type and to obtain a global distribution by taking a weighted mixture of the individual deviation distributions. The weighting factors would be determined by the frequencies with which the different types of errors occur.

This information was not available for this study. Therefore, to model the probability density function of Equation 11 it is assumed that all lateral errors or deviations follow the same probability distribution. This distribution may then be determined on the basis of a sample of data describing lateral deviations of aircraft from their tracks. It is usually modelled as a mixture of two distributions. These two distributions are:

- The core distribution, which represents errors that derive from standard navigation system deviations. These errors are always present, as navigation systems are not perfect and they have a certain precision.
- The tail distribution, which represents gross navigation errors (GNE), that corresponds to what has been denominated before as non-nominal performance.

It should also be noted that not all atypical errors are large in magnitude and that in most cases it is impossible to determine with certainty if a given observed lateral error arose from the core or from the tail term of the distribution.

Therefore, the overall probability density of lateral navigation errors can be written as:

$$f_y(y_1) = (1-\alpha) \times f_1(y_1) + \alpha \times f_2(y_1)$$

Equation 12.

Where:

- $f_1(y_1)$ represents the probability density function that models navigation errors arising from typical deviations of the aircraft navigation systems.
- $f_2(y_1)$ represents the probability density function that models navigation errors arising from typical deviations of the aircraft navigation systems.
- α represents the percentage of aircraft that experience such anomalies, whose distribution of lateral deviations is $f_2(y_1)$.
- (1-α) represents the percentage of aircraft that do not experience such anomalies in their lateral deviations.

To make the tail distribution conservative, the tail distribution is often taken as a double exponential distribution, because of its thick tail.

ARINC, [Ref. 2], also considered a zero mean double exponential distribution for the core term as in the North Pacific collision risk analysis.

The same distribution is used in this study. So,

$$f_1(y_1) = \frac{1}{2a_1} exp - \frac{y_1}{a_1}$$

Equation 13.

$$f_2(y_1) = \frac{1}{2a_2} exp - \frac{y_1}{a_2}$$

Equation 14.

Substituting Equation 13 and Equation 14 in Equation 12:

$$f_y(y_1) = (1-\alpha) \times \frac{1}{2a_1} exp - \frac{y_1}{a_1} + \alpha \frac{1}{2a_2} exp - \frac{y_1}{a_2}$$

Equation 15.

The parameter a_1 is determined by the RNP value, since this value indicates that 95% of the deviations are under that value. So, a_1 is obtained solving the following integral:

$$\int_{-RNP}^{RNP} f_1(y_1) dy_1 = 0.95$$

Equation 16.

The value for a_1 is then:

$$a_1 = -\frac{RNP}{\log 0.05}$$

Equation 17.

Using Equation 17:

$$a_1 = 3.338\ NM \quad (RNP10)$$

As far as the value of a_2 is concerned, in [Ref. 9] it is pointed out that, for a given value of α, $P_y(S_y)$ is maximized taking $a_2 = S_y$. In this case, the minimum separation between tracks is $S_y = 50\ NM$, and therefore, $a_2 = 50\ NM$.

Knowing a_2, it is possible to obtain the lateral deviations interval within which the aircraft would be with a 95% probability. To do it, the integral of the probability density function is calculated in the unknown interval. The result is a relation between the known parameter a_2 and the maximum unknown lateral deviation that define the 95% interval.

$$\int_{-x}^{x} f_2(y_1) dy_1 = 0.95\,; \rightarrow a_2 = -\frac{x}{\log 0.05}$$

Equation 18.

Thus, taking $a_2 = 50\ NM$, 95% of the lateral deviations will be within the interval $[-150{,}150]$ NM.

The remaining parameter to be fixed in order to define completely the probability density function is α.

This parameter may be interpreted as the probability of an individual aircraft experiencing an anomaly resulting in its distribution of lateral deviations having the scale factor a_2, instead of a_1, or as the proportion of aircraft experiencing anomalies in their lateral navigation performance.

To calculate the weighting factor α it has been used as a reference the Appendix A of the study made by ARINC [Ref. 2], summarized in Annex 1. In 2015, no lateral deviations were reported in Canaries[4], SAL, Dakar and Recife. Nevertheless, one LHD reported in Dakar and another in Recife have been also considered as lateral deviations, as information in flight plans in the two adjacent FIR/UIRs was different from the information registered in the LHD and no additional information has been obtained. Information about these considered deviations is shown in Table 7.

FIR/UIR	Date	Route in flight plan	Entry point	Deviation
Dakar	090915	UN873	BIKOM	430 NM
Recife	030915	UN873	ERETU	90 NM

Table 7.
Lateral deviations reported in 2015.

Therefore, the same assumptions made in [Ref. 2] and [Ref. 6] can be considered, i.e., one aircraft experiencing a lateral navigation anomaly has been observed in each FIR/UIR, and the value of α can be obtained using next equation:

$$\alpha = 1 - 0.05^{1/n}$$

Equation 19.

where n is the annual number of flights. As only this number is available for Canaries, extrapolations have been performed to estimate the annual flights for the other UIR/FIRs, using the number of flights of July. Table 8 shows the number of aircraft in July in each FIR and the number of aircraft estimated using the correspondence with the Canaries FIR. Data in cursive indicates if the value is estimated.

Considered period	Canaries	SAL1	SAL2	Dakar1	Dakar2	Recife
July 2015	2145	1471	1490	1624	1646	1791
Jan-Dic 2015	23254	*15947*	*16153*	*17606*	*17844*	*19416*

Table 8.
Number of aircraft considered for the α calculation.

Using Equation 19 and taking the number of aircraft indicated in Table 8, different values of α have been calculated for each FIR. Table 9 summarizes the assumptions and the obtained results.

FIR	α
Canaries	$1.2882*10^{-4}$
SAL1	$1.8784*10^{-4}$

[4] *In fact, one lateral deviation was reported, but in that deviation the ATC Clearance was obtained, so it must not be considered.*

FIR	α
SAL2	$1.8544*10^{-4}$
Dakar1	$1.7014*10^{-4}$
Dakar2	$1.6787*10^{-4}$
Recife	$1.5428*10^{-4}$

Table 9.
α for each FIR.

Once the parameters a_1, a_2 and α are defined, the probability density function of the lateral navigation errors is completely modelled.

Using Equation 11, the lateral overlap probability obtained for the different lateral separations between routes existing in the Corridor are the following ones:

RNP10 S_{ymin}=50NM	$P_y(50)$	$P_y(90)$	$P_y(110)$	$P_y(140)$
Canaries	$7.435*10^{-8}$	$2.399*10^{-8}$	$1.608*10^{-8}$	$0.883*10^{-8}$
SAL1	$11.439*10^{-8}$	$4.049*10^{-8}$	$2.714*10^{-8}$	$1.489*10^{-8}$
SAL2	$11.148*10^{-8}$	$3.936*10^{-8}$	$2.638*10^{-8}$	$1.448*10^{-8}$
Dakar1	$10.303*10^{-8}$	$3.569*10^{-8}$	$2.392*10^{-8}$	$1.313*10^{-8}$
Dakar2	$11.022*10^{-8}$	$3.891*10^{-8}$	$2.608*10^{-8}$	$1.432*10^{-8}$
Recife	$9.643*10^{-8}$	$3.263*10^{-8}$	$2.187*10^{-8}$	$1.200*10^{-8}$

Table 10.
Lateral overlap probability for different separations between routes with RNP10.

The probability increases when the spacing between the routes decreases, as it was expected.

3.9. Lateral occupancy

In Equation 1 there are two occupancy terms, one for same direction occupancy and another one for opposite direction occupancy.

Same direction occupancy is defined as the average number of aircraft that are, in relation to the typical aircraft:

- flying in the same direction as it;
- nominally flying on tracks one lateral separation standard away;
- nominally at the same flight level as it; and
- within a longitudinal segment centred on it.

The above definition has been expanded to include tracks that are separated by more than one lateral separation standard because there is a significant collision risk arising from the probability of overlap between non adjacent tracks.

The length of the longitudinal segment, $2*S_x$, is usually considered to be the length equivalent to 20 minutes of flight at 480 kts. It has been verified that the relationship between S_x and the occupancy is quite linear.

A similar set of criteria can be used to define opposite direction occupancy, just replacing "flying in the same direction as it" by "flying in the opposite direction".

Occupancy, in general, relates to the longitudinal overlap probability and can be obtained from:

$$E_y = \frac{2T_y}{H}$$

Equation 20.

Where:

- T_y represents the total proximity time generated in the system.
- H represents the total number of flight hours generated in the system during the considered period of time.

In Equation 20, the factor 2 allows the conversion of number of collisions into number of accidents.

Two methods can be used to calculate occupancies: "steady state flow model" and "direct estimation from time at waypoint passing". In this study the used method has been the second one.

This method calculates the number of proximate pairs comparing the time at which aircraft on one route pass a waypoint with the time at which aircraft on a parallel route pass the homologous waypoint. When the difference between passing times is less than certain value, 10 minutes in this case, it is considered that there is a proximate pair in that pair of routes.

Then, occupancy can be calculated using the following expression:

$$E_y = \frac{2n_y}{n}$$

Equation 21.

Where n_y is the number of proximate pairs and n is the total number of aircraft.

A more detailed explanation of each method can be found in Annex 2.

As lateral overlap probability depends on lateral spacing between routes and, as it has been said in section 2, routes in the EUR/SAM Corridor are not equally spaced, the terms $P_y(S_y)E_{ysame}$ and $P_y(S_y)E_{yopposite}$ in Equation 1 must be split into several terms.

It can be seen in Table 10 that $P_y(90)$ is about 35% of $P_y(50)$, $P_y(110)$ is about 23% of $P_y(50)$ and $P_y(140)$ is about 13% of $P_y(50)$. So, their contributions to the lateral collision risk cannot be ignored and Equation 1, should be written as follows:

$$N_{ay} = \{P_y(50) \cdot E_{y_{same}} + P_y(90) \cdot E^{*}_{y_{same}} + P_y(140) \cdot E^{**}_{y_{same}}\} \cdot P_z(0) \cdot \frac{\lambda_y}{S_x} \cdot \left\{\frac{|\overline{\Delta v}|}{2 \cdot \lambda_x} + \frac{|\overline{\dot{y}}|}{2 \cdot \lambda_y} + \frac{|\overline{\dot{z}}|}{2 \cdot \lambda_z}\right\} + \{P_y(90) \cdot E_{y_{opposite}} + P_y(110) \cdot E^{*}_{y_{opposite}} + P_y(140) \cdot E^{**}_{y_{oppposite}}\} \cdot P_z(0) \cdot \frac{\lambda_y}{S_x} \cdot \left\{\frac{2 \cdot |\bar{v}|}{2 \cdot \lambda_x} + \frac{|\overline{\dot{y}}|}{2 \cdot \lambda_y} + \frac{|\overline{\dot{z}}|}{2 \cdot \lambda_z}\right\}$$

Equation 22.

Where $E_{y_{same}}$ denotes same direction occupancy for routes UN-873/UN-857; $E^{*}_{y_{same}}$, same direction occupancy for routes UN-866/UN-873 and $E^{**}_{y_{same}}$, same direction occupancy for routes UN-866/UN-857; $E_{y_{opposite}}$, opposite direction occupancy for routes UN-866/UN-873; $E^{*}_{y_{opposite}}$, opposite direction occupancy for routes UN-741/UN-866 and $E^{**}_{y_{oppposite}}$, opposite direction occupancy for routes UN-866/UN-857.

Therefore, three same occupancy values and three opposite direction occupancy values must be computed.

3.9.1. Traffic growth hypothesis

This study presents the collision risk calculated from data corresponding from 1st July 2015 to 31st July 2015, but it also presents an estimate of the collision risk over a 10 years horizon.

To do that, it is necessary to know the traffic forecast for that period of time in the studied airspace. Taking into account the last data given by STATFOR-EUROCONTROL for the high-growth scenario, [Ref. 18], the annual traffic growth rate for the traffic flows in the Canary Islands airspace would be 5.2%.

3.9.2. Lateral occupancy obtained values

This section presents the same direction and opposite direction lateral occupancy values provided by the CRM programme for the current time and an estimate of the occupancy until 2025, with the annual traffic growth rate indicated before, 5.2%.

3.9.2.a. Canaries

Table 11 shows the number of aircraft and the number of same and opposite direction proximate pairs detected on the four routes, from 1st July 2015 till 31st July 2015 in the Canaries UIR.

Number of flights	July 2015
Number of flights on UN-741	233

Number of flights	July 2015
Number of flights on UN-866	451
Number of flights on UN-873	1187
Number of flights on UN-857	274
Total number of flights	2145
Number of same direction proximate pairs for tracks UN-866/UN-873	20
Number of same direction proximate pairs for tracks UN-866/UN-857	9
Number of same direction proximate pairs for tracks UN-873/UN-857	45
Number of opposite direction proximate pairs for tracks UN-741/UN-866	2
Number of opposite direction proximate pairs for tracks UN-866/UN-873	12
Number of opposite direction proximate pairs for tracks UN-866/UN-857	2

Table 11.
Lateral occupancy parameters in the Canaries UIR.

Assuming an annual traffic growth rate of 5.2%, the occupancies for the next 10 years are summarized in Table 12. It holds that occupancy is approximately proportional to traffic flow rate:

5.2% annual traffic growth		2015	2017	2019	2021	2023	2025
Same direction lateral occupancy	UN-873/UN-857 (E_{ysame})	0.0419	0.0464	0.0514	0.0569	0.0629	0.0697
	UN-866/UN-873 (E^{*}_{ysame})	0.0186	0.0206	0.0228	0.0253	0.0280	0.0310
	UN-866/UN-857 (E^{**}_{ysame})	0.0084	0.0093	0.0103	0.0114	0.0126	0.0139
Opposite direction lateral occupancy	UN-866/UN-873 ($E_{yopposite}$)	0.0112	0.0124	0.0137	0.0152	0.0168	0.0186
	UN-741/UN-866 ($E^{*}_{yopposite}$)	0.0019	0.0021	0.0023	0.0025	0.0028	0.0031
	UN-866/UN-857 ($E^{**}_{yopposite}$)	0.0019	0.0021	0.0023	0.0025	0.0028	0.0031

Table 12.
Lateral occupancy estimate for the Canaries until 2025 with an annual traffic growth rate of 5.2%.

3.9.2.b. SAL1

Table 13 shows the number of aircraft and the number of same and opposite direction proximate pairs detected on the four routes, from 1st July 2015 till 31st July 2015 in SAL1.

Number of flights	July 2015
Number of flights on UN-741	218
Number of flights on UN-866	407
Number of flights on UN-873	669
Number of flights on UN-857	177
Total number of flights	1471
Number of same direction proximate pairs for tracks UN-866/UN-873	23
Number of same direction proximate pairs for tracks UN-866/UN-857	5
Number of same direction proximate pairs for tracks UN-873/UN-857	18
Number of opposite direction proximate pairs for tracks UN-741/UN-866	4
Number of opposite direction proximate pairs for tracks UN-866/UN-873	2
Number of opposite direction proximate pairs for tracks UN-866/UN-857	0

Table 13.
Lateral occupancy parameters in SAL1.

Assuming an annual traffic growth rate of 5.2%, the occupancies for the next 10 years are summarized in Table 14. It holds that occupancy is approximately proportional to traffic flow rate:

5.2% annual traffic growth		2015	2017	2019	2021	2023	2025
Same direction lateral occupancy	UN-873/UN-857 (E_{ysame})	0.0245	0.0271	0.0299	0.0332	0.0367	0.0406
	UN-866/UN-873 (E^{*}_{ysame})	0.0313	0.0346	0.0383	0.0424	0.0469	0.0519
	UN-866/UN-857 (E^{**}_{ysame})	0.0068	0.0075	0.0083	0.0092	0.0102	0.0113
Opposite direction lateral occupancy	UN-866/UN-873 ($E_{yopposite}$)	0.0027	0.0030	0.0033	0.0037	0.0041	0.0045
	UN-741/UN-866 ($E^{*}_{yopposite}$)	0.0054	0.0060	0.0067	0.0074	0.0082	0.0090
	UN-866/UN-857 ($E^{**}_{yopposite}$)	0.0000	0.0000	0.0000	0.0000	0.0000	0.0000

Table 14.
Lateral occupancy estimate for SAL1 until 2025 with an annual traffic growth rate of 5.2%.

3.9.2.c. SAL2

Table 15 shows the number of aircraft and the number of same and opposite direction proximate pairs detected on the four routes, from 1st July 2015 till 31st July 2015 in SAL2.

Number of flights	July 2015
Number of flights on UN-741	200
Number of flights on UN-866	410
Number of flights on UN-873	703
Number of flights on UN-857	177
Total number of flights	1490
Number of same direction proximate pairs for tracks UN-866/UN-873	17
Number of same direction proximate pairs for tracks UN-866/UN-857	1
Number of same direction proximate pairs for tracks UN-873/UN-857	34
Number of opposite direction proximate pairs for tracks UN-741/UN-866	0
Number of opposite direction proximate pairs for tracks UN-866/UN-873	2
Number of opposite direction proximate pairs for tracks UN-866/UN-857	1

Table 15.
Lateral occupancy parameters in SAL2.

Assuming an annual traffic growth rate of 5.2%, the occupancies for the next 10 years are summarized in Table 16. It holds that occupancy is approximately proportional to traffic flow rate:

5.2% annual traffic growth		2015	2017	2019	2021	2023	2025
Same direction lateral occupancy	UN-873/UN-857 (E_{ysame})	0.0458	0.0506	0.0560	0.0620	0.0686	0.0760
	UN-866/UN-873 (E^{*}_{ysame})	0.0229	0.0253	0.0280	0.0310	0.0343	0.0380
	UN-866/UN-857 (E^{**}_{ysame})	0.0013	0.0015	0.0016	0.0018	0.0020	0.0022
Opposite direction lateral occupancy	UN-866/UN-873 ($E_{yopposite}$)	0.0027	0.0030	0.0033	0.0036	0.0040	0.0045
	UN-741/UN-866 ($E^{*}_{yopposite}$)	0.0000	0.0000	0.0000	0.0000	0.0000	0.0000
	UN-866/UN-857 ($E^{**}_{yopposite}$)	0.0013	0.0015	0.0016	0.0018	0.0020	0.0022

Table 16.
Lateral occupancy estimate for SAL2 until 2025 with an annual traffic growth rate of 5.2%.

3.9.2.d. Dakar1

Table 17 shows the number of aircraft and the number of same and opposite direction proximate pairs detected on the four routes, from 1st July 2015 till 31st July 2015 in Dakar1.

Number of flights	July 2015
Number of flights on UN-741	273
Number of flights on UN-866	429
Number of flights on UN-873	750
Number of flights on UN-857	172
Total number of flights	1624
Number of same direction proximate pairs for tracks UN-866/UN-873	29
Number of same direction proximate pairs for tracks UN-866/UN-857	2
Number of same direction proximate pairs for tracks UN-873/UN-857	36
Number of opposite direction proximate pairs for tracks UN-741/UN-866	7
Number of opposite direction proximate pairs for tracks UN-866/UN-873	2
Number of opposite direction proximate pairs for tracks UN-866/UN-857	1

Table 17.
Lateral occupancy parameters in Dakar1.

Assuming an annual traffic growth rate of 5.2%, the occupancies for the next 10 years are summarized in Table 18. It holds that occupancy is approximately proportional to traffic flow rate:

5.2% annual traffic growth		2015	2017	2019	2021	2023	2025
Same direction lateral occupancy	UN-873/UN-857 (E_{ysame})	0.0443	0.0490	0.0543	0.0601	0.0665	0.0736
	UN-866/UN-873 (E^{*}_{ysame})	0.0357	0.0395	0.0437	0.0484	0.0536	0.0593
	UN-866/UN-857 (E^{**}_{ysame})	0.0025	0.0027	0.0030	0.0033	0.0037	0.0041
Opposite direction lateral occupancy	UN-866/UN-873 ($E_{yopposite}$)	0.0025	0.0027	0.0030	0.0033	0.0037	0.0041
	UN-741/UN-866 ($E^{*}_{yopposite}$)	0.0862	0.0095	0.0106	0.0117	0.0129	0.0143
	UN-866/UN-857 ($E^{**}_{yopposite}$)	0.0012	0.0014	0.0015	0.0017	0.0018	0.0020

Table 18.
Lateral occupancy estimate for Dakar1 until 2025 with an annual traffic growth rate of 5.2%.

3.9.2.e. Dakar2

Table 19 shows the number of aircraft and the number of same and opposite direction proximate pairs detected on the four routes, from 1st July 2015 till 31st July 2015 in Dakar2.

Number of flights	July 2015
Number of flights on UN-741	275
Number of flights on UN-866	435
Number of flights on UN-873	763
Number of flights on UN-857	173
Total number of flights	1646
Number of same direction proximate pairs for tracks UN-866/UN-873	27
Number of same direction proximate pairs for tracks UN-866/UN-857	2
Number of same direction proximate pairs for tracks UN-873/UN-857	38
Number of opposite direction proximate pairs for tracks UN-741/UN-866	0
Number of opposite direction proximate pairs for tracks UN-866/UN-873	1
Number of opposite direction proximate pairs for tracks UN-866/UN-857	1

Table 19.
Lateral occupancy parameters in Dakar2.

Assuming an annual traffic growth rate of 5.2%, the occupancies for the next 10 years are summarized in Table 20. It holds that occupancy is approximately proportional to traffic flow rate:

5.2% annual traffic growth		2015	2017	2019	2021	2023	2025
Same direction lateral occupancy	UN-873/UN-857 (E_{ysame})	0.0462	0.0511	0.0565	0.0626	0.0693	0.0767
	UN-866/UN-873 (E^{*}_{ysame})	0.0328	0.0363	0.0402	0.0445	0.0492	0.0545
	UN-866/UN-857 (E^{**}_{ysame})	0.0024	0.0027	0.0030	0.0033	0.0034	0.0040
Opposite direction lateral occupancy	UN-866/UN-873 ($E_{yopposite}$)	0.0012	0.0013	0.0015	0.0016	0.0018	0.0020
	UN-741/UN-866 ($E^{*}_{yopposite}$)	0.0000	0.0000	0.0000	0.0000	0.0000	0.0000
	UN-866/UN-857 ($E^{**}_{yopposite}$)	0.0012	0.0013	0.0015	0.0016	0.0018	0.0020

Table 20.
Lateral occupancy estimate for Dakar2 until 2025 with an annual traffic growth rate of 5.2%.

3.9.2.f. Recife

Table 21 shows the number of aircraft and the number of same and opposite direction proximate pairs detected on the four routes, from 1st July 2015 till 31st July 2015 in Recife.

Number of flights	July 2015
Number of flights on UN-741	442
Number of flights on UN-866	419
Number of flights on UN-873	749
Number of flights on UN-857	181
Total number of flights	1791
Number of same direction proximate pairs for tracks UN-866/UN-873	30
Number of same direction proximate pairs for tracks UN-866/UN-857	2
Number of same direction proximate pairs for tracks UN-873/UN-857	30
Number of opposite direction proximate pairs for tracks UN-741/UN-866	3
Number of opposite direction proximate pairs for tracks UN-866/UN-873	2
Number of opposite direction proximate pairs for tracks UN-866/UN-857	0

Table 21.
Lateral occupancy parameters in Recife.

Assuming an annual traffic growth rate of 5.2%, the occupancies for the next 10 years are summarized in Table 22. It holds that occupancy is approximately proportional to traffic flow rate:

5.2% annual traffic growth		2015	2017	2019	2021	2023	2025
Same direction lateral occupancy	UN-873/UN-857 (E_{ysame})	0.0335	0.0371	0.0410	0.0454	0.0502	0.0556
	UN-866/UN-873 (E^{*}_{ysame})	0.0335	0.0371	0.0410	0.0454	0.0502	0.0556
	UN-866/UN-857 (E^{**}_{ysame})	0.0022	0.0025	0.0027	0.0030	0.0033	0.0037
Opposite direction lateral occupancy	UN-866/UN-873 ($E_{yopposite}$)	0.0022	0.0025	0.0027	0.0030	0.0033	0.0037
	UN-741/UN-866 ($E^{*}_{yopposite}$)	0.0033	0.0037	0.0041	0.0045	0.0050	0.0056
	UN-866/UN-857 ($E^{**}_{yopposite}$)	0.0000	0.0000	0.0000	0.0000	0.0000	0.0000

Table 22.
Lateral occupancy estimate for Recife until 2025 with an annual traffic growth rate of 5.2%.

3.10. Lateral collision risk

Once all the parameters of Equation 22 are obtained, it is possible to calculate the lateral collision risk for the current scenario. This value must not exceed the maximum allowed, for which the system is considered to be safe. This threshold, denominated TLS (Target Level of Safety), has been set to $TLS = 5 \cdot 10^{-9}$. It means that $5 \cdot 10^{-9}$ accidents per flight hour are the maximum accepted.

3.10.1. Lateral collision risk obtained values

In the current system, with RNP10, two unidirectional routes and two bidirectional routes, the collision risk values obtained until 2025 in the different locations are the ones shown in the following sections.

3.10.1.a. Canaries

Lateral collision risk in Canaries location, assuming an annual traffic growth rate of 5.2%, is shown in Table 23 and Figure 25:

Lateral collision risk	5.2% annual traffic growth
2015	$1.4050*10^{-9}$
2016	$1.4781*10^{-9}$
2017	$1.5549*10^{-9}$
2018	$1.6358*10^{-9}$
2019	$1.7209*10^{-9}$
2020	$1.8103*10^{-9}$
2021	$1.9045*10^{-9}$
2022	$2.0035*10^{-9}$
2023	$2.1077*10^{-9}$
2024	$2.2173*10^{-9}$
2025	$2.3326*10^{-9}$

Table 23.
Lateral collision risk for the period 2015-2025 in the Canaries.

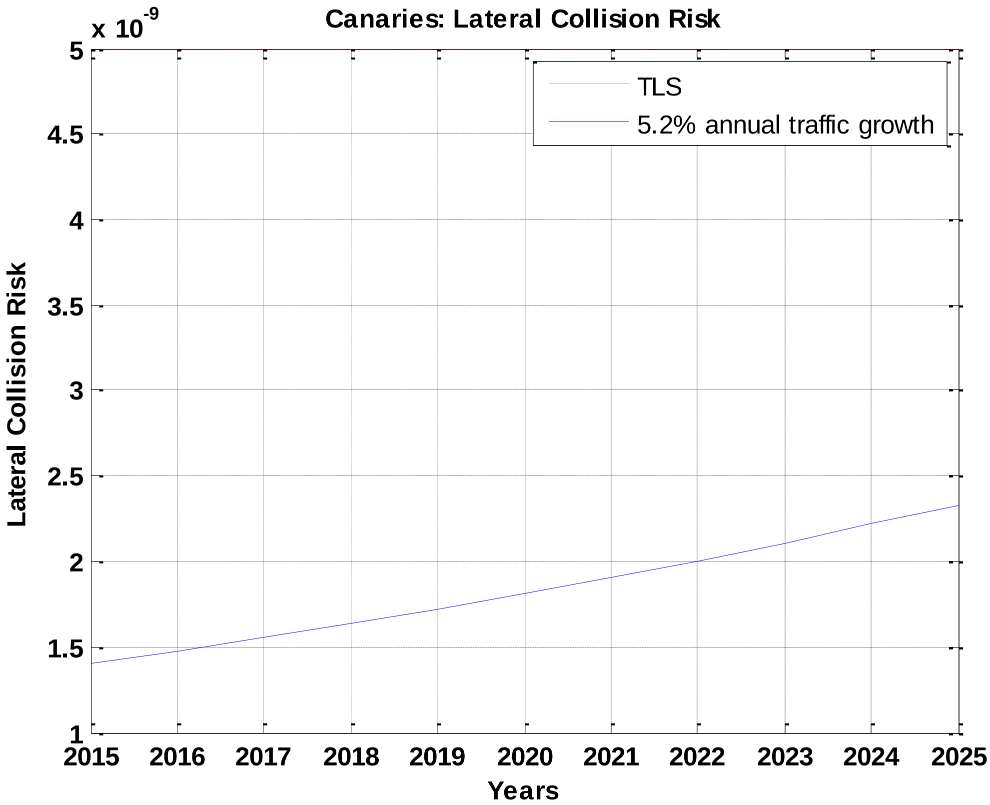

Figure 25.
Lateral collision risk for the period 2015-2025 in the Canaries.

3.10.1.b. SAL1

Lateral collision risk in SAL1 location, assuming an annual traffic growth rate of 5.2%, is shown in Table 24 and Figure 26:

Lateral collision risk	5.2% annual traffic growth
2015	$1.5538*10^{-9}$
2016	$1.6346*10^{-9}$
2017	$1.7196*10^{-9}$
2018	$1.8090*10^{-9}$
2019	$1.9031*10^{-9}$
2020	$2.0021*10^{-9}$
2021	$2.1062*10^{-9}$
2022	$2.2157*10^{-9}$
2023	$2.3309*10^{-9}$
2024	$2.4521*10^{-9}$
2025	$2.5796*10^{-9}$

Table 24.
Lateral collision risk for the period 2015-2025 in SAL1.

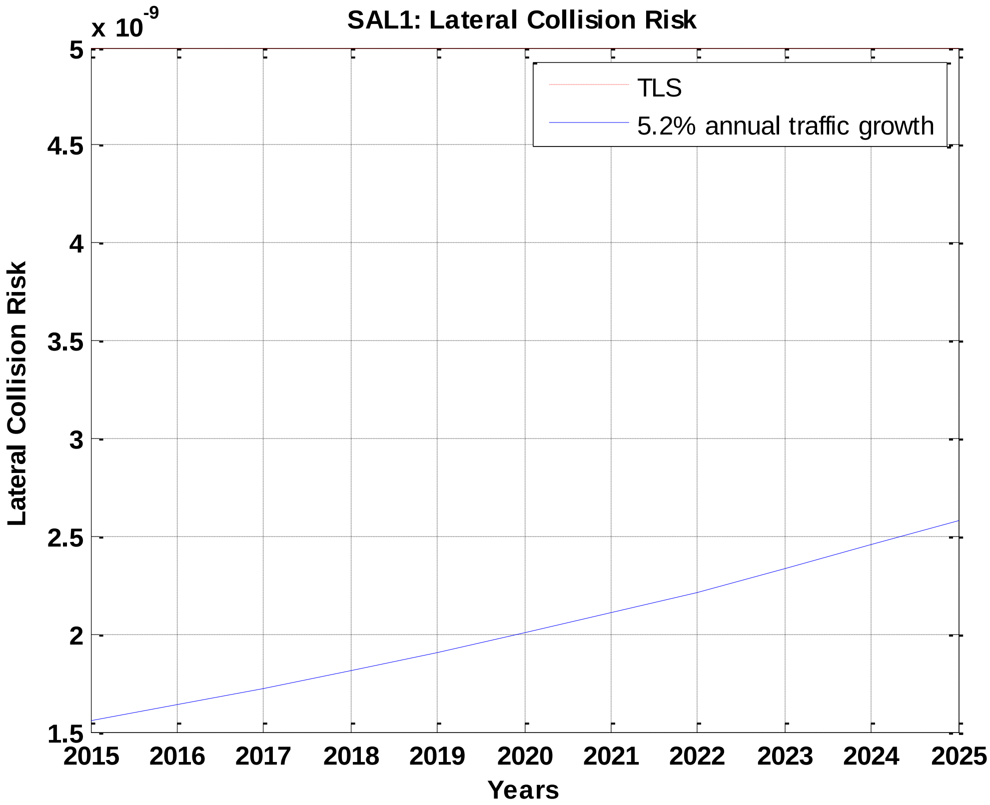

Figure 26.
Lateral collision risk for the period 2015-2025 in SAL1.

3.10.1.c. SAL2

Lateral collision risk in SAL2 location, assuming an annual traffic growth rate of 5.2%, is shown in Table 25 and Figure 27:

Lateral collision risk	5.2% annual traffic growth
2015	$1.4843*10^{-9}$
2016	$1.5615*10^{-9}$
2017	$1.6427*10^{-9}$
2018	$1.7281*10^{-9}$
2019	$1.8180*10^{-9}$
2020	$1.9125*10^{-9}$
2021	$2.0120*10^{-9}$
2022	$2.1166*10^{-9}$
2023	$2.2267*10^{-9}$
2024	$2.3424*10^{-9}$
2025	$2.4643*10^{-9}$

Table 25.
Lateral collision risk for the period 2015-2025 in SAL2.

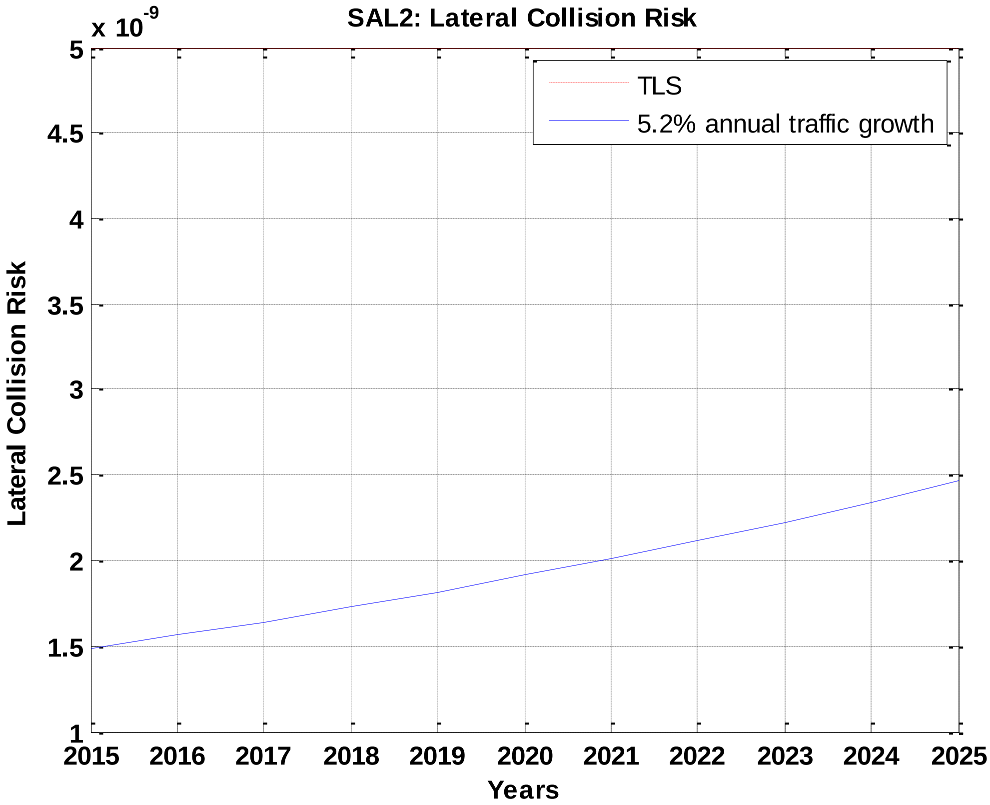

Figure 27.
Lateral collision risk for the period 2015-2025 in SAL2.

3.10.1.d. Dakar1

Lateral collision risk in Dakar1 location, assuming an annual traffic growth rate of 5.2%, is shown in Table 26 and Figure 28:

Lateral collision risk	5.2% annual traffic growth
2015	$2.0662*10^{-9}$
2016	$2.1736*10^{-9}$
2017	$2.2867*10^{-9}$
2018	$2.4056*10^{-9}$
2019	$2.5307*10^{-9}$
2020	$2.6623*10^{-9}$
2021	$2.8007*10^{-9}$
2022	$2.9463*10^{-9}$
2023	$3.0995*10^{-9}$
2024	$3.2607*10^{-9}$
2025	$3.4303*10^{-9}$

Table 26.
Lateral collision risk for the period 2015-2025 in Dakar1.

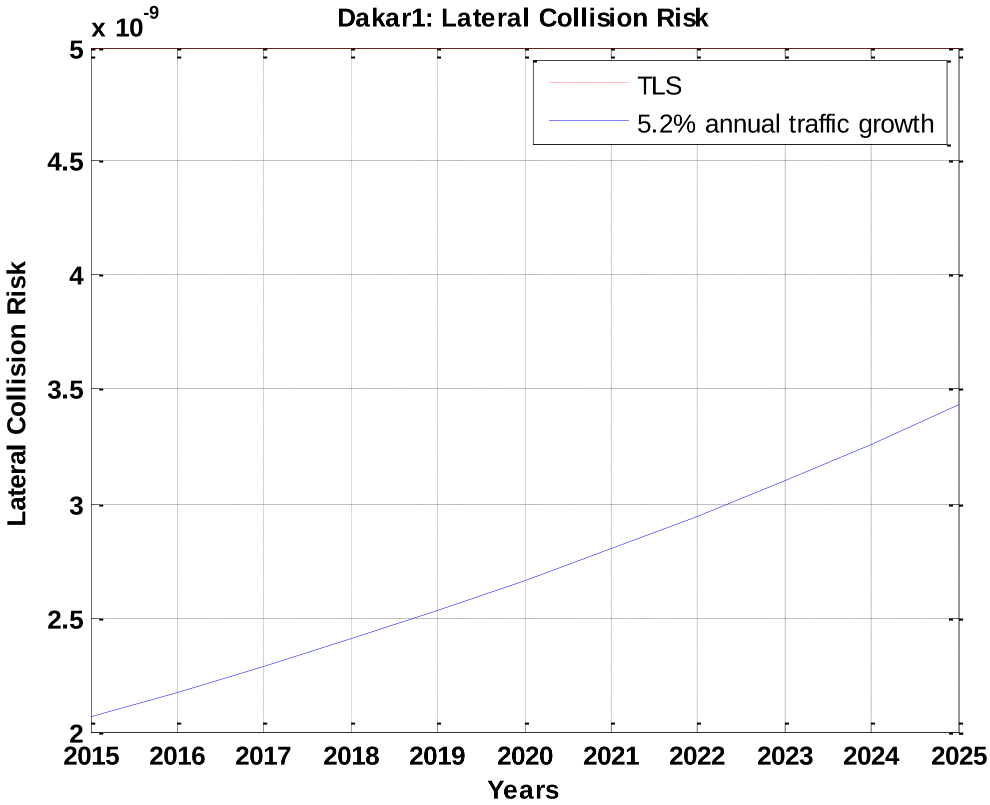

Figure 28.
Lateral collision risk for the period 2015-2025 in Dakar1.

3.10.1.e. Dakar2

Lateral collision risk in Dakar2 location, assuming an annual traffic growth rate of 5.2%, is shown in Table 27 and Figure 29:

Lateral collision risk	5.2% annual traffic growth
2015	$1.5371*10^{-9}$
2016	$1.6171*10^{-9}$
2017	$1.7012*10^{-9}$
2018	$1.7896*10^{-9}$
2019	$1.8829*10^{-9}$
2020	$1.9806*10^{-9}$
2021	$2.0836*10^{-9}$
2022	$2.1919*10^{-9}$
2023	$2.3059*10^{-9}$
2024	$2.4258*10^{-9}$
2025	$2.5520*10^{-9}$

Table 27.
Lateral collision risk for the period 2015-2025 in Dakar2.

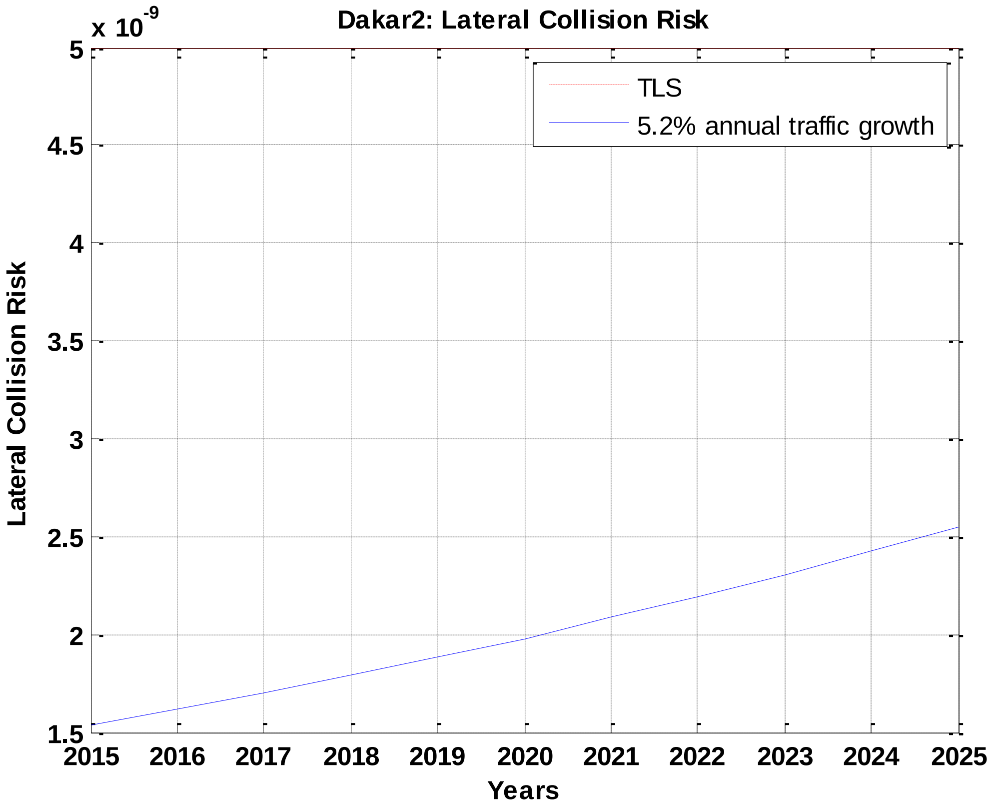

Figure 29.
Lateral collision risk for the period 2015-2025 in Dakar2.

3.10.1.f. Recife

Lateral collision risk in Recife location, assuming an annual traffic growth rate of 5.2%, is shown in Table 28 and Figure 30:

Lateral collision risk	5.2% annual traffic growth
2015	$1.2168*10^{-9}$
2016	$1.2800*10^{-9}$
2017	$1.3466*10^{-9}$
2018	$1.4166*10^{-9}$
2019	$1.4903*10^{-9}$
2020	$1.5678*10^{-9}$
2021	$1.6493*10^{-9}$
2022	$1.7351*10^{-9}$
2023	$1.8253*10^{-9}$
2024	$1.9202*10^{-9}$
2025	$2.0201*10^{-9}$

Table 28.
Lateral collision risk for the period 2015-2025 in Recife.

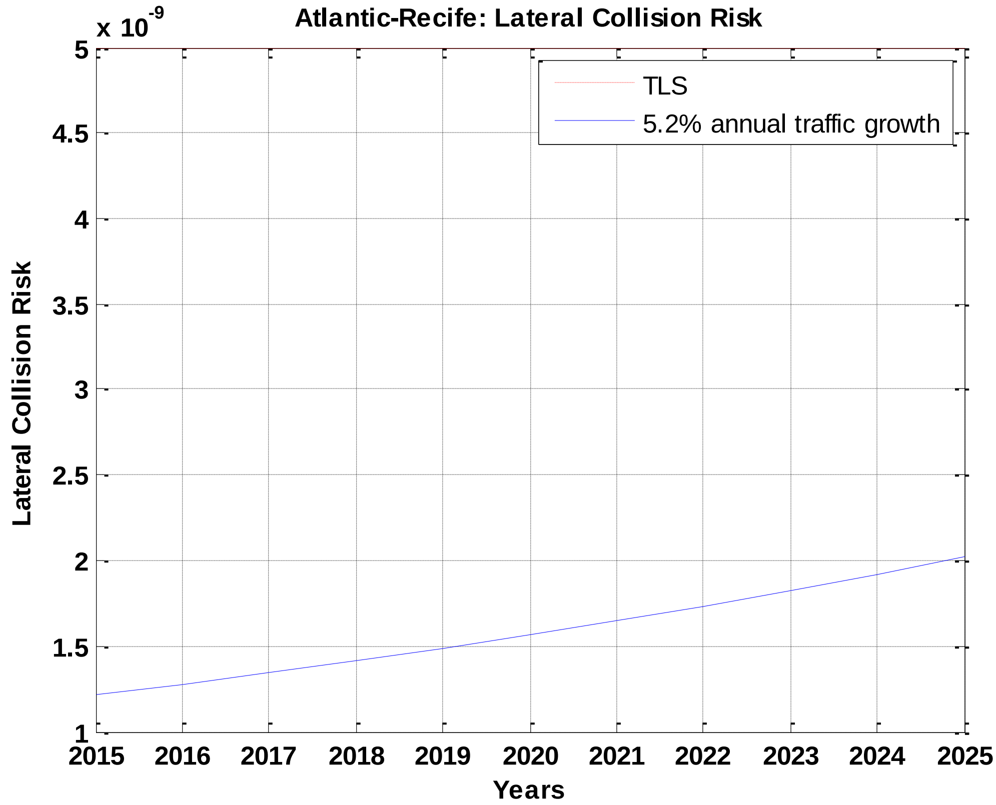

Figure 30.
Lateral collision risk for the period 2015-2025 in Recife.

3.10.2. Considerations on the results

3.10.2.a. Parallel routes

Lateral collision risk is below the $TLS = 5 \cdot 10^{-9}$ with the current traffic flow and it is estimated that, considering 5.2% as the annual traffic growth rate, the TLS would not be exceeded in the period under consideration.

The values obtained for the lateral collision risk are similar to those ones presented in the previous collision risk assessments, [Ref.5], [Ref.6] and [Ref.7]. It has also been confirmed that the results are similar in all the analysed locations.

3.10.2.b. DCT Area routes

Although traffic on the DCT area routes has not been considered, it is assumed that risk due to this routes will not dramatically change the results obtained. The reasoning for this assumption is based on the following points:

- Traffic on all these routes represents approximately 4% of the total traffic in Canaries
- However, most of this traffic is located beyond 150 NM from the UN-741 airway. If we only consider the proximate traffic, traffic in this routes would represent 1.5% of the traffic in the Corredor.
- The closer route to UN-741, ROSTA-XIGLU-NADIR, is southbound traffic, and it is also the most used among the nearby routes (0.77% of the traffic in the Corredor).

Taking this into account, it can be concluded:

- As traffic on the routes is separated longitudinally at the Canaries as if it was UN-741 traffic, there is a scarce probability of having proximate pairs between this route and route UN-741.
- The contribution to risk of DCT Area routes is considered to be small due to:
  - The reduced number of aircraft on DCT Area routes implies a low probability of having proximate pairs between these pairs of routes.
  - The large separation between routes: 110 NM and 90 NM minimum in the Canaries, which increases along the Corridor till GOBEG.

4. Vertical collision risk assessment

4.1. Introduction

Vertical collision risk, i.e. the risk due to the loss of vertical separation between aircraft on adjacent flight levels is generally made up of three traffic components, namely same direction traffic, opposite direction traffic and crossing traffic.

Vertical collision risk models for same and opposite direction traffic are similar to those ones for lateral collision risk presented before. They apply to aircraft in straight and level flight. This condition can be assumed to be satisfied within the EUR/SAM Corridor. Nevertheless, some operational causes of height deviations may lead to an aircraft climbing or descending through other flight levels, requiring a different type of modelling.

There are two requirements that must be achieved to consider the airspace vertically safe. They are the following ones:

- In accordance with ICAO Guidance Material, [Ref. 12], the risk of mid-air collision in the vertical dimension within RVSM airspace, due to technical height keeping performance, shall meet a Target Level of Safety of $2.5 \cdot 10^{-9}$ fatal accidents per flight hour.
- In accordance with ICAO Guidance Material, [Ref. 12], the management of the overall vertical collision risk within RVSM airspace shall meet a Target Level of Safety of $5.0 \cdot 10^{-9}$ fatal accidents per flight hour.

In the following sections, the technical vertical risk and the overall vertical risk are assessed.

4.2. Technical vertical collision risk assessment

Technical vertical risk represents the risk of a collision between aircraft on adjacent flight levels due to normal or typical height deviations of RVSM approved aircraft. It is attributable to the height-keeping errors that result from the combination of altimetry system errors (ASE) and autopilot performance in the vertical dimension.

4.2.1. Collision risk model

The Reich model used for lateral collision risk can also be applied to calculate vertical collision risk between aircraft on adjacent flight levels of the same track, flying in either the same or the opposite direction. In this case the model is expressed by this equation:

$$N_{az} = P_Z(S_Z) \cdot P_y(0) \cdot \frac{\lambda_x}{S_x} \cdot \left\{ E_{z_{same}} \cdot \left[\frac{|\Delta \bar{v}|}{2 \cdot \lambda_x} + \frac{|\overline{\dot{y}}|}{2 \cdot \lambda_y} + \frac{|\overline{\dot{z}}|}{2 \cdot \lambda_z} \right] + E_{z_{opposite}} \cdot \left[\frac{2 \cdot |\bar{v}|}{2 \cdot \lambda_x} + \frac{|\overline{\dot{y}}|}{2 \cdot \lambda_y} + \frac{|\overline{\dot{z}}|}{2 \cdot \lambda_z} \right] \right\}$$

Equation 23.

Where:

- N_{az} is the expected number of accidents (two per each aircraft collision) per flight hour due to the loss of vertical separation.

- S_Z is the minimum vertical separation.
- $P_Z(S_Z)$ is the probability of vertical overlap of aircraft nominally flying on adjacent flight levels of the same track.
- $P_y(0)$ is the probability of lateral overlap of aircraft nominally flying on the same track.
- $E_{z_{same}}$ is the same direction vertical occupancy, i.e. the average number of same direction aircraft flying on adjacent flight levels of the same track within segments of length $2S_x$ centred on the typical aircraft.
- $E_{z_{opposite}}$ is the opposite direction vertical occupancy, i.e. the average number of opposite direction aircraft flying on adjacent flight levels of the same track within segments of length $2S_x$ centred on the typical aircraft.
- S_x is the length of the longitudinal window used in the calculation of occupancies.
- λ_x is the average length of an aircraft.
- λ_y is the average width of an aircraft.
- λ_z is the average height of an aircraft.
- $|\Delta\bar{v}|$ is the average relative along-track speed of two aircraft flying on the same track in the same direction.
- $|\bar{v}|$ is the average ground speed of an aircraft.
- $|\overline{\dot{y}}|$ is the average lateral cross-track speed between aircraft flying on the same track.
- $|\overline{\dot{z}}|$ is the average relative vertical speed of aircraft flying on the same track.

As it can be seen in Equation 23, the elements of the collision risk model for same and opposite direction traffic are the probabilities of overlap and the average durations of overlaps in the different co-ordinate directions. In the model for same and opposite direction traffic, overlap of two aircraft is defined as overlap of rectangular boxes enveloping the aircraft. It is also assumed that during a situation of overlap, the sides of the boxes remain parallel.

Similar elements play a part in a model of vertical collision risk on crossing routes, but in a more complicated way. Due to the geometry of a crossing, the sides of the rectangular boxes enveloping the aircraft will not be parallel during a situation of horizontal overlap. As a result, a different estimation of the average duration of an overlap has to be done. This problem has been addressed by modelling the aircraft by cylinders and calculating the average duration of an overlap from the overlap of the circular cross sections of the cylinders. The diameter of the cylinders is taken as the largest dimension from both the length and the wingspan of the aircraft.

Another difference to take into account is that, for a pair of crossing routes, the probability of horizontal overlap cannot be factored into the probabilities of overlap in the longitudinal and lateral directions.

The vertical collision risk model for crossing routes on the basis of the cylindrical aircraft model can be expressed as:

$$N_{aZ}(cross) = P_Z(S_Z) \cdot P_h(\theta) \cdot E_z(\theta) \cdot \left\{ \frac{v_{rel}(\theta)}{\frac{\pi\lambda_h}{2}} + \frac{|\overline{\dot{z}}|}{2 \cdot \lambda_z} \right\}$$

Equation 24.

Where the relative velocity, $v_{rel}(\theta)$, is given by:

$$v_{rel}(\theta) = \sqrt{v_1^2 + v_2^2 - 2v_1 v_2 \cos(\theta)}$$

Equation 25.

The new parameters are:

- θ: the angle between two crossing routes, i.e. the angle between the aircraft headings.
- λ_h: the average diameter of a cylinder representing an aircraft. It is the largest of the average aircraft wingspan or fuselage length.
- S_h: horizontal separation among aircraft on crossing routes. It is used for the calculation of $E_z(\theta)$ values.
- $E_z(\theta)$: twice the probability of horizontal overlap of circles representing horizontal cross sections of aircraft on crossing routes.
- v_{rel}: the average relative horizontal speed between aircraft flying on crossing routes.
- $P_h(\theta)$: the probability of horizontal overlap for two aircraft at adjacent flight levels on routes crossing at angle θ.

When there are several pairs of crossing routes with different crossing angles θ_i, i=1,....,n, the model can be applied to each pair of routes and combined subsequently to give:

$$N_{aZ}(cross) = P_Z(S_Z) \cdot \sum_{1}^{n} P_h(\theta_i) \cdot E_z(\theta_i) \cdot \left\{ \frac{v_{rel}(\theta_i)}{\frac{\pi\lambda_h}{2}} + \frac{|\overline{\dot{z}}|}{2 \cdot \lambda_z} \right\}$$

Equation 26.

where n is the number of groups made from crossing routes with similar angles of intersection.

When the number of crossing angles is relatively large, Equation 26 can be approximated by the model of Equation 24 by taking conservative estimates of $E_z(\theta_i)$ and $v_{rel}(\theta_i)$ valid for each value of i, i=1,....,n.

The vertical collision risk model for crossing tracks can be combined with the model for same and opposite direction traffic to give the complete technical vertical collision risk model for the RVSM safety assessment for the EUR/SAM Corridor in the SAT, i.e.

$$N_{aZ} = P_Z(S_Z) \cdot P_y(0) \cdot \frac{\lambda_x}{S_x} \cdot \left\{ E_{z_{same}} \cdot \left[\frac{|\Delta \bar{v}|}{2 \cdot \lambda_x} + \frac{|\overline{\dot{y}}|}{2 \cdot \lambda_y} + \frac{|\overline{\dot{z}}|}{2 \cdot \lambda_z} \right] + E_{z_{opposite}} \cdot \left[\frac{2 \cdot |\bar{v}|}{2 \cdot \lambda_x} + \frac{|\overline{\dot{y}}|}{2 \cdot \lambda_y} + \frac{|\overline{\dot{z}}|}{2 \cdot \lambda_z} \right] \right\} + P_Z(S_Z) \cdot \sum_{1}^{n} P_h(\theta_i) \cdot E_z(\theta_i) \cdot \left\{ \frac{v_{rel}(\theta_i)}{\frac{\pi \lambda_h}{2}} + \frac{|\overline{\dot{z}}|}{2 \cdot \lambda_z} \right\}$$

Equation 27.

4.2.2. Average aircraft dimensions: λ_x, λ_y, λ_z, λ_h

Table 3 showed the average aircraft dimensions for the lateral collision risk model. Clearly, the same dimensions apply to the vertical model. In addition, the vertical model for crossing traffic needs the average diameter of a cylinder enveloping the aircraft. Table 29 shows the pertinent average aircraft dimensions.

Location	Value Length (λ_x)		Wingspan (λ_y)		Height (λ_z)		Diameter (λ_h)	
	Value (ft)	Value (NM)	Value (ft)	Value (NM)	Value (ft)	Value (NM)	Value (ft)	Value (NM)
Canaries	187.52	0.0309	170.38	0.0280	51.20	0.0084	187.52	0.0309
SAL1	214.71	0.0353	197.24	0.0325	56.58	0.0093	214.71	0.0353
SAL2	211.52	0.0348	194.18	0.0320	55.82	0.0092	211.52	0.0348
Dakar1	209.37	0.0345	191.90	0.0316	55.39	0.0091	209.37	0.0345
Dakar2	209.26	0.0344	191.97	0.0316	55.42	0.0091	209.26	0.0344
Recife	211.47	0.0348	193.50	0.0318	55.92	0.0092	211.47	0.0348

Table 29.
Average aircraft dimensions for the vertical collision risk model.

4.2.3. Probability of lateral overlap: $P_y(0)$

The probability of lateral overlap for aircraft nominally flying at adjacent flight levels of the same path is denoted by $P_y(0)$. It is defined by:

$$P_y(0) = \int_{-\lambda_y}^{\lambda_y} f^{y_{12}}(y) dy$$

Equation 28.

Where $f^{y_{12}}(y)$ denotes the probability density of the lateral distance y_{12} between two aircraft with lateral deviations y_1 and y_2, nominally at the same track, i.e.

$$y_{12} = y_1 - y_2$$

Equation 29.

And

$$f^{y_{12}} = \int_{-\infty}^{\infty} f^{y}(y_1) f^{y}(y_1 - y) dy_1$$

Equation 30.

Equation 30 assumes that the deviations of the two aircraft are independent and have the same probability density. λ_y denotes the average aircraft width.

Substitution of Equation 30 into Equation 28 gives:

$$P_y(0) = \int_{-\lambda_y}^{\lambda_y} \int_{-\infty}^{\infty} f^{y}(y_1) f^{y}(y_1 - y) dy_1 dy$$

Equation 31.

This last equation can be approximated by:

$$P_y(0) \approx 2\lambda_y \int_{-\infty}^{\infty} f^{y}(y_1) f^{y}(y_1) dy_1$$

Equation 32.

The probability density $f^{y}(y_1)$ was described in 3.8. Using that function in Equation 32, the resulting estimate based on $\lambda_y = 197.24\ ft$ is $P_y(0) = 0.0048$.

This factor has a significant effect on the risk estimate. Therefore, it should not be underestimated. $P_y(0)$ will increase as the lateral navigational performance of typical aircraft improves, causing a corresponding increase in the collision risk estimate. The RGCSP was aware of this problem and attempted to account for improvements in navigation systems when defining the RVSM global system performance specification. Based on the performance of highly accurate area navigation systems observed in European airspace, which demonstrated lateral path-keeping errors with a standard deviation of 0.3NM, the RGCSP adopted a value of 0.059 as the value of $P_y(0)$ for the global system performance.

Nevertheless, in some collision risk studies, [Ref. 19] and [Ref. 20], the followed approach was to assume that some aircraft would have a better lateral performance and considered that a proportion α, $0 \leq \alpha \leq 1$, of the airspace users would be using GNSS navigation, with standard deviation 0.06123NM. The most conservative assumption consists of assuming that the full aircraft population are using GNSS, α=1. Thus, taking the probability density as Gaussian[5], with 0 mean and 0.06123 NM standard deviation, the value obtained with Equation 32 for the lateral

[5] *As the calculation of $P_y(0)$ is dominated by the core of the densities, the choice of the type of the probability density is less critical than for the calculation of $P_y(S_y)$.*

overlap probability is: $P_y(0) = 0.2902$. This value will be considered in this study, although it may be overly conservative for the EUR/SAM Corridor.

4.2.4. Probability of horizontal overlap: $P_h(\theta)$

$P_h(\theta)$ denotes the horizontal overlap probability for crossing routes. The method used in [Ref. 15] for the CAR/SAM region to obtain $P_h(\theta)$ is literally described below:

Lets consider two aircraft, A and B, flying in crossing routes with angle θ, in adjacent levels i and i-1, vertically separated by S_z. The origin of the system of coordinates (x,y), in the horizontal plane, is the crossing point. The axle x coincides with the aircraft route A, that is in the origin (0,0), flying in the positive direction. The angle θ is measured since the axle x in the counter-clockwise direction. The aircraft B is in the position (U_x,U_y), flying to the origin. Consider U the variable that designates the horizontal distance between two aircraft, so that the distance U_h is inside the proximity area given by $S_h = \sqrt{S_x^2 + S_y^2}$. The geometry described can be seen in Figure 31.

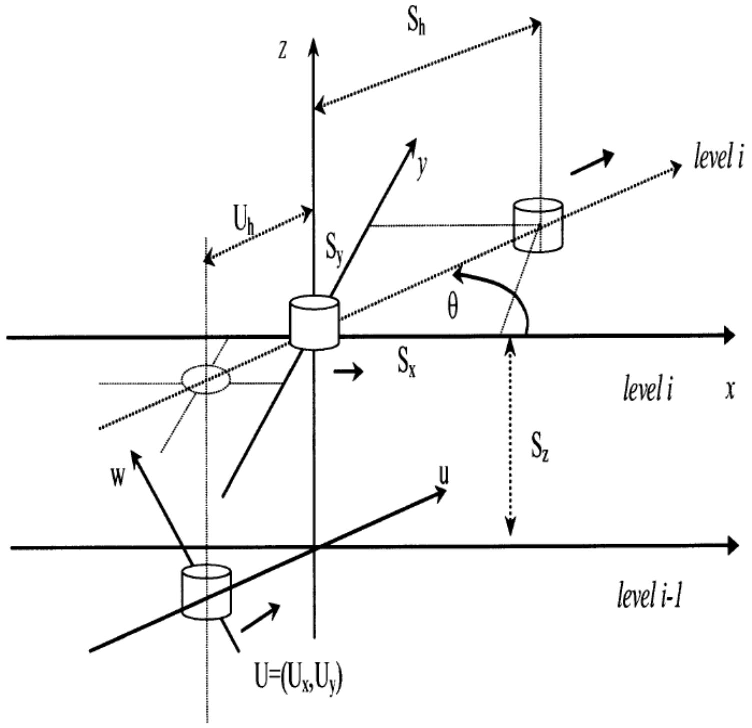

Figure 31.
Geometry of the crossing routes.

Considering that the variables that represent the longitudinal and lateral positions are independent and random, then, mathematically, $P_h(\theta)$ can be expressed by:

$$P_h(\theta) = \frac{h(U)\pi\lambda_h^2}{\int_{-Sh}^{Sh}\int_{-\sqrt{Sh^2-x^2}}^{\sqrt{Sh^2-x^2}} h(U)\,dxdy}$$

Equation 33.

Where h(U) is a density function of horizontal overlap, bi-dimensional, for the aircraft in adjacent flight levels in crossing routes with angle θ, separated by the horizontal distance (U_x,U_y). This last function is given, in its matrix form, by:

$$h(U) = \frac{1}{2\pi\sqrt{\det(M)}}\exp\left(-\frac{1}{2}U^T M^{-1} U\right)$$

Equation 34.

Where, det(M) is the determinant of the covariance matrix M of the two aircraft and U is the matrix position of the aircraft B, given by:

$$U = \begin{pmatrix} U_x \\ U_y \end{pmatrix}$$

Equation 35.

The function h(U) was acquired considering a conservative approach for the longitudinal distribution of the aircraft along-track route. For each aircraft, it was considered that the along-track and lateral deviations, corresponding to its nominal positions, are ruled by normal distributions. Then, for the normal distribution of the longitudinal position, it was assumed that its variance is equal to the variance of the uniform distribution with limits given by the horizontal separation S_h. For the normal distribution of the lateral deviations, the variance is worth σ^2_{rc}. Making the rotation of coordinates of the aircraft B in the system (u,w), to express its position in the system (x,y) of the aircraft A, the covariance matrix M is acquired, and it is given by:

$$M = \begin{pmatrix} (1+cos^2(\theta))\frac{S_h^2}{6} + \frac{\sigma_{rc}^2}{2}sen^2(\theta) & sen(\theta)\cos(\theta)\left(\frac{S_h^2}{6} - \frac{\sigma_{rc}^2}{2}\right) \\ sen(\theta)\cos(\theta)\left(\frac{S_h^2}{6} - \frac{\sigma_{rc}^2}{2}\right) & sen^2(\theta)\frac{S_h^2}{6} + \frac{\sigma_{rc}^2}{2}(1+cos^2(\theta)) \end{pmatrix}$$

Equation 36.

Considering that the normal distribution has its maximum value in the mean point, that in the geometry adopted is the crossing point, and that an aircraft in an adjacent flight level can cross a route intersection with any random distance, h(U) can be assessed only in the point (0,0), that is, for null horizontal separation. In this case, the conservative expression for the horizontal overlap probability is given by:

$$P_h(\theta) = \frac{h(0)\pi\lambda_h^2}{\int_{-Sh}^{Sh}\int_{-\sqrt{Sh^2-x^2}}^{\sqrt{Sh^2-x^2}} h(U)\,dxdy}$$

Equation 37.

This approach is used for any proximity among the aircraft pairs in the crossing routes.

The denominator in Equation 37 can only be obtained by numerical integration.

One interesting property of $P_h(\theta)$ is that $P_h(90º + \theta) = P_h(90º - \theta)$ and $P_h(\theta) = P_h(\theta + 180º)$ in $(U_x, U_y)=(0,0)$.

In [Ref. 16], probability of horizontal overlap for crossing angles between 0° and 90° with two different values of λ_h has been calculated. These results have been compared with the ones obtained by the CRM, being both similar. As an example, for $\lambda_h = 0.02140\ NM$, the value obtained in [Ref. 16] is $P_h(10º) = 1.325 \cdot 10^{-6}$, whilst the value obtained with the CRM is $P_h(10º) = 1.344 \cdot 10^{-6}$. The small differences may be due to numerical integration.

The results obtained by CRM are always slightly higher than those ones presented in [Ref. 16]. Therefore, they can be considered to be conservative.

4.2.4.a. Application to the EUR/SAM Airspace

As it was previously explained, in the EUR/SAM Corridor there is traffic crossing the Corridor in published routes in SAL, Dakar and Recife, but there is also some traffic crossing the Corridor in not-published routes or changing from one route to another. Those trajectories with more than 4 aircraft per month have been analysed.

Probability of horizontal overlap has been calculated for all these routes using Equation 37. The values of S_h and σ_{rc} considered are the same that are used in the CAR/SAM region, i.e., $S_h = 80\ NM$ and $\sigma_{rc} = 0.3\ NM$ (this last value is the one established in the Doc 9574, [Ref. 12])

The obtained results are shown in Table 30, Table 31, Table 32 and Table 33.

Horizontal overlap probability				
Location	**Diameter (λ_h)**	**Route**	**Angles (°)**	**$P_h(\theta)$**
Canaries	**0.0308 NM**	**NORED-ETIBA**	**102-78**	**$0.4812 \cdot 10^{-6}$**

Table 30.
Horizontal overlap probabilities for the Canaries.

Horizontal overlap probability				
Location	Diameter (λ_h)	Route	Angles (°)	$P_h(\theta)$
SAL1	0.0353 NM	UR-976/UA-602	95-85	0.6185*10^{-6}
		ULTEM-LUMPO	90-90	0.6159*10^{-6}
		BAMUX-SEPOM	105-75	0.6394*10^{-6}
		BAMUX-LUMPO	110-70	0.6586*10^{-6}
		BAMUX-ILGAS	97-83	0.6209*10^{-6}
		ULTEM-ILGAS	105-75	0.6394*10^{-6}
		ULTEM-SEPOM	96-84	0.6196*10^{-6}
		SP001-SEPOM	96-84	0.6196*10^{-6}
		IREDO-BL003	133-47	0.8579*10^{-6}
		BULVO-ORABI	156-24	1.5615*10^{-6}
		EDUMO-BI002	126-54	0.7720*10^{-6}
		BL002-CVS	144-36	1.0746*10^{-6}
		NEMDO-BI003	154-26	1.4477*10^{-6}
SAL2	0.0348 NM	KENOX-MOGSA	120-60	0.6972*10^{-6}
		SNT-BOTNO	142-38	0.9944*10^{-6}
		BAMUX-KENOX	163-17	2.1119*10^{-6}
		CARME-KENOX	149-31	1.1931*10^{-6}
		SVT-KENOX	151-29	1.2687*10^{-6}
		BULVO-ORABI	156-24	1.5152*10^{-6}
		MARIA-IREDO	108-72	0.6309*10^{-6}
		EXTER-CARME	108-72	0.6309*10^{-6}

Table 31.
Horizontal overlap probabilities for SAL.

Horizontal overlap probability				
Location	Diameter (λ_h)	Route	Angles (°)	$P_h(\theta)$
Dakar1	0.0345 NM	UL-435	97-83	0.5904*10^{-6}
		ENUGO-APIGU	96-84	0.5892*10^{-6}
		APOXA-GONSA	91-89	0.5858*10^{-6}
		SAGRO-LIRAX	96-84	0.5892*10^{-6}
		XUVIT-DIGUN	158-22	1.6132*10^{-6}
		TARIM-DIGUN	169-11	3.1713*10^{-6}
		SAGRO-BUXON	125-55	0.7245*10^{-6}
		SAGRO-MOSOK	137-43	0.8771*10^{-6}
		LIRAX-IRAVU	153-27	1.3287*10^{-6}
Dakar2	0.0344 NM	IP006-NANIK	152-28	1.2830*10^{-6}
		IP007-NANIK	160-20	1.7661*10^{-6}
		IP008-NANIK	169-11	3.1681*10^{-6}
		IP008-MOSAD	162-18	1.9557*10^{-6}
		IRAVU-MESAB	154-26	1.3752*10^{-6}

Table 32.
Horizontal overlap probabilities for Dakar.

Horizontal overlap probability				
Location	Diameter (λ_h)	Route	Angles (°)	$P_h(\theta)$
Recife	0.0348 NM	UL-695	96-84	0.6011*10^{-6}

Table 33.
Horizontal overlap probabilities for Recife.

4.2.5. Relative velocities

Equation 27 contains four relative speed parameters, $2|\bar{v}|$, $|\Delta\bar{v}|$, $|\overline{\dot{y}}|$ and $|\overline{\dot{z}}|$ for the same/opposite vertical risk and relative speeds for each one of the crossing pairs of routes, $v_{rel}(\theta_i)$.

The average along track speed $2|\bar{v}|$ is taken as in the lateral collision risk model.

Regarding $|\Delta\bar{v}|$, it has been calculated, as in the lateral case, from the differences between the speeds of all the pairs of aircraft that constitute a vertical proximate pair in the same direction.

Location	Vertical average relative longitudinal speeds			
	Southbound (kts)	Northbound (kts)	Average (kts)	Considered value
Canaries	20.5254	14.0149	17.2701	18
SAL1	36.9121	37.4274	37.1698	38
SAL2	51.7587	10.8737	31.3162	32
Dakar1	29.1671	40.0717	34.6194	35
Dakar2	65.6627	24.8496	45.2561	46
Recife	23.8830	24.7825	24.3327	25

Table 34.
Vertical average relative longitudinal speeds.

For the vertical collision risk model, $|\overline{\dot{y}}|$ is the mean of the modulus of the relative cross-track speed between aircraft on the same track. Consequently, there is no operational reason why this relative speed should have a particularly large value. As it was presented in the previous studies, [Ref. 3], [Ref. 5], [Ref. 6] and [Ref. 7], a conservative value, 20 kts, was used based on the assessment made by ARINC in [Ref. 2] and on the AFI Region Assessment, [Ref. 20]. This value has been taken here too.

The mean relative vertical speed of the vertical collision risk model applies to aircraft that have lost their assigned vertical separation minimum of S_z. The value $|\overline{\dot{z}}| = 1.5\ kts$ will be taken here as in the lateral collision risk assessment.

As far as relative speed in crossing routes is concerned, it is obtained by:

$$v_{rel}(\theta_i) = \sqrt{v_1^2 + v_2^2 - 2v_1v_2\cos(\theta_i)}$$

Equation 38.

where v_1 and v_2 are the average speeds in each one of the routes and θ, the intersection angle. The relative speeds used in this study are summarized in Table 35, Table 36, Table 37, Table 38, Table 39 and Table 40. (V_1 refers to the average speed on the corresponding parallel route and V_2, to the crossing route.

Location	Crossing route	V_1 (kts)	V_2 (kts)	θ (°)	$V_{rel}(\theta)$ (kts)
Canaries	NORED-ETIBA	471.67	473.52	78	594.83
				102	734.55

Table 35.
Relative speeds in crossings (Canaries).

Location	Crossing route	V_1 (kts)	V_2 (kts)	θ (°)	$V_{rel}(\theta)$ (kts)
SAL1	UR-976/UA-602	460.51	473.36	85	630.99
				95	688.57
	ULTEM-LUMPO	460.51	457.10	90	648.85
	BAMUX-LUMPO	460.51	480.12	70	539.76
				110	770.60
	BAMUX-SEPOM	460.51	489.84	75	579.01
				105	754.18
	BAMUX-ILGAS	460.51	468.75	83	615.78
				97	696.00
	ULTEM-ILGAS	460.51	475.16	75	569.72
				105	742.38
	ULTEM-SEPOM	460.51	498.34	84	642.21
				96	713.02
	SP001-SEPOM	466.08	498.34	84	645.77
				96	717.03
	IREDO-BL003	454.30	472.32	47	369.86
				133	849.80
	BULVO-ORABI	466.08	481.16	24	197.49
				156	926.55
	EDUMO-BI002	444.32	433.24	54	398.52
				126	781.93
	BL002-CVS	444.32	462.39	36	280.71
				144	862.35
	NEMDO-BI003	464.29	442.32	26	205.06
				154	883.38

Table 36.
Relative speeds in crossings (SAL1).

Location	Crossing route	V_1 (kts)	V_2 (kts)	θ (°)	$V_{rel}(\theta)$ (kts)
SAL2	KENOX-MOGSA	464.93	475.84	60	470.48
				120	814.75
	SNT-BOTNO	465.07	445.78	38	297.10
				142	861.25
	BAMUX-KENOX	447.93	486.00	17	143.09
				163	923.69
	CARME-KENOX	463.71	488.00	31	255.41
				149	917.13
	SVT-KENOX	447.93	458.41	29	227.16
				151	877.48
	BULVO-ORABI	466.01	481.17	24	197.49
				156	926.49
	MARIA-IREDO	463.71	480.24	72	555.00
				108	763.74
	EXTER-CARME	463.71	448.60	72	536.42
				108	738.18

Table 37.
Relative speeds in crossings (SAL2).

Location	Crossing route	V_1 (kts)	V_2 (kts)	θ (°)	$V_{rel}(\theta)$ (kts)
Dakar1	UL-435	462.54	479.10	83	624.07
				97	705.32
	ENUGO-APIGU	462.54	490.89	84	638.31
				96	708.79
	APOXA-GONSA	462.54	481.26	89	661.65
				91	673.29
	SAGRO-LIRAX	462.54	501.44	84	645.68
				96	716.85
	XUVIT-DIGUN	473.61	481.69	22	182.45
				158	937.75
	TARIM-DIGUN	473.61	465.37	11	90.37
				169	934.66
	SAGRO-BUXON	454.80	478.84	25	431.64
				155	828.23
	SAGRO-MOSOK	454.80	469.40	43	338.99
				137	859.90
	LIRAX-IRAVU	466.40	464.35	27	217.29
				153	905.04

Table 38.
Relative speeds in crossings (Dakar1).

Location	Crossing route	V_1 (kts)	V_2 (kts)	θ (°)	$V_{rel}(\theta)$ (kts)
Dakar2	IP006-NANIK	465.48	513.50	28	241.37
				152	949.97
	IP007-NANIK	465.48	486.62	20	166.64
				160	937.64
	IP008-NANIK	465.48	478.53	11	91.41
				169	939.66
	IP008-MOSAD	465.48	436.67	18	143.97
				162	891.06
	IRAVU-MESAB	463.19	464.35	26	208.65
				154	903.77

Table 39.
Relative speeds in crossings (Dakar2).

Location	Crossing route	V_1 (kts)	V_2 (kts)	θ (°)	$V_{rel}(\theta)$ (kts)
Recife	UL-695	459.57	469.74	84	621.87
				96	690.64

Table 40.
Relative speeds in crossings (Recife).

4.2.6. Vertical overlap probability: $P_z(S_z)$

The probability of vertical overlap of a pair of aircraft nominally flying at adjacent flight levels separated by S_z is denoted $P_z(S_z)$. It is defined by:

$$P_z(S_z) = \int_{-\lambda_z}^{\lambda_z} f^{z_{12}}(z)dz$$

Equation 39.

Where $f^{z_{12}}(z)$ denotes the probability density of the vertical distance z_{12} between the two aircraft. This distance may be defined as:

$$z_{12} = S_z + z_1 - z_2$$

Equation 40.

with z_1 and z_2 representing the height-keeping deviations of two aircraft. Height-keeping deviations of aircraft are usually defined in terms of Total Vertical Error (TVE), measured in geometric feet:

$$TVE = actual\ pressure\ altitude\ flown\ by\ aircraft - assigned\ altitude$$

Assuming that the height-keeping deviations of the two aircraft are independent and denoting their probability densities by $f_1^{TVE}(z_1)$ and $f_2^{TVE}(z_1)$, the probability density $f^{z_{12}}(z)$ and the probability of vertical overlap can be written as:

$$f^{z_{12}}(z) = \int_{-\infty}^{\infty} f_1^{TVE}(z_1) f_2^{TVE}(z_1)(S_z + z_1 - z_2) dz_1$$

Equation 41.

$$P_z(S_z) = \int_{-\lambda_z}^{\lambda_z} \int_{-\infty}^{\infty} f_1^{TVE}(z_1) f_2^{TVE}(z_1)(S_z + z_1 - z_2) dz_1\, dz$$

Equation 42.

This equation can be approximated by:

$$P_z(S_z) \approx 2\lambda_z \int_{-\infty}^{\infty} f_1^{TVE}(z_1) f_2^{TVE}(z_1)(S_z + z_1) dz_1$$

Equation 43.

The probability distribution of the height-keeping deviations, $f^{TVE}(z)$, depends on the height-keeping characteristics of the aircraft as specified by the MASPS. Data on the height-keeping performance of MASPS-approved aircraft can be obtained by means of aircraft height monitoring. Currently, height monitoring data are not available from the SAT. However, as the majority of the aircraft types in the EUR/SAM Corridor are also flying in the European RVSM height monitoring programme, these data can be used.

$f^{TVE}(z)$, can be obtained modelling separately the two components of TVE: Altimetry System Error (ASE) and Flight Technical Error (FTE):

$$TVE = ASE + FTE$$

Equation 44.

Where:

ASE=actual pressure altitude flown by aircraft – displayed altitude

FTE=displayed altitude – assigned altitude

Assuming that the two components are statistically independent:

$$f^{TVE}(z) = \int_{-\infty}^{\infty} f^{ASE}(a) f^{FTE}(z - a) da$$

Equation 45.

In practice, FTE is difficult to determine and it is approximated by Assigned Altitude Deviation (AAD):

AAD=transponded altitude – assigned altitude

Equation 44 can then be approximated by:

$$f^{TVE}(z) = \int_{-\infty}^{\infty} f^{ASE}(a) f^{AAD}(z-a)da$$

Equation 46.

The difference between FTE and AAD is referred to as correspondence error. It arises due to the rounding of the altimeter reading before transmission by the aircraft transponder. Data on AAD can be obtained by evaluating archived mode C data. Figure 32 shows a diagram of the components of the Total Vertical Error:

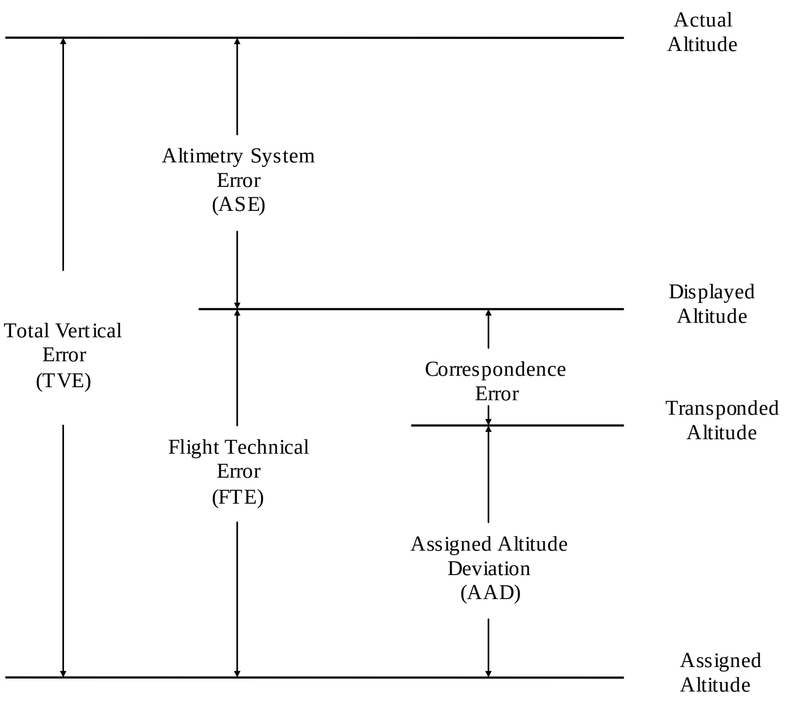

Figure 32.
Breakdown of height-keeping errors.

The modelling of the two component densities, ASE and AAD, is described below.

4.2.6.a. ASE distribution modelling

The overall ASE distribution is a combination of ASE distributions for each aircraft monitoring group, weighted by the proportion of flights made by the group, i.e.

$$f^{ASE}(a) = \sum_{i=1}^{n_{tg}} \beta_i f_i^{ASE}(a)$$

Equation 47.

where n_{tg} denotes the number of different aircraft type groups, β_i is the proportion of flight time contributed by aircraft type group i and $f_i^{ASE}(a)$ is the probability density of the ASE of aircraft type group i, i=1,.....,n_{tg}. Each monitoring group's ASE probability density, $f_i^{ASE}(a)$, is the result of both within and between airframe ASE variability of all the airframes making up the group.

The probability densities $f_i^{ASE}(a)$ are to be determined on the basis of height monitoring data of RVSM approved aircraft. As it was mentioned before, such monitoring data are not available from the SAT. However, as the normal height-keeping performance of RVSM approved aircraft is not dependent on the region of operation, HMU data collected in other ICAO Regions may be used for the modelling of a monitoring group's ASE probability density, $f_i^{ASE}(a)$.

As in previous risk assessments, the RVSM Tool, developed by Eurocontrol, has been used to model the monitoring group's ASE probability densities, $f_i^{ASE}(a)$, for the aircraft that fly in the EUR/SAM Corridor, to obtain the overall ASE distribution and to calculate the vertical overlap probability, $P_z(1000)$. Eurocontrol monitoring data from 2014 and 2015 have been used for this purpose.

4.2.6.b. AAD distribution modelling

AAD performance is subdivided into typical and atypical performance. For the assessment of technical vertical risk, only typical AAD will be taken into account for the AAD component of TVE. All data on atypical AAD will be included in the assessment of the vertical risk due to all causes.

In [Ref. 16] typical AAD performance is taken to be that which is not greater than 300 ft in magnitude and any AAD greater than that value is considered to be atypical.

AAD data on typical performance should be obtained from the height monitoring process, while AAD data on atypical performance should be obtained from incident reports.

The typical AAD distribution to be used in this study has been obtained using the Eurocontrol RVSM Tool with the aircraft monitoring groups of the EUR/SAM Corridor of the year 2015.

4.2.6.c. TVE distribution modelling

Substitution of the ASE and AAD densities of the foregoing two subsections into Equation 46 yields the TVE density $f^{TVE}(z)$. Then, with the 2015 traffic and height-keeping performances information, the probability of vertical overlap has been calculated by means of Equation 44, using the Eurocontrol RVSM Tool, being the resulting values $P_z(1000) = 2.0405 \cdot 10^{-9}$ and $P_z(0) = 0.3989$.

4.2.7. Vertical occupancy

Vertical occupancy can be defined for same and opposite direction traffic in the same way as lateral occupancy. Thus, "same direction, single separation minimum vertical occupancy" is the average number of aircraft, which are, in relation to the typical aircraft:

- flying in the same direction as it;
- nominally on the same track as it;
- nominally flying at flight levels one vertical separation minimum away from it; and
- within a longitudinal segment centred on it, whose length is $2S_x$.

A similar set of criteria can be used to define opposite direction vertical occupancy.

Therefore,

$$E_z = \frac{2T_z}{H}$$

Equation 48.

Where:

- T_z: The total same (opposite) direction proximity time generated in the system, i.e. the total time spent by same (opposite) direction aircraft pairs on the same flight paths at adjacent flight levels and within a longitudinal distance S_x of each other; and
- H: The total number of flying hours generated in the system during the period considered.

The same method used to estimate lateral occupancy, "direct estimation from time at waypoint passing", can also be used to estimate same and opposite direction vertical occupancy. In this case, the condition that the points utilized should be approximately on a plane at right angles to the track system is automatically satisfied for aircraft on the same track. Thus, occupancy can be obtained using the following equation:

$$E_z = \frac{2n_z}{n}$$

Equation 49.

where n_z is the total number of vertically proximate pairs and n is the total number of aircraft.

It was verified that the relationship between S_x and vertical occupancy was linear. The vertical collision risk has been calculated on the basis of $S_x = 80NM$.

For crossing routes, with intersection angle θ, a similar procedure can be used to obtain the vertical occupancy, $E(\theta)$. It is given by:

$$E_z(\theta) = \begin{cases} \frac{t_{sh}(\theta)}{t_F}\frac{2K(\theta)}{N}; for\ t_{sh} < t_F \\ \frac{2K(\theta)}{N}; \qquad for\ t_{sh} > t_F \end{cases}$$

Equation 50.

Where,

- N is the number of aircraft in the system during the observation period,
- $K(\theta_i)$ is the number of aircraft pairs in the crossing routes with angle θ_i,
- t_{sh} is the average proximity time of pairs of aircraft in the crossing routes with angle θ
- t_F is the average flight time in the crossing routes,

In this assessment, as it was done in the CAR/SAM study, the conservative expression $^{2K(\theta)}/_N$ will be used.

The "direct estimation from time at waypoint passing", can also be used in this case to estimate crossing occupancy. The way proximate events are obtained is explained in Annex 2.

4.2.7.a. Obtained vertical occupancy values

This section presents the vertical occupancy values provided by the CRM programme for the current time and an estimate of the occupancy until 2025, with the annual traffic growth rate previously indicated, 5.2%.

a. Canaries

Table 41 shows some results on same and opposite vertical occupancy in Canaries location, based on traffic levels representative of 2015.

Number of flights	July 2015
Number of flights on UN-741	233
Number of flights on UN-866	451
Number of flights on UN-873	1187
Number of flights on UN-857	274
Total number of flights	2145
Number of same direction vertical proximate pairs for tracks UN-741	25
Number of same direction vertical proximate pairs for tracks UN-866	34
Number of opposite direction vertical proximate pairs for tracks UN-873	86
Number of opposite direction vertical proximate pairs for tracks UN-857	4
Total number of same direction proximate events	59
Total number of opposite direction proximate events	90
Same direction vertical occupancy (S_x=80NM)	0.0550
Opposite direction vertical occupancy (S_x=80NM)	0.0839

Table 41.
Vertical occupancy due to same and opposite direction traffic in the Canaries location with current traffic levels.

Apart from the traffic on the main routes, in the Canaries airspace there are some not-published crossing trajectories, as it was explained before. The number of flights on these routes can be found in the following table:

Number of flights	July 2015
Number of flights on NORED-ETIBA	6
Number of flights on main routes (UN-741, UN-866, UN-873 and UN-857)	2145
Total number of flights	2151

Table 42.
Number of flights in the Canaries airspace.

All the flights on the crossing routes are already included in the number of flights on the main routes. Therefore, the total number of aircraft in this case is 2145.

To calculate crossing occupancies, it is necessary to obtain the number of proximate pairs, i.e., the number of pairs for which horizontal separation is less than S_h. The value selected for S_h is set to the value used in the CAR/SAM study, [Ref. 16], i.e. $S_h = 80NM$.

Proximate events can be obtained comparing differences of passing times at the crossing point. The time window to be used in each case depends on the speeds and intersection angle of the routes, as it is explained in Annex 2. The values obtained for the Canaries are shown in Table 43, where v_1 refers to the average speed on the corresponding parallel route, v_2 refers to the average speed on the crossing route, and θ_1 and θ_2 are the two possible crossing angles, depending on the headings.

Time windows for crossing routes					
Route	Point	v1 (kts)	v2 (kts)	θ (°)	t (min)
NORED-ETIBA	---	471.67	473.52	102°	17
				78°	13

Table 43.
Time windows for crossing occupancies in the Canaries.

With these time windows, the number of proximate pairs obtained can be seen in Table 44.

Number of proximate events due to crossing traffic				
Route	**Point**	**θ (°)**	**Flight levels**	**Number of events**
NORED-ETIBA	NORED	102°	Same	0
			Adjacent	0
		78°	Same	0
			Adjacent	0
	USOTI	102°	Same	0
			Adjacent	1
		78°	Same	0
			Adjacent	1
	ISOKA	102°	Same	0
			Adjacent	0
		78°	Same	0
			Adjacent	1
	ETIBA	102°	Same	0
			Adjacent	0
		78°	Same	0
			Adjacent	0

Table 44.
Number of proximate events due to crossing traffic in the Canaries.

Once vertical occupancy is calculated based on current traffic levels, it is possible to estimate the occupancy in the following years taking into account the annual traffic growth rate forecasted. Vertical occupancy values from 2015 to 2025 with an annual traffic growth rate of 5.2% are shown in Table 45.

5.2% annual traffic growth			2015	2017	2019	2021	2023	2025
Same direction vertical occupancy			0.0550	0.0609	0.0674	0.0746	0.0825	0.0913
Opposite direction vertical occupancy			0.0839	0.0929	0.1028	0.1137	0.1259	0.1393
Crossing occupancy	NORED-ETIBA	102°	0.0009	0.0010	0.0011	0.0013	0.0014	0.0015
		78°	0.0019	0.0021	0.0023	0.0025	0.0028	0.0031

Table 45.
Vertical occupancy estimate for the Canaries until 2025 with an annual traffic growth rate of 5.2%

b. SAL1

Table 46 collects some results on same and opposite vertical occupancy in SAL1, obtained with data from July 2015.

Number of flights	July 2015
Number of flights on UN-741	218
Number of flights on UN-866	407
Number of flights on UN-873	669
Number of flights on UN-857	177
Total number of flights	1471
Number of same direction vertical proximate pairs for tracks UN-741	26
Number of same direction vertical proximate pairs for tracks UN-866	34
Number of opposite direction vertical proximate pairs for tracks UN-873	18
Number of opposite direction vertical proximate pairs for tracks UN-857	0
Total number of same direction proximate events	60
Total number of opposite direction proximate events	18
Same direction vertical occupancy (S_x=80NM)	0.0816
Opposite direction vertical occupancy (S_x=80NM)	0.0244

Table 46.
Vertical occupancy due to same and opposite direction traffic in SAL1 location with current traffic levels.

Apart from the traffic on the main routes, in SAL1 there is also some traffic crossing the Corridor on routes UR-976/UA-602 and on not-published routes. The number of flights on these routes can be found in the following table:

Number of flights	July 2015
Number of flights on UR-976/UA-602	156
Number of flights on ULTEM-LUMPO	96
Number of flights on BAMUX-SEPOM	3
Number of flights on BAMUX-LUMPO	4
Number of flights on BAMUX-ILGAS	90
Number of flights on ULTEM-ILGAS	15
Number of flights on ULTEM-SEPOM	2
Number of flights on SP001-SEPOM	8
Number of flights on IREDO-BL003	9
Number of flights on EDUMO-BI002	8
Number of flights on BL002-CVS	18
Number of flights on NEMDO-BI003	19
Number of flights on BULVO-ORABI	4
Number of flights on main routes (UN-741, UN-866, UN-873 and UN-857)	1471
Total number of flights	1891

Table 47.
Number of flights in SAL1 airspace.

Apart from the crossing routes, all the other flights on the not-published routes are already included in the number of flights on the main routes except for 46 of them. Therefore, the total number of aircraft in this case is 1.891.

The time windows to obtain proximate pairs are, in this case, the ones shown in Table 48.

Time windows for crossing routes					
Route	**Point**	**v1 (kts)**	**v2 (kts)**	**θ (°)**	**t (min)**
UR-976/UA-602	---	460.51	473.36	95	16
				85	14
ULTEM-LUMPO	---	460.51	457.10	90	15
BAMUX-SEPOM	---	460.51	489.84	105	17
				75	13
BAMUX-LUMPO	---	460.51	480.12	110	18
				70	13
BAMUX-ILGAS	---	460.51	468.75	97	16
				83	14
ULTEM-ILGAS	---	460.51	475.16	105	17
				75	13
ULTEM-SEPOM	---	460.51	498.34	96	15
				84	14
SP001-SEPOM	**SP001**	466.08	498.34	96	15
				84	14
IREDO-BL003	**IREDO**	444.32	472.32	133	27
				47	12
	BL003	464.28	472.32	133	26
				47	12
EDUMO-BI002	**BI002**	444.32	433.24	126	25
				54	13
BL002-CVS[6]	**BL002**	444.32	462.39	144	35
				36	12
NEMDO-BI003	**BI003**	464.28	442.32	155	48
				25	11
BULVO-ORABI	**ORABI**	466.08	481.17	156	49
				24	11

Table 48.
Time windows for crossing occupancies in SAL1.

With these time windows, the number of proximate pairs obtained can be seen in Table 49, Table 50, Table 51 and Table 52.

[6] *This crossing is used in take-offs or landings from/to Amilcar Cabra Airport, so aircraft in CVS are below the RSVM flight levels and this point has not been evaluated.*

Number of proximate events due to crossing traffic				
Route	Point	θ (°)	Flight levels	Number of events
UR-976/UA-602	GAMBA	95	Same	2
			Adjacent	6
		85	Same	0
			Adjacent	0
	IREDO	95	Same	3
			Adjacent	6
		85	Same	2
			Adjacent	15
	CVS	95	Same	25
			Adjacent	1
		85	Same	0
			Adjacent	18
	GAMBA	95	Same	4
			Adjacent	0
		85	Same	0
			Adjacent	0
	ORABI	95	Same	1
			Adjacent	0
		85	Same	0
			Adjacent	3
ULTEM-LUMPO	IRENE	90	Same	0
			Adjacent	1
		90	Same	0
			Adjacent	0
	DORTA	90	Same	7
			Adjacent	3
		90	Same	2
			Adjacent	9
	FUMER	90	Same	11
			Adjacent	6
		90	Same	1
			Adjacent	7
	HALEX	90	Same	3
			Adjacent	3
		90	Same	0
			Adjacent	2

Table 49.
Number of proximate events due to crossing traffic in SAL1 (1).

Number of proximate events due to crossing traffic				
Route	**Point**	**θ (°)**	**Flight levels**	**Number of events**
BAMUX-LUMPO	**BL001**	110	Same	0
			Adjacent	0
		70	Same	0
			Adjacent	0
	BL002	110	Same	0
			Adjacent	0
		70	Same	0
			Adjacent	0
	BL003	110	Same	0
			Adjacent	0
		70	Same	0
			Adjacent	0
	BL004	110	Same	0
			Adjacent	0
		70	Same	0
			Adjacent	0
BAMUX-SEPOM	**BS001**	105	Same	0
			Adjacent	0
		75	Same	1
			Adjacent	0
	BS002	105	Same	0
			Adjacent	0
		75	Same	0
			Adjacent	0
	BS003	105	Same	0
			Adjacent	0
		75	Same	0
			Adjacent	0
	BS004	105	Same	0
			Adjacent	0
		75	Same	0
			Adjacent	1
IREDO-BL003	**IREDO**	133	Same	0
			Adjacent	2
		47	Same	0
			Adjacent	0
	BL003	133	Same	0
			Adjacent	2
		47	Same	0
			Adjacent	0

Table 50.
Number of proximate events due to crossing traffic in SAL1 (2).

Number of proximate events due to crossing traffic				
Route	**Point**	**θ (°)**	**Flight levels**	**Number of events**
ULTEM-SEPOM	IRENE	96	Same	0
			Adjacent	0
		84	Same	0
			Adjacent	0
	RL002	96	Same	0
			Adjacent	0
		84	Same	0
			Adjacent	0
	BL003	96	Same	0
			Adjacent	0
		84	Same	0
			Adjacent	0
	SP001	96	Same	0
			Adjacent	0
		84	Same	0
			Adjacent	0
BAMUX-ILGAS	BI001	97	Same	4
			Adjacent	4
		83	Same	0
			Adjacent	1
	BI002	97	Same	0
			Adjacent	2
		83	Same	3
			Adjacent	3
	BI003	97	Same	6
			Adjacent	3
		83	Same	2
			Adjacent	9
	BI004	97	Same	0
			Adjacent	1
		83	Same	0
			Adjacent	2
EDUMO-BI002	BI002	126	Same	2
			Adjacent	2
		54	Same	0
			Adjacent	0
BL002-CVS	BL002	144	Same	0
			Adjacent	0
		36	Same	0
			Adjacent	0
NEMDO-BI003	BI003	154	Same	0
			Adjacent	4
		26	Same	0
			Adjacent	1

Table 51.
Number of proximate events due to crossing traffic in SAL1 (3).

Number of proximate events due to crossing traffic				
Route	**Point**	**θ (°)**	**Flight levels**	**Number of events**
ULTEM-ILGAS	RL001	105	Same	1
			Adjacent	0
		75	Same	0
			Adjacent	0
	BL002	105	Same	0
			Adjacent	2
		75	Same	0
			Adjacent	0
	BS003	105	Same	0
			Adjacent	2
		75	Same	0
			Adjacent	0
	BI004	105	Same	0
			Adjacent	2
		75	Same	0
			Adjacent	0
SP001-SEPOM	SP001	96	Same	0
			Adjacent	0
		84	Same	0
			Adjacent	0
BULVO-ORABI	ORABI	156	Same	0
			Adjacent	0
		24	Same	0
			Adjacent	0

Table 52.
Number of proximate events due to crossing traffic in SAL1 (4).

It can be seen that a lot of proximate events at the same flight level, within less than 15 minutes of each other. Several reasons are possible for this, such as:

- A tactical flight level change to separate crossing traffic was not included in the provided data;
- There was an error in the time provided in the data;
- The air traffic controller did not register a flight level change;
- The aircraft made contact too late to allow an action by the air traffic controller;
- There was an operational error that was not registered by the air traffic controller and/or by the aircraft;
- Passing times at the crossing point are not precise, due to the need of extrapolation of the traffic data.

Given that such a great amount of proximate events is not possible and that no deviation reports have been received for those aircraft, it will be assumed that they are due to the extrapolation of data and the lack of data regarding flight level changes in the traffic data provided, and they will be considered as adjacent level proximate events. Nevertheless, this hypothesis should be verified when more information is available, because it may have an impact on the results in case that any of the proximate events were, in fact, at the same flight level.

Therefore, in this assessment, for the purpose of accounting for these events in the collision risk model, the "same flight level" crossing proximity events are counted as "adjacent flight level" proximity events. This approach was also followed by ARINC in [Ref. 2]. Nevertheless, if it could be shown that these events were in fact violations of the vertical separation standard, then these events should be treated as large height keeping deviations and be accounted for in the total vertical collision risk.

With these considerations, vertical occupancy values from 2015 to 2025 with an annual traffic growth rate of 5.2% are shown in Table 53.

5.2% annual traffic growth			2015	2017	2019	2021	2023	2025
Same direction vertical occupancy			0.0816	0.0903	0.0999	0.1106	0.1224	0.1354
Opposite direction vertical occupancy			0.0245	0.0271	0.0300	0.0332	0.0367	0.0406
Crossing occupancy	UR-976/UA-602	95°	0.0543	0.0601	0.0665	0.0736	0.0814	0.0901
		85°	0.0429	0.0475	0.0526	0.0582	0.0644	0.0713
	ULTEM-LUMPO	90°	0.0622	0.0688	0.0762	0.0843	0.0933	0.1032
	BAMUX-LUMPO	110°	0.0000	0.0000	0.0000	0.0000	0.0000	0.0000
		70°	0.0000	0.0000	0.0000	0.0000	0.0000	0.0000
	BAMUX-SEPOM	105°	0.0000	0.0000	0.0000	0.0000	0.0000	0.0000
		75°	0.0025	0.0027	0.0030	0.0034	0.0037	0.0041
	ULTEM-SEPOM	96°	0.0000	0.0000	0.0000	0.0000	0.0000	0.0000
		84°	0.0000	0.0000	0.0000	0.0000	0.0000	0.0000
	BAMUX-ILGAS	97°	0.0248	0.0274	0.0304	0.0336	0.0372	0.0411
		83°	0.0248	0.0274	0.0304	0.0336	0.0372	0.0411
	ULTEM-ILGAS	103°	0.0091	0.0100	0.0111	0.0123	0.0134	0.0150
		77°	0.0013	0.0014	0.0016	0.0017	0.0019	0.0021
	SP001-SEPOM	96°	0.0000	0.0000	0.0000	0.0000	0.0000	0.0000
		84°	0.0000	0.0000	0.0000	0.0000	0.0000	0.0000
	IREDO-BL003	133°	0.0045	0.0050	0.0055	0.0061	0.0068	0.0075
		47°	0.0000	0.0000	0.0000	0.0000	0.0000	0.0000
	EDUMO-BI002	126°	0.0024	0.0027	0.0030	0.0033	0.0037	0.0041
		54°	0.0024	0.0027	0.0030	0.0033	0.0037	0.0041
	BL002-CVS	144°	0.0000	0.0000	0.0000	0.0000	0.0000	0.0000
		36°	0.0000	0.0000	0.0000	0.0000	0.0000	0.0000
	NEMDO-BI003	154°	0.0049	0.0054	0.0060	0.0066	0.0073	0.0081
		26°	0.0012	0.0013	0.0015	0.0016	0.0018	0.0020
	BULVO-ORABI	156°	0.0000	0.0000	0.0000	0.0000	0.0000	0.0000
		24°	0.0000	0.0000	0.0000	0.0000	0.0000	0.0000

Table 53.
Vertical occupancy estimate for SAL1 until 2025 with an annual traffic growth rate of 5.2%.

c. SAL2

Table 54 collects some results on same and opposite vertical occupancy in SAL2, obtained with data from the July 2015.

Number of flights	July 2015
Number of flights on UN-741	200
Number of flights on UN-866	410
Number of flights on UN-873	703
Number of flights on UN-857	177
Total number of flights	1490
Number of same direction vertical proximate pairs for tracks UN-741	20
Number of same direction vertical proximate pairs for tracks UN-866	28
Number of opposite direction vertical proximate pairs for tracks UN-873	29
Number of opposite direction vertical proximate pairs for tracks UN-857	2
Total number of same direction proximate events	48
Total number of opposite direction proximate events	31
Same direction vertical occupancy (S_x=80NM)	0.0646
Opposite direction vertical occupancy (S_x=80NM)	0.0417

Table 54.
Vertical occupancy due to same and opposite direction traffic in SAL2 location with current traffic levels.

Apart from the traffic on the main routes, in SAL2 there is also some traffic crossing the Corridor on not-published routes. The number of flights on these routes can be found in the following table:

Number of flights	July 2015
Number of flights on KENOX-MOGSA	5
Number of flights on SNT-BOTNO	9
Number of flights on BAMUX-KENOX	24
Number of flights on CARME-KENOX	9
Number of flights on SVT-KENOX	4
Number of flights on BULVO-ORABI	4
Number of flights on MARIA-IREDO	50
Number of flights on EXTER-CARME	4
Number of flights on main routes (UN-741, UN-866, UN-873 and UN-857)	1490
Total number of flights	1590

Table 55.
Number of flights in SAL2 airspace.

Apart from the crossing route KENOX-MOGSA, all the other flights on the not-published routes are already included in the number of flights on the main routes except for 95 of them. Therefore, the total number of aircraft in this case is 1.590.

The time windows to obtain proximate pairs are, in this case, the ones shown in Table 56.

Time windows for crossing routes					
Route	**Point**	**v1 (kts)**	**v2 (kts)**	**θ (°)**	**t (min)**
KENOX-MOGSA	---	464.93	475.84	120°	21
				60°	12
SNT-BOTNO	**BOTNO**	465.07	445.78	142°	33
				38°	12
BAMUX-KENOX	**KENOX**	447.93	486.00	163°	70
				17°	11
CARME-KENOX	**CARME**	479.49	487.76	149°	38
				31°	11
	KENOX	447.93	488.26	148°	38
				32°	11
SVT-KENOX	**KENOX**	447.93	458.41	151°	43
				29°	11
BULVO-ORABI	**BULVO**	466.01	481.17	156°	49
				24°	11
MARIA-IREDO[7]	**MARIA**	447.93	480.24	108°	18
				72°	13
EXTER-CARME	**EXTER**	447.93	448.60	107°	18
				73°	14
	CARME	479.63	448.60	108°	18
				72°	13

Table 56.
Time windows for crossing occupancies in SAL2.

With these time windows, the number of proximate pairs obtained can be seen in Table 58 and Table 58.

[7] *This crossing has not been evaluated in IREDO because all the aircraft in this route join the UR-976/UA-602 airway.*

Number of proximate events due to crossing traffic				
Route	**Point**	**θ (°)**	**Flight levels**	**Number of events**
KENOX-MOGSA	KENOX	120°	Same	0
			Adjacent	0
		60°	Same	0
			Adjacent	0
	DENER	120°	Same	0
			Adjacent	0
		60°	Same	0
			Adjacent	0
	RODRI	120°	Same	0
			Adjacent	1
		60°	Same	0
			Adjacent	0
	INESS	120°	Same	0
			Adjacent	0
		60°	Same	0
			Adjacent	0
SNT-BOTNO	BOTNO	142°	Same	0
			Adjacent	1
		38°	Same	0
			Adjacent	0
BAMUX-KENOX	KENOX	163°	Same	0
			Adjacent	0
		17°	Same	0
			Adjacent	3
CARME-KENOX	CARME	149°	Same	0
			Adjacent	3
		31°	Same	0
			Adjacent	0
	KENOX	148°	Same	0
			Adjacent	0
		32°	Same	0
			Adjacent	0
SVT-KENOX	KENOX	151°	Same	0
			Adjacent	0
		29°	Same	0
			Adjacent	0
BULVO-ORABI	BULVO	156°	Same	0
			Adjacent	4
		24°	Same	0
			Adjacent	0
MARIA-IREDO	MARIA	108°	Same	0
			Adjacent	0
		72°	Same	0
			Adjacent	0

Table 57.
Number of proximate events due to crossing traffic in SAL2 (1).

Number of proximate events due to crossing traffic				
Route	**Point**	**θ (°)**	**Flight levels**	**Number of events**
EXTER-CARME	**EXTER**	107°	Same	0
			Adjacent	0
		73°	Same	0
			Adjacent	2
	CARME	108°	Same	0
			Adjacent	0
		72°	Same	0
			Adjacent	0

Table 58.
Number of proximate events due to crossing traffic in SAL2 (2).

Here again, as it happened in SAL1, there are at least 2 proximate events at the same flight level within 12 minutes of each other. The same reasons explained before are of application here.

No deviation reports have been received for these cases either, and therefore, the hypothesis of considering proximate events at the same flight level as proximate at adjacent flight levels will also be made for this location. Nevertheless, this hypothesis should be verified.

With these considerations, once vertical occupancy is calculated based on current traffic levels, it is possible to estimate the occupancy in the following years taking into account the annual traffic growth rate forecasted. Vertical occupancy values from 2015 to 2025 with an annual traffic growth rate of 5.2% are shown in Table 59.

5.2% annual traffic growth			2015	2017	2019	2021	2023	2025
Same direction vertical occupancy			0.0646	0.0715	0.0791	0.0876	0.0969	0.1073
Opposite direction vertical occupancy			0.0417	0.0462	0.0511	0.0566	0.0626	0.0693
Crossing occupancy	KENOX-MOGSA	120°	0.0013	0.0014	0.0015	0.0017	0.0019	0.0021
		60°	0.0000	0.0000	0.0000	0.0000	0.0000	0.0000
	SNT-BOTNO	142°	0.0013	0.0014	0.0015	0.0017	0.0019	0.0021
		38°	0.0000	0.0000	0.0000	0.0000	0.0000	0.0000
	BAMUX-KENOX	163°	0.0000	0.0000	0.0000	0.0000	0.0000	0.0000
		17°	0.0038	0.0042	0.0046	0.0051	0.0056	0.0063
	CARME-KENOX	149°	0.0038	0.0042	0.0045	0.0051	0.0057	0.0063
		31°	0.0000	0.0000	0.0000	0.0000	0.0000	0.0000
	SVT-KENOX	151°	0.0000	0.0000	0.0000	0.0000	0.0000	0.0000
		29°	0.0000	0.0000	0.0000	0.0000	0.0000	0.0000
	BULVO-ORABI	156°	0.0050	0.0056	0.0062	0.0068	0.0076	0.0084
		24°	0.0000	0.0000	0.0000	0.0000	0.0000	0.0000
	MARIA-IREDO	108°	0.0000	0.0000	0.0000	0.0000	0.0000	0.0000
		72°	0.0000	0.0000	0.0000	0.0000	0.0000	0.0000
	EXTER-CARME	107°	0.0000	0.0000	0.0000	0.0000	0.0000	0.0000
		73°	0.0025	0.0028	0.0031	0.0034	0.0038	0.0042

Table 59.
Vertical occupancy estimate for SAL2 until 2025 with an annual traffic growth rate of 5.2%

d. Dakar1

Table 60 collects some results on same and opposite vertical occupancy in Dakar1, obtained with data from July 2015.

Number of flights	July 2015
Number of flights on UN-741	273
Number of flights on UN-866	429
Number of flights on UN-873	750
Number of flights on UN-857	172
Total number of flights	1624
Number of same direction vertical proximate pairs for tracks UN-741	20
Number of same direction vertical proximate pairs for tracks UN-866	25
Number of opposite direction vertical proximate pairs for tracks UN-873	27
Number of opposite direction vertical proximate pairs for tracks UN-857	2
Total number of same direction proximate events	45
Total number of opposite direction proximate events	29
Same direction vertical occupancy (S_x=80NM)	0.0554
Opposite direction vertical occupancy (S_x=80NM)	0.0357

Table 60.
Vertical occupancy due to same and opposite direction traffic in Dakar1 location with current traffic levels.

Apart from the traffic on the main routes, in Dakar1 there is also some traffic crossing the Corridor on routes UL-435, other routes that cross the Corridor and on not-published routes. The number of flights on these routes can be found in the following table:

Number of flights	July 2015
Number of flights on UL-435	44
Number of flights on ENUGO-APIGU	4
Number of flights on APOXA-GONSA	1
Number of flights on SAGRO-LIRAX	1
Number of flights on XUVIT-DIGUN	8
Number of flights on TARIM-DIGUN	22
Number of flights on SAGRO-BUXON	7
Number of flights on SAGRO-MOSOK	17
Number of flights on LIRAX-IRAVU	15
Number of flights on main routes (UN-741, UN-866, UN-873 and UN-857)	1624
Total number of flights	1716

Table 61.
Number of flights in Dakar1 airspace.

Besides the four crossing routes (UL-435, ENUGO-APIGU, APOXA-GONSA and GARKO-LIRAX), the flights on the other not-published routes are already included in the number of flights on the main routes except for 42 of them. Therefore, the total number of aircraft in this case is 1716.

The time windows to obtain proximate pairs are, in this case, the ones shown in Table 62.

Time windows for crossing routes					
Route	**Point**	**v1 (kts)**	**v2 (kts)**	**θ (°)**	**t (min)**
UL-435	---	462.54	479.10	97	16
				83	14
ENUGO-APIGU	---	462.54	490.89	96	15
				84	14
APOXA-GONSA	---	462.54	481.26	91	15
				89	15
SAGRO-LIRAX	---	462.54	501.44	96	15
				84	14
XUVIT-DIGUN	**DIGUN**	473.61	481.69	158	53
				22	11
TARIM-DIGUN	**DIGUN**	473.61	465.37	169	107
				11	11
SAGRO-BUXON	**SAGRO**	473.61	478.84	125	22
				55	12
	BUXON	435.99	478.84	124	23
				56	12
SAGRO-MOSOK	**SAGRO**	473.61	469.40	137	28
				43	11
	MOSOK	435.99	469.40	137	29
				43	12
LIRAX-IRAVU	**LIRAX**	466.91	464.35	153	45
				27	11

Table 62.
Time windows for crossing occupancies in Dakar1.

With these time windows, the number of proximate pairs obtained can be seen in Table 63, Table 64 and Table 65.

Number of proximate events due to crossing traffic				
Route	**Point**	**θ (°)**	**Flight levels**	**Number of events**
UL-435	**DIGUN**	97	Same	1
			Adjacent	3
		83	Same	0
			Adjacent	1
	BUXON	97	Same	2
			Adjacent	2
		83	Same	2
			Adjacent	2
	ASEBA	97	Same	2
			Adjacent	0
		83	Same	0
			Adjacent	8
	MAROA	97	Same	0
			Adjacent	0
		83	Same	0
			Adjacent	4
ENUGO-APIGU	**ENUGO**	96	Same	0
			Adjacent	0
		84	Same	1
			Adjacent	1
	RIXAD	96	Same	0
			Adjacent	0
		84	Same	0
			Adjacent	0
	VOMER	96	Same	0
			Adjacent	0
		84	Same	0
			Adjacent	0
	APIGU	96	Same	0
			Adjacent	0
		84	Same	0
			Adjacent	0

Table 63.
Number of proximate events due to crossing traffic in Dakar1 (1).

Number of proximate events due to crossing traffic				
Route	**Point**	**θ (°)**	**Flight levels**	**Number of events**
APOXA-GONSA	APOXA	91	Same	0
			Adjacent	0
		89	Same	0
			Adjacent	0
	MOSOK	91	Same	0
			Adjacent	0
		89	Same	0
			Adjacent	0
	GROBA	91	Same	0
			Adjacent	1
		89	Same	0
			Adjacent	0
	GONSA	91	Same	0
			Adjacent	0
		89	Same	0
			Adjacent	0
SAGRO-LIRAX	SAGRO	96	Same	0
			Adjacent	0
		84	Same	0
			Adjacent	0
	LIMUK	96	Same	0
			Adjacent	0
		84	Same	0
			Adjacent	1
	SEMOG	96	Same	0
			Adjacent	0
		84	Same	0
			Adjacent	0
	LIRAX	96	Same	0
			Adjacent	0
		84	Same	0
			Adjacent	0
XUVIT-DIGUN	DIGUN	158	Same	1
			Adjacent	0
		22	Same	0
			Adjacent	1
TARIM-DIGUN	DIGUN	169	Same	0
			Adjacent	0
		11	Same	0
			Adjacent	1

Table 64.
Number of proximate events due to crossing traffic in Dakar1 (2).

Number of proximate events due to crossing traffic				
Route	**Point**	**θ (°)**	**Flight levels**	**Number of events**
SAGRO-BUXON	**SAGRO**	125	Same	0
			Adjacent	3
		55	Same	0
			Adjacent	0
	BUXON	124	Same	0
			Adjacent	0
		56	Same	0
			Adjacent	0
SAGRO-MOSOK	**SAGRO**	137	Same	0
			Adjacent	0
		43	Same	0
			Adjacent	1
	MOSOK	137	Same	2
			Adjacent	1
		43	Same	0
			Adjacent	0
LIRAX-IRAVU	**LIRAX**	153	Same	0
			Adjacent	1
		27	Same	0
			Adjacent	0

Table 65.
Number of proximate events due to crossing traffic in Dakar1 (3).

Here again, as it happened in all the locations previously analyzed, there are proximate events at the same flight level. The same reasons explained before are of application here.

No deviation reports have been received for these cases either, and therefore, the hypothesis of considering proximate events at the same flight level as proximate at adjacent flight levels will also be made for this location. Nevertheless, this hypothesis should be verified.

With these considerations, once vertical occupancy is calculated based on current traffic levels, it is possible to estimate the occupancy in the following years taking into account the annual traffic growth rate forecasted. Vertical occupancy values from 2015 to 2025 with an annual traffic growth rate of 5.2% are shown in Table 66.

5.2% annual traffic growth			2015	2017	2019	2021	2023	2025
Same direction vertical occupancy			0.0554	0.0613	0.0679	0.0751	0.0831	0.0920
Opposite direction vertical occupancy			0.0357	0.0395	0.0437	0.0484	0.0536	0.0593
Crossing occupancy	UL-435	97°	0.0112	0.0133	0.0147	0.0163	0.0180	0.0199
		83°	0.0204	0.0226	0.0250	0.0276	0.0306	0.0338
	ENUGO-APIGU	96°	0.0000	0.0000	0.0000	0.0000	0.0000	0.0000
		84°	0.0024	0.0026	0.0029	0.0032	0.0036	0.0040
	APOXA-GONSA	91°	0.0012	0.0013	0.0015	0.0016	0.0018	0.0020
		89°	0.0000	0.0000	0.0000	0.0000	0.0000	0.0000
	SAGRO-LIRAX	96°	0.0000	0.0000	0.0000	0.0000	0.0000	0.0000
		84°	0.0012	0.0013	0.0015	0.0016	0.0018	0.0020
	XUVIT-DIGUN	158°	0.0012	0.0013	0.0014	0.0016	0.0018	0.0019
		22°	0.0012	0.0013	0.0014	0.0016	0.0018	0.0019
	TARIM-DIGUN	169°	0.0000	0.0000	0.0000	0.0000	0.0000	0.0000
		11°	0.0012	0.0013	0.0014	0.0016	0.0018	0.0019
	SAGRO-BUXON	125°	0.0035	0.0039	0.0043	0.0047	0.0052	0.0058
		55°	0.0000	0.0000	0.0000	0.0000	0.0000	0.0000
	SAGRO-MOSOK	137°	0.0035	0.0039	0.0043	0.0047	0.0052	0.0058
		43°	0.0012	0.0013	0.0014	0.0016	0.0017	0.0019
	LIRAX-IRAVU	153°	0.0012	0.0013	0.0014	0.0016	0.0017	0.0019
		27°	0.0000	0.0000	0.0000	0.0000	0.0000	0.0000

Table 66.
Vertical occupancy estimate for Dakar1 until 2025 with an annual traffic growth rate of 5.2%

e. Dakar2

Table 67 collects some results on same and opposite vertical occupancy in Dakar2, obtained with data from July 2015.

Number of flights	July 2015
Number of flights on UN-741	275
Number of flights on UN-866	435
Number of flights on UN-873	763
Number of flights on UN-857	173
Total number of flights	1646
Number of same direction vertical proximate pairs for tracks UN-741	17
Number of same direction vertical proximate pairs for tracks UN-866	27
Number of opposite direction vertical proximate pairs for tracks UN-873	32
Number of opposite direction vertical proximate pairs for tracks UN-857	1
Total number of same direction proximate events	44
Total number of opposite direction proximate events	33
Same direction vertical occupancy (S_x=80NM)	0.0535
Opposite direction vertical occupancy (S_x=80NM)	0.0401

Table 67.
Vertical occupancy due to same and opposite direction traffic in Dakar2 location with current traffic levels.

Apart from the traffic on the main routes, in Dakar2 there is also some traffic crossing the Corridor on not-published routes. The number of flights on these routes can be found in the following table:

Number of flights	July 2015
Number of flights on IP006-NANIK	14
Number of flights on IP007-NANIK	77
Number of flights on IP008-NANIK	74
Number of flights on IP008-MOSAD	12
Number of flights on IRAVU-MESAB	15
Number of flights on main routes (UN-741, UN-866, UN-873 and UN-857)	1646
Total number of flights	1826

Table 68.
Number of flights in Dakar2 airspace.

The flights on the other not-published routes are already included in the number of flights on the main routes except for 180 of them. Therefore, the total number of aircraft in this case is 1826.

The time windows to obtain proximate pairs are, in this case, the ones shown in Table 69.

Time windows for crossing routes					
Route	Point	v1 (kts)	v2 (kts)	θ (°)	t (min)
IP006-NANIK	NANIK	471.14	513.50	152	41
				28	11
IP007-NANIK	NANIK	471.14	486.62	160	58
				20	11
IP008-NANIK	NANIK	471.14	478.53	169	107
				11	11
IP008-MOSAD	MOSAD	471.14	436.67	162	68
				18	11
IRAVU-MESAB	MESAB	463.19	464.34	154	46
				26	11

Table 69.
Time windows for crossing occupancies in Dakar2.

With these time windows, the number of proximate pairs obtained can be seen in Table 70.

Number of proximate events due to crossing traffic				
Route	**Point**	**θ (°)**	**Flight levels**	**Number of events**
IP006-NANIK	**NANIK**	152	Same	0
			Adjacent	0
		28	Same	0
			Adjacent	0
IP007-NANIK	**NANIK**	160	Same	0
			Adjacent	0
		20	Same	3
			Adjacent	12
IP008-NANIK	**NANIK**	169	Same	0
			Adjacent	0
		11	Same	4
			Adjacent	10
IP008-MOSAD	**MOSAD**	162	Same	0
			Adjacent	0
		18	Same	0
			Adjacent	2
IRAVU-MESAB	**MESAB**	154	Same	2
			Adjacent	6
		26	Same	0
			Adjacent	1

Table 70.
Number of proximate events due to crossing traffic in Dakar2.

Here again, as it happened in all the locations previously analysed, there are proximate events at the same flight level. The same reasons explained before are of application here.

No deviation reports have been received for these cases either, and therefore, the hypothesis of considering proximate events at the same flight level as proximate at adjacent flight levels will also be made for this location. Nevertheless, this hypothesis should be verified.

With these considerations, once vertical occupancy is calculated based on current traffic levels, it is possible to estimate the occupancy in the following years taking into account the annual traffic growth rate forecasted. Vertical occupancy values from 2015 to 2025 with an annual traffic growth rate of 5.2% are shown in Table 71.

5.2% annual traffic growth			2015	2017	2019	2021	2023	2025
Same direction vertical occupancy			0.0535	0.0592	0.0655	0.0725	0.0802	0.0888
Opposite direction vertical occupancy			0.0401	0.0444	0.0491	0.0544	0.0602	0.0666
Crossing occupancy	IP006-NANIK	152°	0.0000	0.0000	0.0000	0.0000	0.0000	0.0000
		28°	0.0000	0.0000	0.0000	0.0000	0.0000	0.0000
	IP007-NANIK	160°	0.0000	0.0000	0.0000	0.0000	0.0000	0.0000
		20°	0.0164	0.0182	0.0201	0.0223	0.0246	0.0273
	IP008-NANIK	169°	0.0000	0.0000	0.0000	0.0000	0.0000	0.0000
		11°	0.0153	0.0170	0.0188	0.0208	0.0230	0.0255
	IP008-MOSAD	162°	0.0000	0.0000	0.0000	0.0000	0.0000	0.0000
		18°	0.0022	0.0024	0.0027	0.0030	0.0033	0.0036
	IRAVU-MESAB	154°	0.0088	0.0097	0.0107	0.0119	0.0131	0.0145
		26°	0.0011	0.0012	0.0013	0.0015	0.0016	0.0018

Table 71.
Vertical occupancy estimate for Dakar2 until 2025 with an annual traffic growth rate of 5.2%

f. Recife

Table 72 collects some results on same and opposite vertical occupancy in Recife, obtained with data from July 2015.

Number of flights	July 2015
Number of flights on UN-741	442
Number of flights on UN-866	419
Number of flights on UN-873	749
Number of flights on UN-857	181
Total number of flights	1791
Number of same direction vertical proximate pairs for tracks UN-741	51
Number of same direction vertical proximate pairs for tracks UN-866	20
Number of opposite direction vertical proximate pairs for tracks UN-873	54
Number of opposite direction vertical proximate pairs for tracks UN-857	3
Total number of same direction proximate events	71
Total number of opposite direction proximate events	57
Same direction vertical occupancy (S_x=80NM)	0.0793
Opposite direction vertical occupancy (S_x=80NM)	0.0636

Table 72.
Vertical occupancy due to same and opposite direction traffic in Recife location with current traffic levels.

Apart from the traffic on the main routes, in Recife there is also some traffic crossing the Corridor on routes UL-695/UL-375 and on not-published routes. The number of flights on these routes can be found in the following table:

Number of flights	July 2015
Number of flights on UL-695/UL-375	39
Number of flights on main routes (UN-741, UN-866, UN-873 and UN-857)	1791
Total number of flights	1840

Table 73.
Number of flights in Recife airspace.

The time windows to obtain proximate pairs are, in this case, the ones shown in Table 74.

Time windows for crossing routes					
Route	**Point**	**v1 (kts)**	**v2 (kts)**	**θ (°)**	**t (min)**
UL-695	---	459.57	469.74	96	16
				84	14

Table 74.
Time windows for crossing occupancies in Recife.

With these time windows, the number of proximate pairs obtained can be seen in Table 75.

Number of proximate events due to crossing traffic				
Route	**Point**	**θ (°)**	**Flight levels**	**Number of events**
UL-695	**DIKEB**	96	Same	0
			Adjacent	0
		84	Same	0
			Adjacent	4
	OBKUT	96	Same	0
			Adjacent	0
		84	Same	0
			Adjacent	0
	ORARO	96	Same	0
			Adjacent	0
		84	Same	0
			Adjacent	0
	NOISE	96	Same	2
			Adjacent	0
		84	Same	0
			Adjacent	0

Table 75.
Number of proximate events due to crossing traffic in Recife.

As it occurred in other locations, some proximate pairs at the same flight level have been detected. In this case, at least 2 of the proximate pairs found are at the same flight level within 14 minutes of each other.

As no large height deviation reports have been received for these events, it will be considered that they are proximate events at adjacent flight levels, as it has been done in other locations, assuming that they are due to the need of extrapolation and the lack of data about flight level changes. Nevertheless, this hypothesis should be verified, because it may have an impact on the results, as it has been explained before.

With these considerations, once vertical occupancy is calculated based on current traffic levels, it is possible to estimate the occupancy in the following years taking into account the annual traffic growth rate forecasted. Vertical occupancy values from 2015 to 2025 with an annual traffic growth rate of 5.2% are shown in Table 76.

5.2% annual traffic growth			2015	2017	2019	2021	2023	2025
Same direction vertical occupancy			0.0793	0.0877	0.0971	0.1075	0.1189	0.1316
Opposite direction vertical occupancy			0.0636	0.0704	0.0779	0.0863	0.0955	0.1057
Crossing occupancy	UL-695	96°	0.0022	0.0024	0.0027	0.0030	0.0033	0.0036
		84°	0.0044	0.0048	0.0053	0.0059	0.0066	0.0073

Table 76.
Vertical occupancy estimate for Recife until 2025 with an annual traffic growth rate of 5.2%

4.2.8. Technical vertical collision risk

The technical vertical collision risk values obtained until 2025 in the different locations are the ones summarized in the following sections.

4.2.8.a. Canaries

Table 77 shows the estimate of the vertical collision risk, in Canaries location, considering that the traffic growth factor is 5.2% per annum. These results can also be seen in Figure 33.

Technical Vertical Collision risk	5.2% annual traffic growth
2015	$3.1082*10^{-10}$
2016	$3.2698*10^{-10}$
2017	$3.4398*10^{-10}$
2018	$3.6187*10^{-10}$
2019	$3.8069*10^{-10}$
2020	$4.0048*10^{-10}$
2021	$4.2131*10^{-10}$
2022	$4.4321*10^{-10}$
2023	$4.6626*10^{-10}$
2024	$4.9051*10^{-10}$
2025	$5.1601*10^{-10}$

Table 77.
Technical vertical collision risk for the period 2015-2025 in the Canaries.

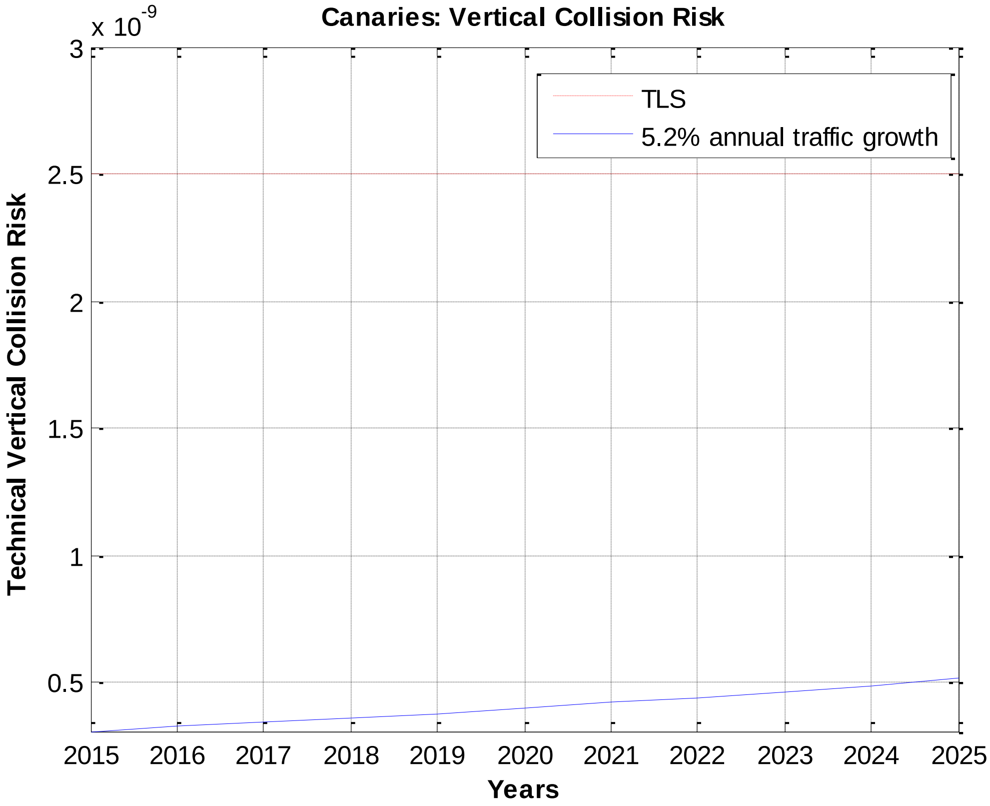

Figure 33.
Technical vertical collision risk for the period 2015-2025 in the Canaries.

4.2.8.b. SAL1

Table 78 shows the estimate of the vertical collision risk, in Canaries location, considering the traffic growth factor as 5.2% per annum. These results can also be seen in Figure 34.

Technical Vertical Collision risk	5.2% annual traffic growth
2015	$1.0946*10^{-10}$
2016	$1.1515*10^{-10}$
2017	$1.2114*10^{-10}$
2018	$1.2744*10^{-10}$
2019	$1.3406*10^{-10}$
2020	$1.4104*10^{-10}$
2021	$1.4837*10^{-10}$
2022	$1.5609*10^{-10}$
2023	$1.6420*10^{-10}$
2024	$1.7274*10^{-10}$
2025	$1.8172*10^{-10}$

Table 78.
Technical vertical collision risk for the period 2015-2025 in SAL1.

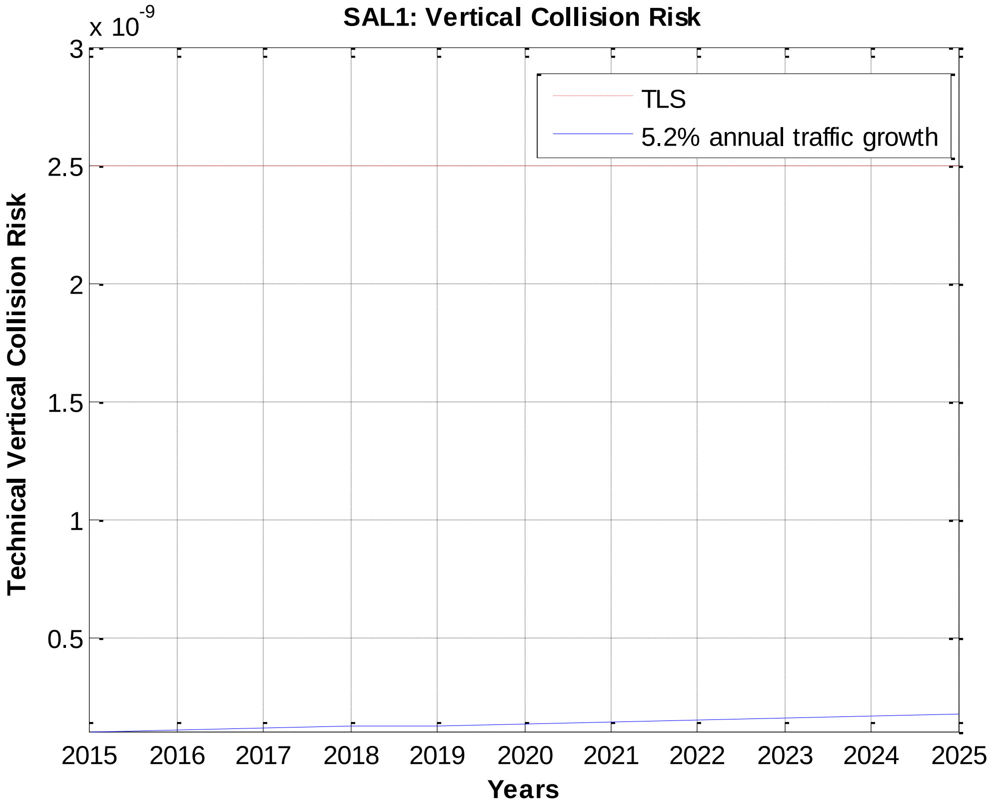

Figure 34.
Technical vertical collision risk for the period 2015-2025 in SAL1.

4.2.8.c. SAL2

Table 79 shows the estimate of the vertical collision risk, in Canaries location, considering that the traffic growth factor is 5.2% per annum. These results can also be seen in Figure 35.

Technical Vertical Collision risk	5.2% annual traffic growth
2015	$1.6257*10^{-10}$
2016	$1.7102*10^{-10}$
2017	$1.7992*10^{-10}$
2018	$1.8927*10^{-10}$
2019	$1.9911*10^{-10}$
2020	$2.0947*10^{-10}$
2021	$2.2036*10^{-10}$
2022	$2.3182*10^{-10}$
2023	$2.4387*10^{-10}$
2024	$2.5655*10^{-10}$
2025	$2.6989*10^{-10}$

Table 79.
Technical vertical collision risk for the period 2015-2025 in SAL2.

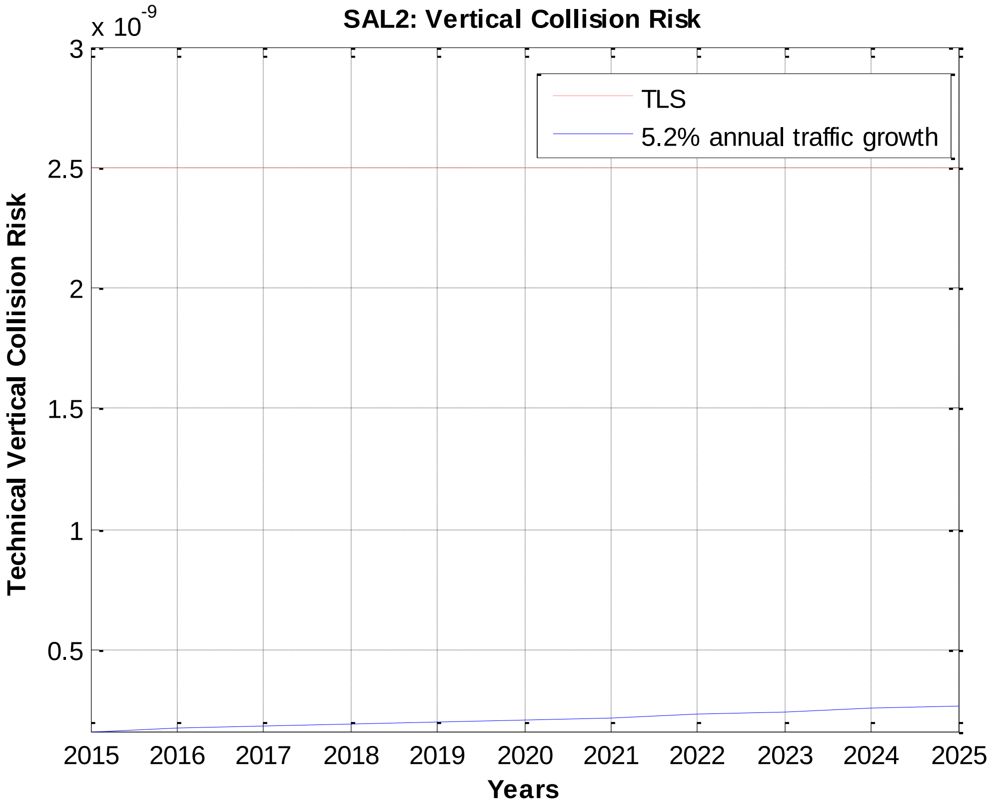

Figure 35.
Technical vertical collision risk for the period 2015-2025 in SAL2.

4.2.8.d. Dakar1

Table 80 shows the estimate of the vertical collision risk, in Canaries location, considering that the traffic growth factor is 5.2% per annum. These results can also be seen in Figure 36.

Technical Vertical Collision risk	5.2% annual traffic growth
2015	$1.3961*10^{-10}$
2016	$1.4687*10^{-10}$
2017	$1.5451*10^{-10}$
2018	$1.6254*10^{-10}$
2019	$1.7099*10^{-10}$
2020	$1.7988*10^{-10}$
2021	$1.8924*10^{-10}$
2022	$1.9908*10^{-10}$
2023	$2.0943*10^{-10}$
2024	$2.2032*10^{-10}$
2025	$2.3178*10^{-10}$

Table 80.
Technical vertical collision risk for the period 2015-2025 in Dakar1.

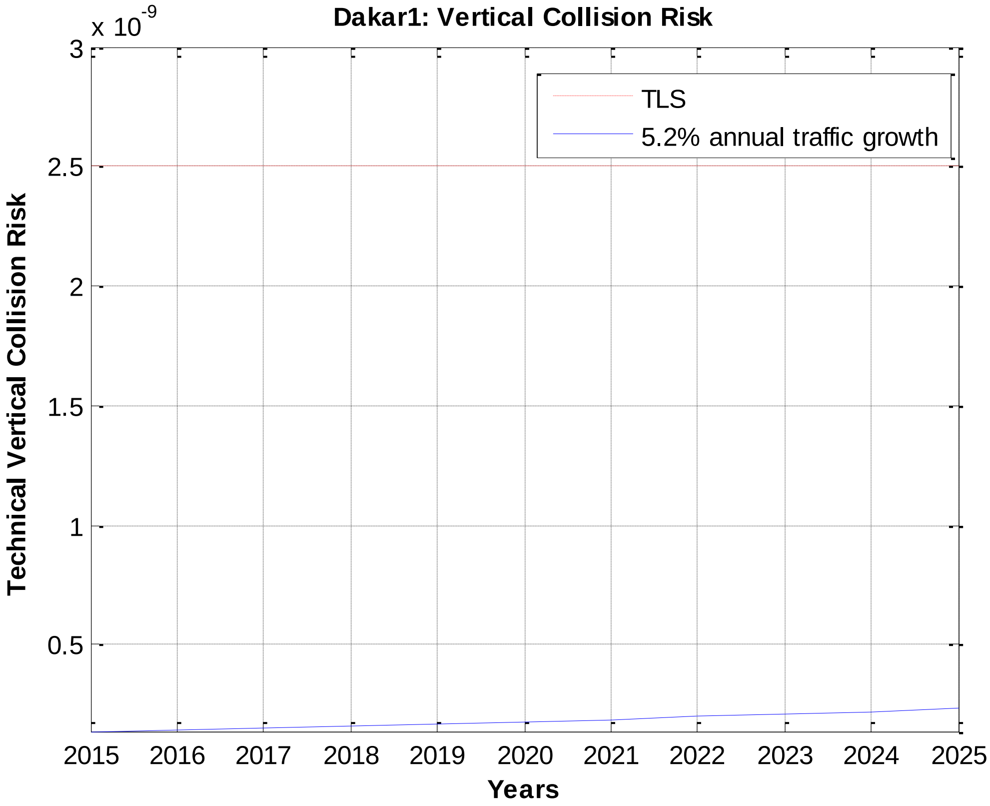

Figure 36.
Technical vertical collision risk for the period 2015-2025 in Dakar1.

4.2.8.e. Dakar2

Table 81 shows the estimate of the vertical collision risk, in Canaries location, considering that the traffic growth factor is 5.2% per annum. These results can also be seen in Figure 37.

Technical Vertical Collision risk	5.2% annual traffic growth
2015	$1.5693*10^{-10}$
2016	$1.6509*10^{-10}$
2017	$1.7368*10^{-10}$
2018	$1.8271*10^{-10}$
2019	$1.9221*10^{-10}$
2020	$2.0220*10^{-10}$
2021	$2.1272*10^{-10}$
2022	$2.2378*10^{-10}$
2023	$2.3542*10^{-10}$
2024	$2.4766*10^{-10}$
2025	$2.6054*10^{-10}$

Table 81.
Technical vertical collision risk for the period 2015-2025 in Dakar2.

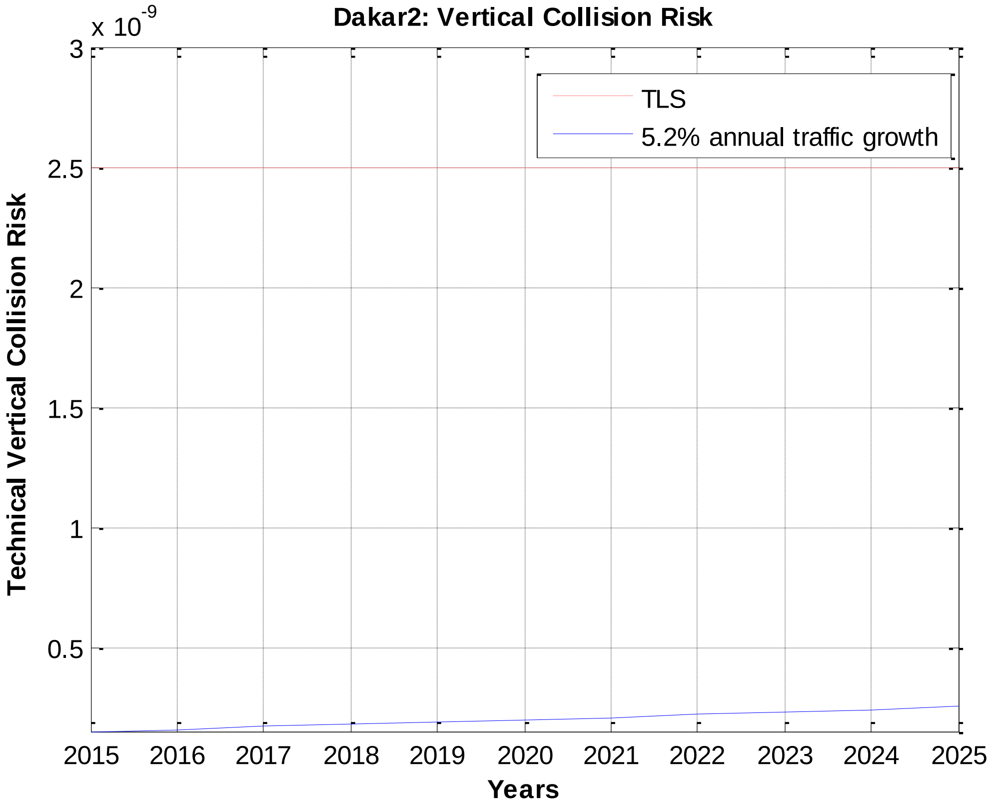

Figure 37.
Technical vertical collision risk for the period 2015-2025 in Dakar2.

4.2.8.f. Recife

Table 82 shows the estimate of the vertical collision risk, in Canaries location, considering that the traffic growth factor is 5.2% per annum. These results can also be seen in Figure 38.

Technical Vertical Collision risk	5.2% annual traffic growth
2015	$2.3852*10^{-10}$
2016	$2.5092*10^{-10}$
2017	$2.6397*10^{-10}$
2018	$2.7769*10^{-10}$
2019	$2.9213*10^{-10}$
2020	$3.0733*10^{-10}$
2021	$3.2331*10^{-10}$
2022	$3.4012*10^{-10}$
2023	$3.5780*10^{-10}$
2024	$3.7641*10^{-10}$
2025	$3.9598*10^{-10}$

Table 82.
Technical vertical collision risk for the period 2015-2025 in Recife.

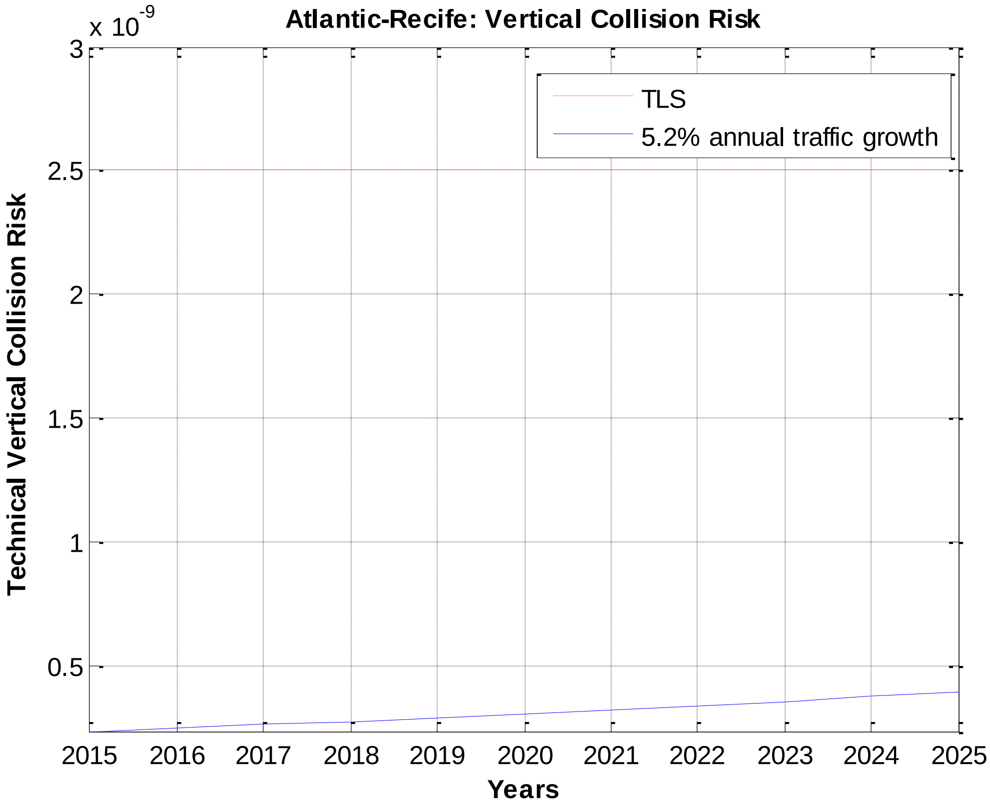

Figure 38.
Technical vertical collision risk for the period 2015-2025 in Recife.

4.2.9. Considerations on the results

4.2.9.a. Parallel and crossing routes

It can be seen that the estimates of the technical vertical risk are below the technical TLS even in 2025 being similar the values obtained in all the locations.

Comparing these results with those obtained in [Ref. 7], it should be noted that the new values are lower. This is primarily due to the increase in the new value of $P_z(1000)$ for the year 2015 ($2.0405*10^{-9}$ instead of $6.84*10^{-9}$ used in [Ref. 7]).

4.2.9.b. DCT Area routes

Although traffic on the direct routes (DCT Area) has not been considered, it is assumed that the risk due to these routes will not dramatically change the results obtained for technical vertical risk. This is due to the fact that on these routes there is mainly traffic on even or odd levels and, therefore, there will not be proximate pairs at adjacent flight levels of the same route.

4.3. Total vertical collision risk assessment

In order to assess the total vertical risk, the risk due to large, atypical height deviations[8] must be assessed and added to the technical vertical risk

Whilst the technical vertical risk for aircraft on non-adjacent flight levels is negligible in comparison with those on adjacent flight levels, the same is not true for the risk due to atypical height deviations.

Atypical height deviations can be due to exceptional technical errors or due to operational errors.

Altitude deviations resulting from exceptional technical errors are subdivided into five categories, according to the cause of deviation. These are:

- Turbulence: Incidents in which an aircraft deviates from its assigned altitude as a result of pressure turbulence, or turbulence from another aircraft.
- TCAS: false RA-TCAS alerts when there is no other aircraft nearby.
- TCAS: nuisance RA-TCAS alerts against an aircraft that is not posing a threat; for example, an aircraft that is climbing to the level below.
- Autopilot failure: the aircraft deviates from its assigned flight level due to a malfunction in the autopilot system.
- Other technical malfunctions: for example, an electrical fault or engine problem.

On the other side, altitude deviations due to operational errors are due to ATC-pilot loop errors and incorrect clearances. These include:

- Climb/descend without ATC clearance.
- Failure to climb/descend as cleared.
- Entry to RVSM airspace at an incorrect level.
- ATC system loop error (e.g. pilot misunderstands clearance or ATC issues incorrect clearance).
- Errors in coordination of the transfer of control responsibility between adjacent ATC units, resulting in flight at incorrect flight level.

A large atypical deviation can follow three main paths, which are illustrated in Figure 39. The figure depicts a scenario where aircraft 1 should climb to a certain flight level. The correct path of the aircraft is shown by the solid line. The three possible types of deviation which aircraft 1 might make are depicted by dotted line paths A, B and C.

[8] *A RVSM large height deviation (LHD) is defined as any vertical deviation of 90 metres/300 feet or more from the flight level expected to be occupied by the flight.*

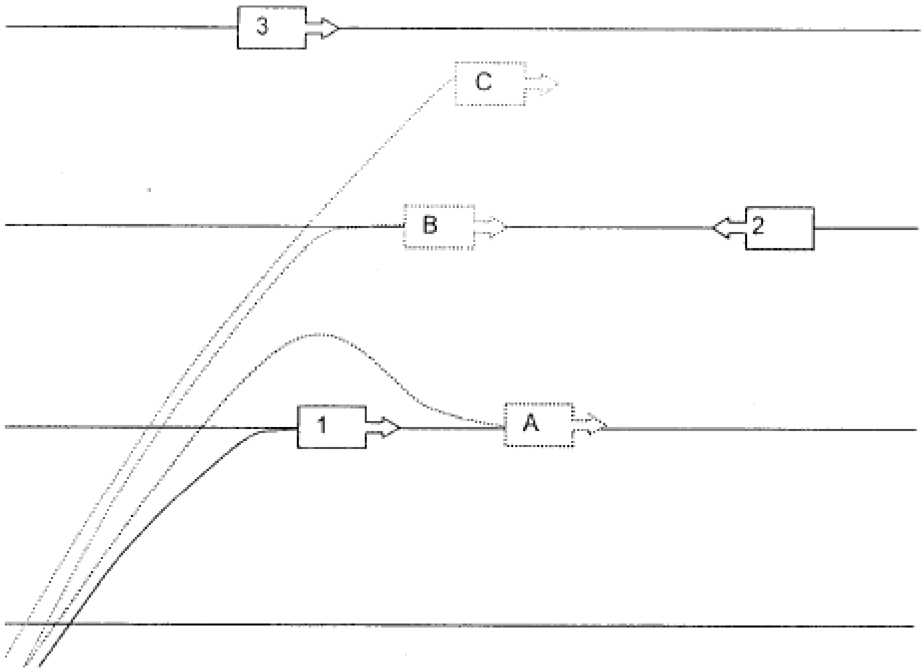

Figure 39.
Illustration of the basic deviation paths.

In scenario A, aircraft 1 fails to capture its correct flight level, and performs a height bust. In scenario B, aircraft 1 climbs to and joins an incorrect flight level and in scenario C, aircraft 1 climbs through an incorrect level.

Height deviations due to TCAS do not usually involve whole number of flight levels, i.e. climbing or descending through one or more flight levels without clearance or levelling off at a wrong flight level, but may be much larger than the normal deviations of MASPS approved aircraft. However, deviations caused by the remaining types of error may involve whole number of flight levels.

Related to this, a distinction between large height deviations involving whole numbers of flight levels and large height deviations not involving whole numbers of flight levels was made for the NAT and different models for the associated probabilities of vertical overlap were developed. These models are described in the following section.

Finally, according with the ICAO recommendations ([Ref. 28]), large height deviations can be classified as reflected in Table 83. This classification has been used in the EUR/SAM Corredor.

Tipos LHD	
Código	Descripción LHD
A	Flight crew fails to climb or descend the aircraft as cleared
B	Flight crew climbing or descending without ATC clearance
C	Incorrect operation or interpretation of airborne equipment
D	ATC system loop error
E	ATC transfer of control coordination errors due to human factors
F	ATC transfer of control coordination errors due to technical issues
G	Aircraft contingency leading to sudden inability to maintain level
H	Airborne equipment failure and unintentional or undetected level change
I	Turbulence or other weather related cause
J	TCAS resolution advisory and flight crew correctly responds
K	TCAS resolution advisory and flight crew incorrectly responds
L	Non-approved aircraft is provided with RVSM separation
M	Other

Table 83.
LHD classification according to ICAO.

4.3.1. Vertical Collision Risk models for large height deviations

The models used to estimate the risk due to large height deviations differ from the technical vertical risk model only in the computation of the probability of vertical overlap, Pz, and the relative vertical speed, $|\bar{\dot{z}}|$.

Three sub-models will be used for large height deviations not involving whole numbers of flight levels, aircraft climbing or descending through a flight level and aircraft levelling off at a wrong level.

4.3.1.a. Aircraft levelling off at a wrong level

To estimate the vertical overlap probability for events where an aircraft joins an incorrect level it is necessary to estimate the probability that an aircraft is at an incorrect level, P_i, and then multiply this by the probability that two aircraft nominally at the same level will be in vertical overlap ($P_z(0)$).

The probability that an aircraft is flying at an incorrect level, Pi, is estimated from the proportion of the total flying time spent at an incorrect level. It is determined by summing the individual times spent at an incorrect level for each large height deviation and dividing this by the total system flight time.

An aircraft levelling off at a wrong flight level is still in level flight and, therefore, the same type of collision risk model is applicable as for aircraft at adjacent flight levels but with a modified calculation of the probability of vertical overlap. The collision risk in this case is given by:

$$N_{aZ}^{wl} = P_y(0) \cdot \frac{\lambda_x}{S_x} \cdot \left\{ P_z^{wl}(S_z)_{same} E_{z_{same}} \cdot \left[\frac{|\Delta\bar{v}|}{2 \cdot \lambda_x} + \frac{|\dot{\bar{y}}|}{2 \cdot \lambda_y} + \frac{|\dot{\bar{z}}|}{2 \cdot \lambda_z} \right] + P_z^{wl}(S_z)_{opp} E_{z_{opp}} \cdot \left[\frac{2 \cdot |\bar{v}|}{2 \cdot \lambda_x} + \frac{|\dot{\bar{y}}|}{2 \cdot \lambda_y} + \frac{|\dot{\bar{z}}|}{2 \cdot \lambda_z} \right] \right\} + \frac{P_Z(0) \times t^{wl}}{T} \cdot \sum_{1}^{n} P_h(\theta_i) \cdot E_z(\theta_i) \cdot \left\{ \frac{v_{rel}(\theta_i)}{\frac{\pi \lambda_h}{2}} + \frac{|\dot{\bar{z}}|}{2 \cdot \lambda_z} \right\}$$

Equation 51.

where the superscript "wl" refers to levelling off at a wrong level and $P_z^{wl}(S_z)$ is given by:

$$P_z^{wl}(S_z)_{same} = \frac{P_Z(0) \times t_{same}^{wl}}{T} \qquad P_z^{wl}(S_z)_{opp} = \frac{P_Z(0) \times t_{opp}^{wl}}{T}$$

Equation 52.

In these equations the different parameters are:

- N_{aZ}^{wl}: the expected number of fatal aircraft accidents per flight hour due to aircraft levelling off at a wrong flight level.
- $P_z^{wl}(S_z)$: is the probability of vertical overlap due to aircraft levelling off at a wrong flight level. The subscript "same" indicates same direction and "opp" opposite direction.
- $P_Z(0)$: is the probability of vertical overlap for aircraft nominally flying at the same flight level. It accounts for the normal technical height deviations of aircraft that are flying at the same level and it can be calculated as in 3.3.
- T is the amount of flying time during the period of time the incident data were collected.
- t^{wl} is the total time aircraft have stayed at a wrong flight level after incorrectly levelling off during a period of time with T flying hours. The subscript "same" or "opp" indicates weather there is traffic on the same or opposite direction in this level.

Information on the number of times an aircraft levels off at a wrong level and the duration of its stay at the wrong level are to be obtained from the incident reports.

4.3.1.b. Aircraft climbing or descending through a flight level

The two main elements of a collision risk model for aircraft climbing or descending through a flight level without clearance depend on the probability of two aircraft being in joint longitudinal and vertical overlap and on the average duration of a joint overlap in the vertical plane. The relative vertical speed depends on the rate of climb/descent during the event and determines the angle at which the flight level is crossed.

The model described here is employed for climb/descent rates less than or equal to 4000 ft/min (approximately 40 knots). Slowly descending aircraft are assumed to maintain the same attitude as in level flight and it is assumed that the lateral path-keeping performance is no worse than that for aircraft in level flight. For large height deviations of aircraft with climb/descent rates higher than 40 kts, (emergencies or pressurization failures) a different model should be applied.

The collision risk model for aircraft climbing or descending through a flight level is given by:

$$N_{aZ}^{cl/d} = P_y(0) \cdot \frac{\lambda_x}{S_x} \cdot \left\{ P_z^{cl/d}(S_z)_{same} E_{z_{same}} \cdot \left[\frac{|\Delta \bar{v}|}{2 \cdot \lambda_x} + \frac{|\overline{\dot{y}}|}{2 \cdot \lambda_y} + \frac{|\overline{\dot{z}}|}{2 \cdot \lambda_z} \right] + P_z^{cl/d}(S_z)_{opp} E_{z_{opp}} \cdot \left[\frac{2 \cdot |\bar{v}|}{2 \cdot \lambda_x} + \frac{|\overline{\dot{y}}|}{2 \cdot \lambda_y} + \frac{|\overline{\dot{z}}|}{2 \cdot \lambda_z} \right] \right\} + P_z^{cl/d} \cdot \sum_{1}^{n} P_h(\theta_i) \cdot E_z(\theta_i) \cdot \left\{ \frac{v_{rel}(\theta_i)}{\frac{\pi \lambda_h}{2}} + \frac{|\overline{\dot{z}}|}{2 \cdot \lambda_z} \right\}$$

Equation 53.

where the superscript "cl/d" refers to an aircraft climbing or descending through a flight level without a proper clearance.

Per event, that is, an aircraft crossing a flight level, it is in vertical overlap, in average, for t_z flight hours,

$$t_z = \frac{2 \cdot \lambda_z}{|\overline{\dot{z}_c}|}$$

Equation 54.

where λ_z is the average aircraft height and $\overline{\dot{z}_c}$, the relative vertical speed.

Therefore, if N is the total number of flight levels crossed, the total time in vertical overlap for aircraft climbing or descending through a flight level is $N \times t_z$ and the probability of vertical overlap, $P_z^{cl/d}(S_z)$, is given by:

$$P_z^{cl/d}(S_z) = \frac{N \times t_z}{T} = \frac{N \times 2\lambda_z / |\overline{\dot{z}_c}|}{T}$$

Equation 55.

In these equations:

- $N_{aZ}^{cl/d}$ is the expected number of fatal aircraft accidents per flight hour due to aircraft climbing or descending through a flight level without a proper clearance.
- $P_z^{cl/d}(S_z)$ is the probability of vertical overlap due to aircraft climbing or descending through a flight level without a proper clearance. The subscripts "same" and "opp" indicate whether the crossed levels are levels in the same direction or in the opposite direction.

- N is the number of crossed flight levels.
- $\dot{z}_c$ is the average climb or descent rate for aircraft climbing or descending through a flight level without a proper clearance.

Information on the number of incorrect flight level crossings and the pertinent vertical speeds is to be obtained from the incident reports. When the vertical speed is not indicated, a default value is used for the relative vertical speed. This value is usually considered to be 15 knots.

4.3.1.c. Large height deviations not involving whole numbers of flight levels

The vertical collision risk due to large height deviations not involving whole numbers of flight levels can be modelled in the same way as the technical vertical collision risk, i.e.:

$$N_{aZ}^{*} = P_y(0) \cdot \frac{\lambda_x}{S_x} \cdot \left\{ P_z^{*}(S_z)_{same} E_{z_{same}} \cdot \left[\frac{|\Delta \bar{v}|}{2 \cdot \lambda_x} + \frac{|\overline{\dot{y}}|}{2 \cdot \lambda_y} + \frac{|\overline{\dot{z}}|}{2 \cdot \lambda_z} \right] + P_z^{*}(S_z)_{opp} E_{z_{opp}} \cdot \left[\frac{2 \cdot |\bar{v}|}{2 \cdot \lambda_x} + \frac{|\overline{\dot{y}}|}{2 \cdot \lambda_y} + \frac{|\overline{\dot{z}}|}{2 \cdot \lambda_z} \right] \right\} +$$

$$P_z^{*} \cdot \sum_{1}^{n} P_h(\theta_i) \cdot E_z(\theta_i) \cdot \left\{ \frac{v_{rel}(\theta_i)}{\frac{\pi \lambda_h}{2}} + \frac{|\overline{\dot{z}}|}{2 \cdot \lambda_z} \right\}$$

Equation 56.

Superscript "*" is used to distinguish this type of vertical risk from the technical vertical collision risk. The probability of vertical overlap $P_z^{*}(S_z)$ can be calculated in the same way as for the technical vertical collision risk, by means of Equation 43.

4.3.2. Data on EUR/SAM large height deviations

As it has been explained in the previous sections, data needed for the different models should be obtained from the large height deviation reports received from the different UIRs.

The information that has been made available for this assessment can be seen in the following tables, where the time spent at an incorrect flight level, necessary to calculate the risk due to an aircraft levelling off at a wrong level, had to be estimated in the major part of the LHDs, since it was not included in the reports. Therefore, it has been necessary to use default values according to the following set of criteria:

- Coordination error (no notification of the transfer or transfer at unexpected flight level) and detection of the aircraft when entering the UIR: 10 minutes.
- Coordination error (no notification of the transfer) and undetected aircraft in the UIR. The duration of the flight in that UIR, taking into account its speed.

Table 84 indicates the months for which LHD reports have been received. From these LHDs, only those affecting the four main routes have been considered[9]. Table 85, Table 86, Table 87 and Table 88 show the details of the deviations reported in the Canaries, SAL, Dakar and Atlantic-Recife, respectively.

Months	Canarias UIR	SAL Oceanic UIR	Dakar Oceanic UIR	Atlântico-Recife FIR/UIR
Jan-15	Available	Available	Available	“No deviation” report received
Feb-15	Available	Available	Available	Available
Mar-15	Available	Available	Available	“No deviation” report received
Apr-15	Available	Available	Available	“No deviation” report received
May-15	“No deviation” report received	Available	Available	“No deviation” report received
Jun-15	“No deviation” report received	Available	“No deviation” report received	“No deviation” report received
Jul-15	“No deviation” report received	Available	Available	“No deviation” report received
Aug-15	Available	Available	Available	“No deviation” report received
Sep-15	“No deviation” report received	Available	Available	Available
Oct-15	Available	Available	Available	“No deviation” report received
Nov-15	Available	Available	Available	“No deviation” report received
Dec-15	“No deviation” report received	Available	Available	“No deviation” report received

KEY: Available | Not avalaible | “No deviation” report received

Table 84.
Received data from January 2015 to December 2015.

[9] *It has been considered the LHDs that have taken place in the main routes and in incorporations to the main routes coming from the DCT Area.*

Date	Route	Duration	Coordinated FL	Observed FL	Deviation	Cause	Category
140115	UN873	0.0833 h	FL370	FL355	1500 ft	Coordination error	E
310115	UN866	0.0833 h	FL380	FL390	1000 ft	Coordination error	E
150215	UN873	0.0833 h	FL350	FL350	4000 ft	Coordination error	F
180215	UN866	0.0833 h	FL350	FL330	2000 ft	Coordination error	E
140315	UN857	0.0833 h	FL310	FL350	4000 ft	Coordination error	E
070415	UN873	0.0833 h	FL330	FL350	2000 ft	Coordination error	E
180415	UN866	0.0833 h	FL340	FL340	0	Coordination error	E
080515	UN873	0.0833 h	FL390	FL390	0	Coordination error	E
150615	UN873	0.0833 h	FL350	FL350	0	Coordination error	E
190715	UN866	0.0833 h	FL330	FL350	2000 ft	Coordination error	E
140815	UN866	0.25 h	FL380	FL380	0	Coordination error	E
190815	UN857	0.0833 h	FL310	FL350	4000 ft	Coordination error	E
150915	UN873	0.0833 h	-	FL330	-	Coordination error	E
230915	UN857	0.0833 h	FL370	FL390	2000 ft	Coordination error	E
051115	UN866	0.0833 h	FL400	FL400	-	Coordination error	E
201115	UN857	0.0833 h	-	FL330	-	Coordination error	E
141215	UN866	0.0833 h	-	FL400	-	Coordination error	E

Table 85.
Large height deviations reported in the Canaries.

Date	Route	Duration	Coordinated FL	Observed FL	Deviation	Cause	Category
090115	RANDOM	0.0667 h	FL360	FL360	0	Coordination error	E
140115	UN873	0.0333 h	FL330	FL350	2000 ft	Coordination error	E
240215	UN741	1.3333 h	FL350	FL360	1000 ft	Coordination error	E
280215	BAMUX-ILGAS	0.0833 h	FL370	FL360	1000 ft	Coordination error	E
140315	UN857	0.0833 h	-	FL350	0	Coordination error	E
310315	ILGAS-SNT	0.0833 h	FL380	FL360	2000 ft	Coordination error	E
010415	UN873	0.0833 h	-	FL380	0	Coordination error	E
170415	UN873	0.0833 h	FL400	FL400	0	Coordination error	E
190415	UN866	0.0833 h	FL360	FL360	0	Coordination error	E
100515	ILGAS-BAMUX	0.0833 h	FL320	-	0	Coordination error	E
090615	UN857	0.0833 h	FL380	FL380	0	Coordination error	E
110615	UN857	0.0833 h	FL350	FL370	2000 ft	Coordination error	E
200615	UN873	0.0833 h	FL380	FL380	0	Coordination error	E
260615	ULTEM-EVKAS	0.0833 h	FL370	FL360	1000 ft	Coordination error	E
190815	UN873	0.0833 h	FL360	-	-	Coordination error	E
290915	UN866	0.0833 h	-	FL350	-	Coordination error	E

Table 86.
Large height deviations reported in SAL.

Date	Route	Duration	Coordinated FL	Observed FL	Deviation	Cause	Category
140115	UN741	0.0833 h	FL310	FL330	2000 ft	Coordination error	E
090215	UN857	0.0167 h	FL370	-	0 ft	Coordination error	E
240215	UN741	0.0833 h	F350	-	1000 ft	Coordination error	E
240215_2	UN866	0.0833 h	FL390	FL400	1000 ft	Coordination error	E
280215	UN857	0.0833 h	FL350	FL370	2000 ft	Coordination error	E
220315	UN873	0.0833 h	FL350	-	0 ft	Coordination error	E
250315	UN873	0.0833 h	FL380	FL300	8000 ft	Coordination error	E
260315	UN873	0.0833 h	FL400	FL380	2000 ft	Coordination error	E
180415	UL345	0.0833 h	FL310	FL330	2000 ft	Coordination error	E
300415	UN866	0.0833 h	FL370	FL380	1000 ft	Coordination error	E
210515	UN857	0.0833 h	FL370	FL350	2000 ft	Coordination error	E
070715	RANDOM	0.0833 h	FL320	FL340	2000 ft	Coordination error	E
180715	UN873	0.0833 h	FL380	-	-	Coordination error	E
090915	RANDOM	0.0833 h	FL340	-	0 ft	Coordination error	E
100915	UN857	0.0833 h	FL330	FL370	4000 ft	Coordination error	E
130915	UN857	0.0833 h	FL350	FL330	2000 ft	Coordination error	E
140915	UN873	0.0833 h	FL340	FL400	6000 ft	Coordination error	E
131015	UN741	0.0833 h	FL320	FL340	2000 ft	Coordination error	E
141015	UN741	0.0833 h	FL320	FL330	1000 ft	Coordination error	E
311015	RANDOM	0.0833 h	FL340	FL360	2000 ft	Coordination error	E
081115	RANDOM	0.0833 h	FL350	FL330	2000 ft	Coordination error	E
101215	RANDOM	0.0833 h	FL340	FL340	-	Coordination error	E

Table 87.
Large height deviations reported in Dakar.

Date	Route	Duration	Coordinated FL	Observed FL	Deviation	Cause	Category
170215	UN741	0.0833 h	FL320	FL340	2000 ft	Coordination error	E
030915	UN857	0.0833 h	FL320	FL340	2000 ft	Coordination error	E

Table 88.
Large height deviations reported in Recife.

After an analysis of the deviation reports, it can be concluded that all the registered deviations are due to errors in coordination between adjacent ATC units, resulting in either no notification of the transfer or in transfer at an unexpected flight level. All LHDs have been classified as E category, except one that apparently was caused by a technical problem and was classified as F category.

There is one deviation in SAL that lasted 1 hour. In this case, it is due to an aircraft that crossed SAL without being coordinated, and the coordination error was discovered it passed from SAL to Canaries.

4.3.3. Total vertical collision risk

The total vertical risk is the sum of the technical risk and the risks due to large height deviations involving whole numbers of flight levels (both climbing/descending aircraft and level flight aircraft) and the risk due to large height deviations not involving whole numbers of flight levels. As it has been said, it is assumed that the same type of collision risk model applies to the different risk components, being only different the probability of vertical overlap, $P_z(S_z)$, and the average relative vertical speed used in each case. So,

$$N_{az}^{total} = N_{az}^{tech} + N_{az}^{wl} + N_{az}^{cl/d} + N_{az}^{*}$$

Equation 57.

Technical risk has already been calculated in 4.2.8.

Regarding the risk due to large height deviations, as it can be seen in Table 85, Table 86, Table 87 and Table 88, there are no reports due to large height deviations not involving whole numbers of flight levels and $N_{az}^{*} = 0$.

In all the deviations reported due to coordination errors between ATC units for which there is not enough information it is assumed that the level change, if any, took place in the transferring UIR following appropriate clearances and, when the aircraft entered the new UIR, the aircraft was already established at the incorrect flight level. Therefore, in these cases, the number of crossed levels is zero.

As there are no deviations where it can be addressed that there was a change of level, it can be also assumed that $N_{az}^{cl/d} = 0$

Consequently, the only term to be calculated is the risk due to an aircraft levelling off at a wrong level without a proper clearance. Most of the parameters used to calculate this risk have already been presented within the vertical technical collision risk section (4.2). The new value required is the one necessary to calculate the probability of vertical overlap. As it was previously presented:

$$P_z^{wl}(S_z)_{same} = \frac{P_Z(0) \times t_{same}^{wl}}{T}$$

$$P_z^{wl}(S_z)_{opp} = \frac{P_Z(0) \times t_{opp}^{wl}}{T}$$

Equation 58.

In the following tables, relevant data for these calculations have been gathered, namely: the time spent at a wrong level and the total flight time within those months in which a LHD or a “no LHD” reports have been received for each location. As the annual flight time information is only available for the Canaries FIR, the annual flight time in each FIR has been estimated relating the number of aircraft in mid-year in each FIR with the one calculated in the Canaries.

4.3.3.a. Canaries

Table 89 shows the data needed to calculate the vertical risk due to large height deviations in the Canaries location, based on traffic levels representative for the year 2015.

Number of flights	Jan-Dec 2015
Same direction time at incorrect level (h)	1.58 hours
Opposite direction time at incorrect level (h)	0 hours
Total Canaries flight time (h)	17269.17 hours
Total Corridor flight time (h)	91676.52 hours
Wrong level, same direction vertical overlap probability	$3.6572*10^{-5}$
Wrong level, opposite direction vertical overlap probability	0

Table 89.
Operational vertical collision risk parameters in the Canaries.

Table 90 shows the estimate of the total vertical collision risk, sum of the technical vertical risk and the operational vertical risk, in the Canaries location, considering that the traffic growth factor is 5.2% per annum. These results can also be seen in Figure 40.

Total Vertical Collision risk	5.2% annual traffic growth
2015	$1.6703*10^{-7}$
2016	$1.7571*10^{-7}$
2017	$1.8485*10^{-7}$
2018	$1.9446*10^{-7}$
2019	$2.0457*10^{-7}$
2020	$2.1521*10^{-7}$
2021	$2.2640*10^{-7}$
2022	$2.3818*10^{-7}$
2023	$2.5056*10^{-7}$
2024	$2.6359*10^{-7}$
2025	$2.7730*10^{-7}$

Table 90.
Total vertical collision risk for the period 2015-2025 in the Canaries.

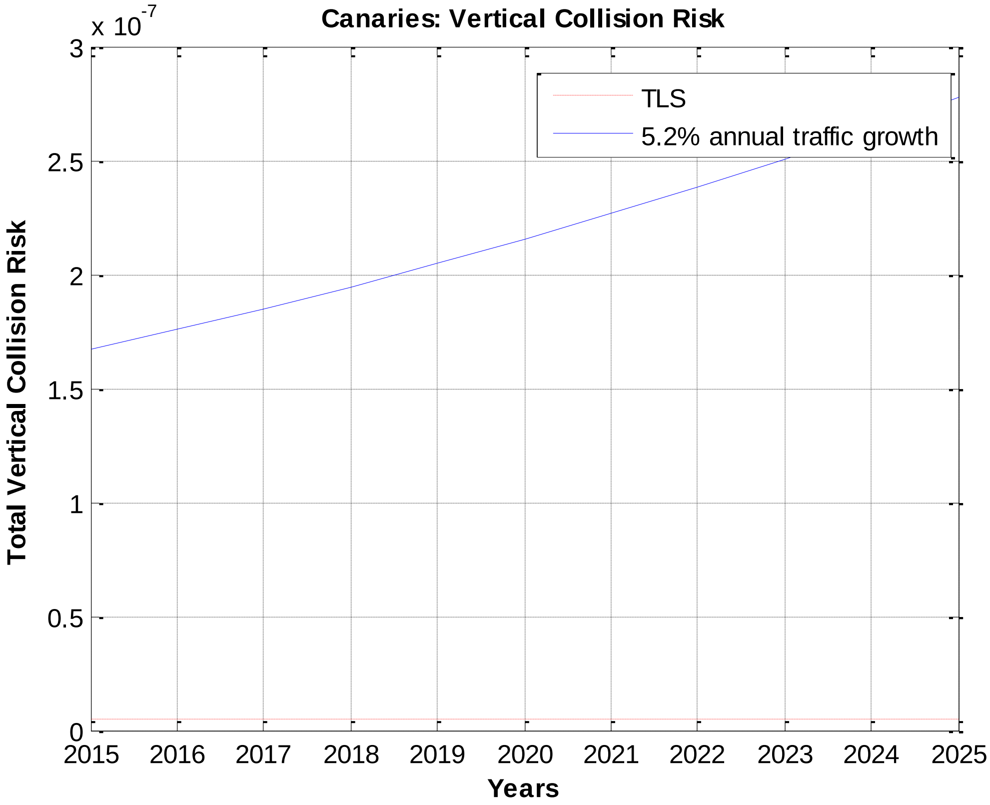

Figure 40.
Total vertical collision risk for the period 2015-2025 in the Canaries.

4.3.3.b. SAL

Table 91 shows the data needed to calculate the vertical risk due to large height deviations in SAL, based on traffic levels representative for the year 2015.

Number of flights	Jan-Dec 2015
Same direction time at incorrect level (h)	2.60 hours
Opposite direction time at incorrect level (h)	0 hours
Total SAL flight time (h)	22447.07 hours
Total Corridor flight time (h)	91676.52 hours
Wrong level, same direction vertical overlap probability	$4.6203*10^{-5}$
Wrong level, opposite direction vertical overlap probability	0

Table 91.
Operational vertical collision risk parameters in SAL locations.

The parameters presented above are used for the calculations in both SAL1 and SAL2 locations. Taking these values into account, operational vertical collision risk is estimated to be $5.3335*10^{-7}$ and $3.3482*10^{-7}$ in SAL1 and SAL2, respectively.

Table 92 shows the estimate of the total vertical collision risk in SAL1 and SAL2 locations considering that the traffic growth factor is 5.2% per annum. These results can also be seen in Figure 41 and Figure 42.

Total Vertical Collision risk	5.2% annual traffic growth	
	SAL1	SAL2
2015	$5.3335*10^{-7}$	$3.3482*10^{-7}$
2016	$5.6108*10^{-7}$	$3.5223*10^{-7}$
2017	$5.9026*10^{-7}$	$3.7055*10^{-7}$
2018	$6.2095*10^{-7}$	$3.8982*10^{-7}$
2019	$6.5324*10^{-7}$	$4.1009*10^{-7}$
2020	$6.8721*10^{-7}$	$4.3141*10^{-7}$
2021	$7.2295*10^{-7}$	$4.5384*10^{-7}$
2022	$7.6054*10^{-7}$	$4.7744*10^{-7}$
2023	$8.0009*10^{-7}$	$5.0227*10^{-7}$
2024	$8.4169*10^{-7}$	$5.2839*10^{-7}$
2025	$8.8546*10^{-7}$	$5.5587*10^{-7}$

Table 92.
Total vertical collision risk for the period 2015-2025 in SAL.

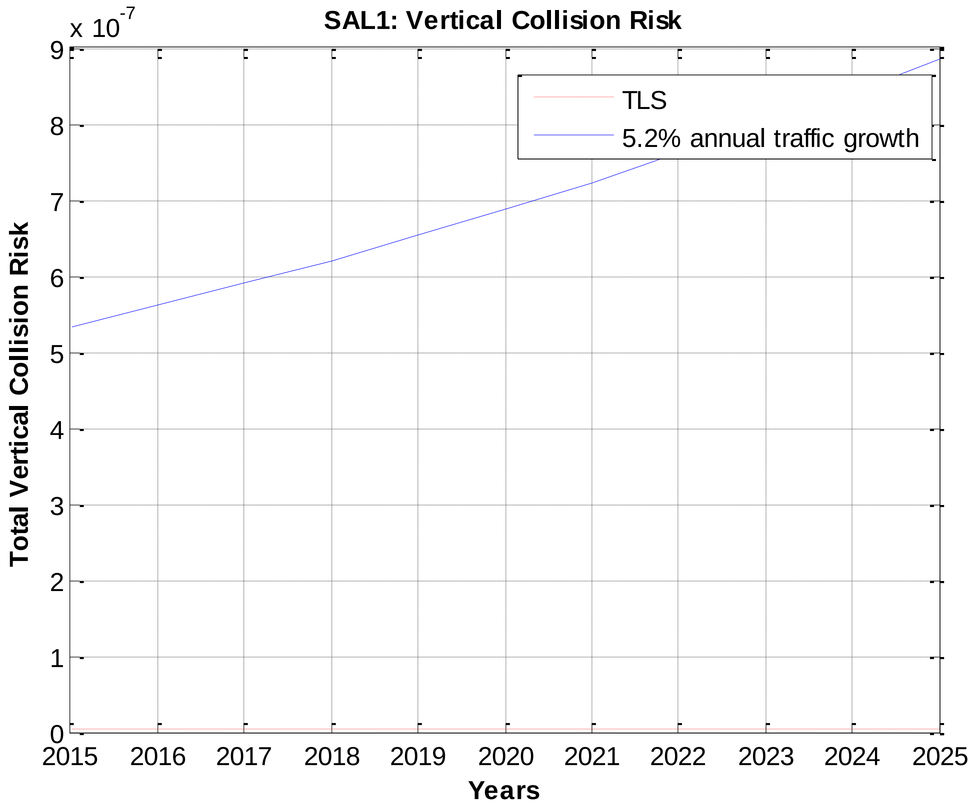

Figure 41.
Total vertical collision risk for the period 2015-2025 in SAL1.

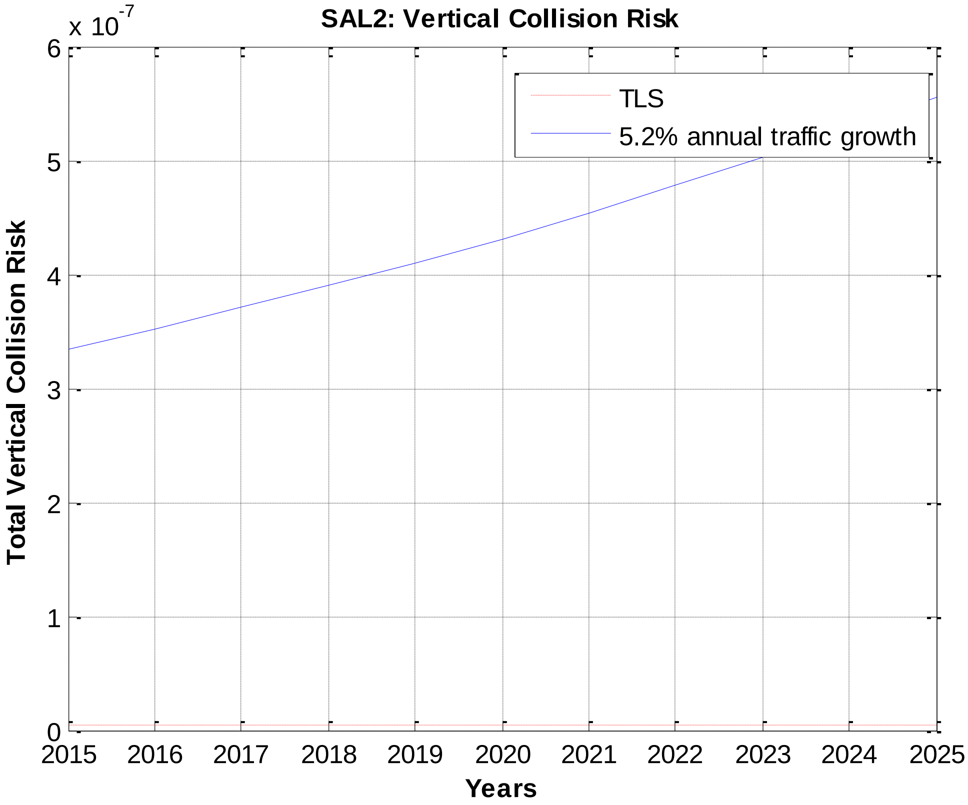

Figure 42.
Total vertical collision risk for the period 2015-2025 in SAL2.

4.3.3.c. Dakar

Table 93 shows the data needed to calculate the vertical risk due to large height deviations in Dakar, based on traffic levels representative for the year 2015.

Number of flights	Jan-Dec 2015
Same direction time at incorrect level (h)	2.08 hours
Opposite direction time at incorrect level (h)	0 hours
Total Dakar flight time (h)	31412.62 hours
Total Corridor flight time (h)	91676.52 hours
Wrong level, same direction vertical overlap probability	$2.6455*10^{-5}$
Wrong level, opposite direction vertical overlap probability	0

Table 93.
Operational vertical collision risk parameters in Dakar locations.

The parameters presented above are used for the calculations in both Dakar1 and Dakar2 locations. Taking these values into account, operational vertical collision risk is estimated to be $1.7778*10^{-7}$ and $1.9914*10^{-7}$ in Dakar1 and Dakar2, respectively.

Table 94 shows the estimate of the total vertical collision risk in Dakar1 and Dakar2 locations considering that the traffic growth factor is 5.2% per annum. These results can also be seen in Figure 43 and Figure 44.

Total Vertical Collision risk	5.2% annual traffic growth	
	Dakar1	Dakar2
2015	$1.7778*10^{-7}$	$1.9914*10^{-7}$
2016	$1.8702*10^{-7}$	$2.0950*10^{-7}$
2017	$1.9675*10^{-7}$	$2.2039*10^{-7}$
2018	$2.0698*10^{-7}$	$2.3185*10^{-7}$
2019	$2.1774*10^{-7}$	$2.4391*10^{-7}$
2020	$2.2906*10^{-7}$	$2.5659*10^{-7}$
2021	$2.4097*10^{-7}$	$2.6994*10^{-7}$
2022	$2.5351*10^{-7}$	$2.8397*10^{-7}$
2023	$2.6669*10^{-7}$	$2.9874*10^{-7}$
2024	$2.8056*10^{-7}$	$3.1427*10^{-7}$
2025	$2.9514*10^{-7}$	$3.3062*10^{-7}$

Table 94.
Total vertical collision risk for the period 2015-2025 in Dakar.

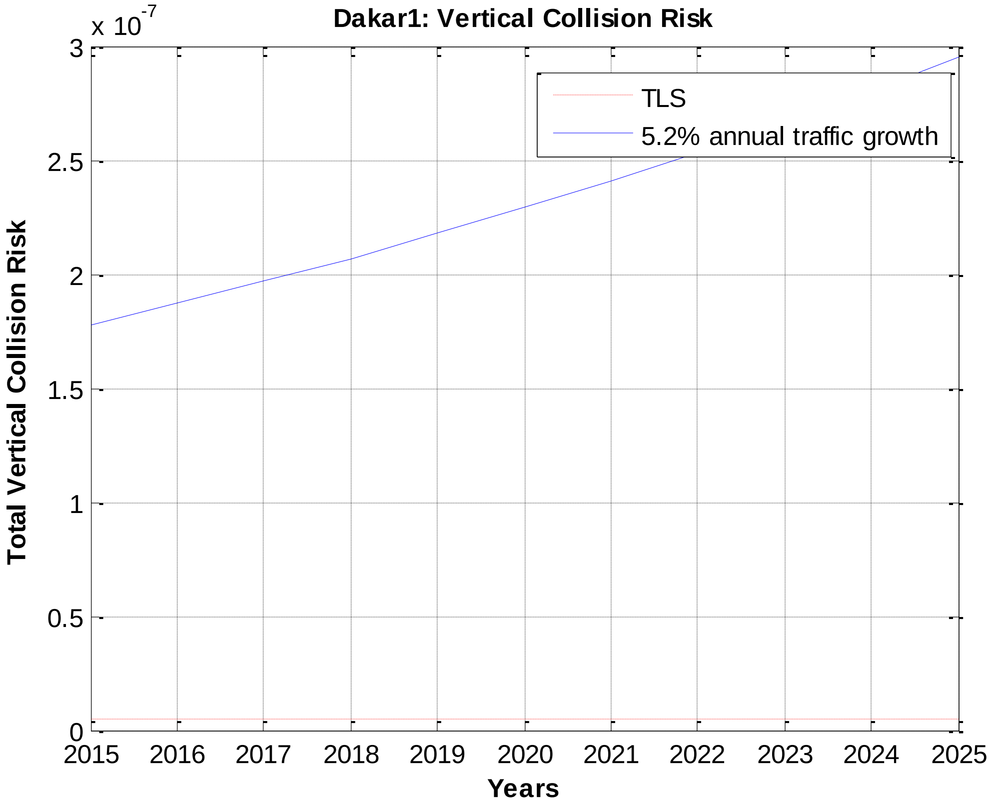

Figure 43.
Total vertical collision risk for the period 2015-2025 in Dakar1.

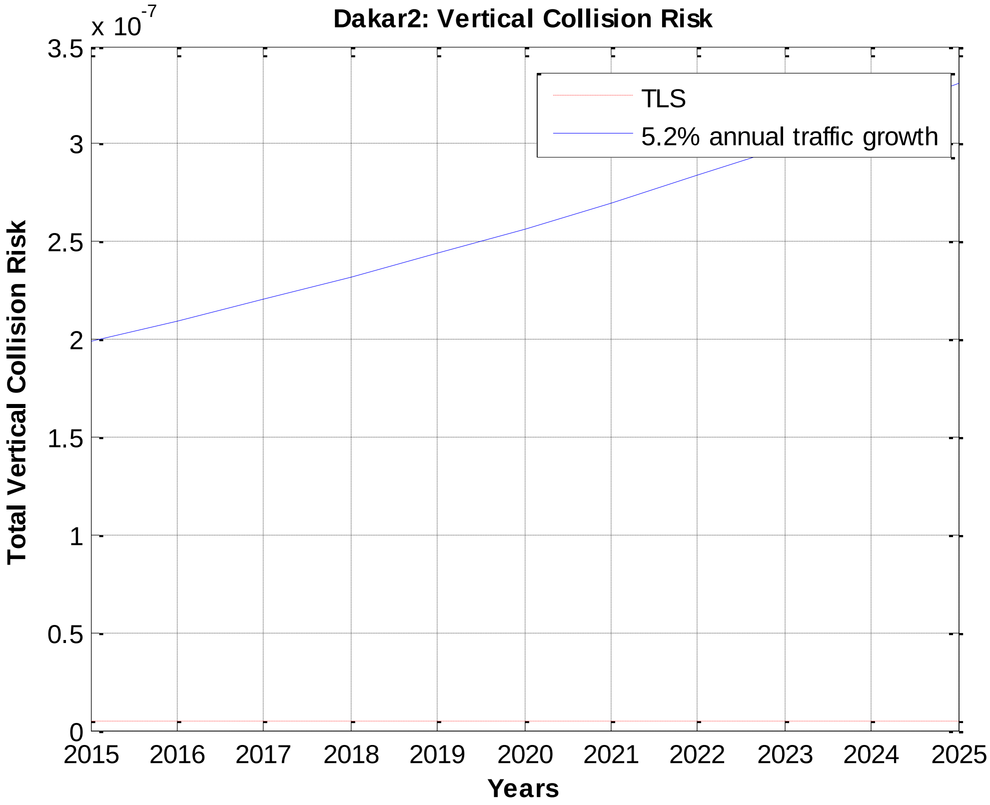

Figure 44.
Total vertical collision risk for the period 2015-2025 in Dakar2.

4.3.3.d. Recife

Table 95 shows the data needed to calculate the vertical risk due to large height deviations in the Recife location, based on traffic levels representative for the year 2015.

Number of flights	Jan-Dec 2015
Same direction time at incorrect level (h)	0.1667 hours
Opposite direction time at incorrect level (h)	0
Total Recife flight time (h)	20547.91 hours
Total Corridor flight time (h)	91676.52 hours
Wrong level, same direction vertical overlap probability	$0.3235*10^{-5}$
Wrong level, opposite direction vertical overlap probability	0

Table 95.
Operational vertical collision risk parameters in the Canaries.

Table 96 shows the estimate of the total vertical collision risk, sum of the technical vertical risk and the operational vertical risk, in the Recife location, considering that the traffic growth factor is 5.2% per annum. These results can also be seen in Figure 45.

Total Vertical Collision risk	5.2% annual traffic growth
2015	$2.4830*10^{-8}$
2016	$2.6122*10^{-8}$
2017	$2.7480*10^{-8}$
2018	$2.8909*10^{-8}$
2019	$3.0412*10^{-8}$
2020	$3.1194*10^{-8}$
2021	$3.3657*10^{-8}$
2022	$3.5407*10^{-8}$
2023	$3.7249*10^{-8}$
2024	$3.9186*10^{-8}$
2025	$4.1223*10^{-8}$

Table 96.
Total vertical collision risk for the period 2015-2025 in Recife.

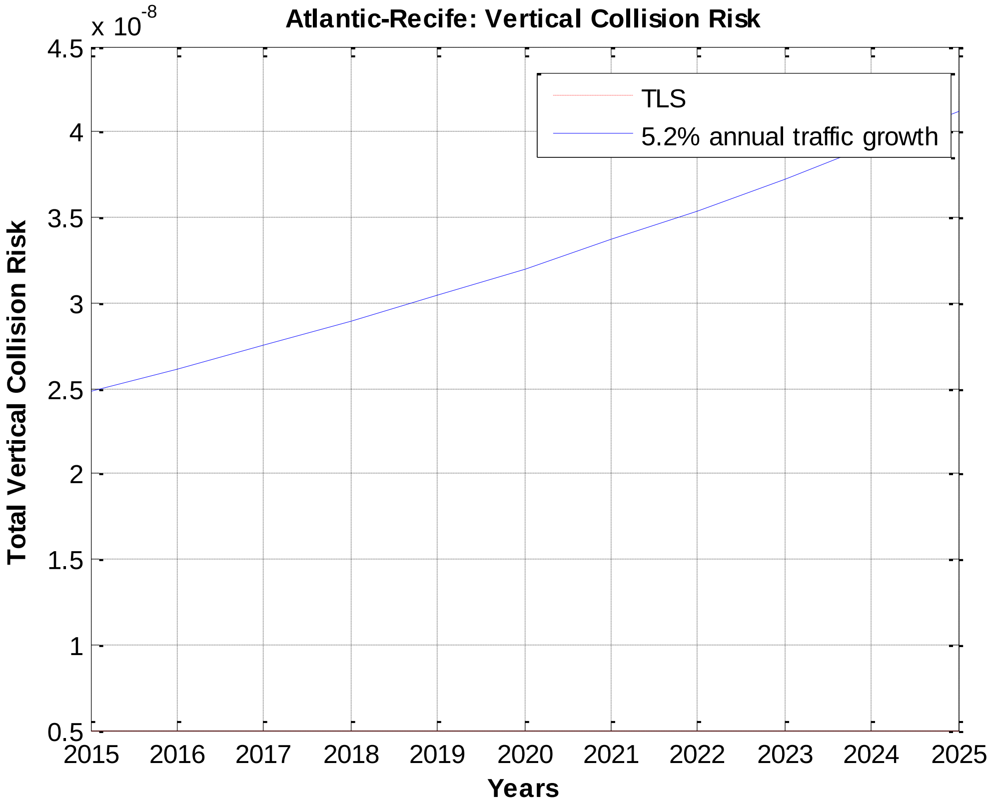

Figure 45.
Total vertical collision risk for the period 2015-2025 in Recife.

4.3.4. Considerations on the results

The total vertical risk calculated using the deviations reported by the States is higher than the TLS in all locations.

In previous safety assessments, [Ref. 5] and [Ref. 7], it was remarked that all the deviations received had been due to a coordination error between ATC units, and they had not been related to RVSM operations. In the same way, it was also explained that the deviation reports indicated that there was not any traffic in conflict. That is also the case of this study.

The same problem, the collision risk being higher than the TLS if coordination errors are taken into account, was already identified in the previous safety assessments and the corresponding conclusions were presented. Unlike [Ref.6], in this case there have not been reported situations with traffic in conflict. Nevertheless, it is also advisable the need of implementing adequate corrective actions to reduce operational errors in the Corridor.

4.3.4.a. Influence of the Py(0) value

As was said in 4.2.3, the selected value of Py(0) can be overly conservative in the Corredor EUR/SAM environment, having this parameter a direct influence in the vertical collision risk results. Alternative calculations have also been made using a value of Py(0)=0.059, which is more similar to the one used in European studies and in the Risk Collision Assessments performed by other Region Monitoring Agencies ([Ref.26], [Ref.27] and [Ref.28]).

Using this value of Py(0)=0.059, the obtained results are shown in Table 97.

FIR/UIR	Vertical risk	
	Technical risk	Total vertical risk
Canaries	$6.3221*10^{-11}$	$34.477*10^{-9}$
SAL1	$2.5270*10^{-11}$	$176.720*10^{-9}$
SAL2	$3.3468*10^{-11}$	$78.195*10^{-9}$
Dakar1	$2.9088*10^{-11}$	$45.279*10^{-9}$
Dakar2	$3.2547*10^{-11}$	$48.874*10^{-9}$
Recife	$4.8569*10^{-11}$	$5.169*10^{-9}$

Table 97.
Technical and total vertical risk using Py(0)=0.059.

As can be seen in Table 97, even if a value of Py(0)=0.059 is used, the results for the total vertical risk would still be above the TLS.

5. Conclusions

Only real traffic data for one month has been received from all Corridor UIRs for this study. Besides, some information was still missing and some inconsistencies have been detected. However, better information is available for large height deviation reports, as information for all FIR/UIR and months has been received. Nevertheless, some conservative assumptions had to be made regarding the modelling of probability densities and the extrapolation of traffic data.

Taking this into account, the following conclusions can be extracted from the analysis in the six different locations considered (the risk associated to the Corridor is considered to be the largest of the values calculated for each location):

- Lateral collision assessments:
  - The probability of lateral overlap increases as the separation between routes decreases, as it was expected. The value obtained for $S_y = 50\,NM$ is between $P_y(50) = 7.435 \cdot 10^{-8}$ and $P_y(50) = 11.022 \cdot 10^{-8}$, depending on the location, whilst the lateral overlap probability obtained for $S_y = 90\,NM$ is between $P_y(90) = 2.399 \cdot 10^{-8}$ and $P_y(90) = 4.049 \cdot 10^{-8}$.
  - For current traffic levels, the lateral collision risk obtained is $2.0662*10^{-9}$, whilst the lateral collision risk estimated for 2025 with an annual traffic growth rate of 5.2% is $3.4303*10^{-9}$. These values do not take into account traffic on the DCT Area route. Nevertheless, due to the randomness of this area and since traffic on this route only represents approximately 4% of the traffic in the Corridor, it is considered that the collision risk due to traffic in this area will not make the collision risk go above the TLS and the system is considered to be laterally safe in the period under consideration.
  - It should be remarked that the values of lateral technical collision risk for 2015 and the projection to the next 10 years, are similar to those obtained in previous collision risk assessments.

- Vertical risk assessment:
  - Vertical risk is split into two parts, one for the technical vertical risk and the second one for the vertical risk due to all causes. The same collision risk model is used for both. The differences are the value of the vertical overlap probability and the relative vertical speed to use in each one.
  - The probability of vertical overlap due to technical causes was based on the probability distribution of Total Vertical Error (TVE). This was obtained by convoluting probability distributions of Altimetry System Errors (ASE) and typical Assigned Altitude Deviation (AAD). In the absence of any direct monitoring data from the EUR/SAM Corridor, 2015 height-keeping data and models from the EUR airspace provided by Eurocontrol have been used.
  - The value of the vertical overlap probability calculated by means of EUROCONTROL RVSM tool with traffic data from the Canaries for 2015, for S_z=1000 ft is $P_z(1000) = 2.0405 \cdot 10^{-9}$.
  - The lateral overlap probability for aircraft nominally flying at adjacent flight levels of the same path, $P_y(0)$ has been obtained conservatively assuming that all aircraft are using GNSS and that

their lateral path-keeping errors standard deviation is 0.0612 NM. The value obtained is $P_y(0) = 0.2905$, much higher than the value assumed by the RGCSP, 0.059.

- The value of the vertical technical collision risk for the current traffic levels is estimated to be $0.3108*10^{-9}$. The technical vertical collision risk estimated for 2025 with an annual traffic growth rate of 5.2% is $0.5160*10^{-9}$. Both values are below the TLS.
- The technical vertical risk obtained in this study is lower than the one obtained in the previous safety assessment. This is mainly because the value for $P_z(1000)$ is lower than the one used in that study.
- The vertical risk due to large height deviations has been calculated using the deviations reported by the States. The total vertical risk calculated using these deviations is much higher than the TLS.
- All the deviations received were due to a coordination error or resulted in a coordination error, and they are not related to RVSM operations.
- The same problem, the collision risk being higher than the TLS if coordination errors are taken into account, was already identified in the previous safety assessments.

It can be concluded that lateral and technical vertical collision risks are below the TLS. Nevertheless, the validity of these results depends on the validity of the assumptions made.

Regarding the total vertical risk, the risk greatly exceeds the TLS even with current traffic levels. In any case, as the main problem, coordination errors, is clearly identified, the use of adequate corrective actions to reduce coordination errors in the Corridor would reduce the risk. These measures should be applied as soon as feasible.

As the accuracy of the assessment greatly depends on the availability and accuracy of the data provided, it is recommended that for next assessments:

- Accurate flight progress data from all FIR/UIRs be made available, including as much information as possible in the traffic samples, to facilitate the verification of traffic flows, distribution and passing frequencies used in the analysis.
- Data on lateral and vertical deviations obtained from radar data and incident reports should be provided in order to improve the estimation of overlap probabilities (a continuous monitoring process is required to obtain a representative data sample on deviations for future assessments).
- All LHDs should be reported and better information about LHDs must be made available, as not always complete information about them has been provided.

6. Reference documentation

[Ref. 1] Atlas South Atlantic Crossing 57C, 22 Dec 05. Air navigation Chart

[Ref. 2] Risk Assessment of RNP10 and RVSM in the South Atlantic Flight Identification Regions Including an Assessment for Limited Implementation of RVSM on RN741. (ARINC)

[Ref. 3] EUR/SAM Corridor: "Double unidirectionality" post-implementation collision risk assessment. NIVY-IDSA-INF-001-1.0-09. January 09.

[Ref. 4] First approach to 2009 Collision Risk Assessment within the EUR/SAM Corridor. NYVI-IDSA-INF-008-1.0/10. May 2010.

[Ref. 5] EUR/SAM Corridor: 2009 Collision risk assessment. NYVI-IDSA-INF-036-1.0/10. December 2010.

[Ref. 6] EUR/SAM Corridor: 2010 Collision risk assessment. NYVI-IDSA-INF-003-1.0/12. February 2012.

[Ref. 7] EUR/SAM Corridor: 2014 Collision risk assessment. NYVI-IDSA-INF-007-1.0/16. February 2016.

[Ref. 8] AIP Spain. AIS. AIC 17/Jan/01

[Ref. 9] Separation and Airspace Safety Panel. A New Parameter for Gross Lateral Errors (SASP-WG/A/2-WP/4, 21/10/01)

[Ref. 10] Manual on airspace planning methodology for the determination of separation minima (ICAO Doc 9689-AN/953)

[Ref. 11] Air Traffic Services Planning manual. Doc 9426 OACI

[Ref. 12] ICAO Document 9574 (2nd edition). Manual on Implementation of a 300m (1000ft) Vertical Separation Minimum between FL290 and FL410 inclusive.

[Ref. 13] RVSM Safety Assessment of the Australian Airspace for the period 1 Jan 2004 through 31 Dec 2004.- RASMAG/3-WP/16 06/06/2005. OACI

[Ref. 14] Summary of the Airspace Safety Review for the RVSM Implementation in Asia Region.- RASMAG/4-WP11 25/10/2005. OACI

[Ref. 15] The EUR RVSM Mathematical Supplement.-MDG/21 DP/01 August 2001.

[Ref. 16] CAR/SAM-Course on Introduction to Safety Assessment. Lima, 19-23/06/06 (www.lima.icao.int)

[Ref. 17] SAT/12-TF/1 Report. Appendix A to the Report on Agenda Item 2: An Update to the Summary of Reduced Vertical Separation Minimum (RVSM) Safety Assessment to Reflect the Operations Safety after the RVSM Implementation in CAR/SAM airspace in January 20th.- 5-9/09/06

[Ref. 18] STATFOR. Eurocontrol Seven-Year Forecast. September 2016.

[Ref. 19] EUR/SAM Risk Assessments. DNV-ADS-INF-23-0.2/06. December 2006

[Ref. 20] Revised Pre-Implementation Collision Risk Assessment for RVSM in the Africa Indian Ocean Region. NLR-CR-2007-637. February 2007

[Ref. 21] Application of offset tracks. NLR. September 2007

[Ref. 22] AIC NR 13/A/08GO 30 October 2008. Bureau NOTAM International de L'Ouest Africain. Pre-Operational Implementation of AFDP, FPASD, ADS and CPDLC within Dakar and Niamey FIRs.

[Ref. 23] AIS-ESPAÑA. AIC 10 May 07. New route orientation on airways UN-741 and UN-866 (Corridor EUR/SAM)

[Ref. 24] AIS-ESPAÑA. AIC 30 July 09. ADS/CPDLC Operational implementation of the SACCAN FANS 1/A System in the Canarias FIR/UIR

[Ref. 25] Updated RMA Manual. SASP/13-WP/44. May 2008

[Ref. 26] "Airspace Safety Review of RVSM in Australian, Nauru, Papua New Guinea and Solomon Islands Airspace. January 2014 to December 2014", "Airspace Safety Review of the RVSM Implementation in Indonesian Airspace. January 2014 To December 2014".

[Ref. 27] "Airspace Safety Review for the RVSM operation In the airspace of Chinese Flight Information Regions. January 2012 - December 2012".

[Ref. 28] "Airspace Safety Review for the RVSM Implementation in Fukuoka Flight Information Region. Jan 2014 To Dec 2014"

[Ref. 29] Doc 9937 Manual of Operating Procedures and Practices for Regional Monitoring Agencies

7. Terminology

AAD	ASSIGNED ALTITUDE DEVIATION
ADS	AUTOMATIC DEPENDENT SURVEILLANCE
ASE	ALTIMETRY SYSTEM ERROR
ATC	AIR TRAFFIC CONTROL
ATS	AIR TRAFFIC SERVICES
DE	DOUBLE EXPONENTIAL DISTRIBUTION
EUR/SAM	EUROPE/SOUTH AMERICA
FIR	FLIGHT INFORMATION REGION
FL	FLIGHT LEVEL
FMC	FLIGHT MANAGEMENT COMPUTER
FTE	FLIGHT TECHNICAL ERROR
G	GAUSSIAN DISTRIBUTION
GL	GENERALISED LAPLACE DISTRIBUTION
HFDL	HIGH FREQUENCY DATA LINK
HMU	HEIGHT MONITORING UNIT
kts	KNOTS
MASPS	MINIMUM AVIATION SYSTEM PERFORMANCE STANDARDS
MDG	MATHEMATICS DRAFTING GROUP (EUROCONTROL)
NAT	NORTH ATLANTIC
NM	NAUTICAL MILE
RGCSP	REVIEW OF THE GENERAL CONCEPT OF SEPARATION PANEL
RMA	REGIONAL MONITORING AGENCY
RNP	REQUIRED NAVIGATION PERFORMANCE
RVSM	REDUCED VERTICAL SEPARATION MINIMUM
SAT	SOUTH ATLANTIC

SATCOM	SATELLITE COMMUNICATIONS
SATMA	SOUTH ATLANTIC MONITORING AGENCY
STATFOR	AIR TRAFFIC STATISTICS AND FORECASTS (EUROCONTROL)
TVE	TOTAL VERTICAL ERROR
UIR	UPPER FLIGHT INFORMATION REGION

8. Annexes

- Annex I: Calculation of α
- Annex II: Methods for occupancy estimate

Annex 1
Calculation of α

A1.1 Calculations for α

On the assumption that ATC and/or the flight crew are able to detect lateral navigation anomalies and are reporting each occurrence thereof, the parameter α can be estimated as the proportion of flights or aircraft where an anomaly occurred. However, that there might exist a high likelihood of underreporting of such errors. To calculate a conservative estimate of α, an upper confidence limit for α will be calculated and used as the estimate for α within the DDE model of the lateral deviations in the proposed RNP10 airspace in the SAT.

A confidence interval for α can be determined by means of the binomial distribution for the number of aircraft X, say, experiencing a lateral navigation anomaly as described above during a certain monitoring period, i.e. in a given number of flights n, say. It holds that:

$$Prob\{X = k\} = \binom{n}{k} \cdot \alpha^k \cdot (1-\alpha)^{n-k}$$

Equation A1.1.

Being k the observed value of ocurrences.

In principle, then, an integer number $A_{\alpha,\beta}$ can be determined for each value of α and β,β > 0 , such that:

$$Prob\{X \geq A_{\alpha,\beta}\} = 1 - \beta$$

Equation A1.2.

i.e. a fraction 1-β of the values of the random variable X are larger than or equal to $A_{\alpha,\beta}$. This means that in the same fraction of cases, the (random) interval [0, X] covers the point $A_{\alpha,\beta}$, i.e. 0≤$A_{\alpha,\beta}$. ≤ X, as illustrated in Figure A1.1.

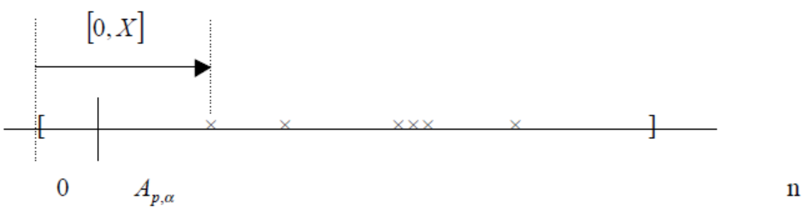

Figure A1.1
The value $A_{\alpha,\beta}$ being covered by the (random) interval [0,X].

The confidence limit for α is obtained by manipulating Equation A2 such that it becomes:

$$Prob\{Y(X)_\beta \geq \alpha\} = 1 - \beta$$

Equation A1.3.

Where $Y(X)_\alpha$ is some appropriate function of the random variable X. The interval $[Y_{low}, Y(X)_\beta]$, where Y_{low} is the lower bound of the domain of the random variable $Y(X)_\beta$ will cover α in a fraction 1-β of cases. The actual value of the confidence limit is obtained by substituting the observed value k of the random variable X into $Y(X)_\beta$.

Now, if $A_{\alpha,\beta}$ is written as:

$$A_{\alpha,\beta} = n\alpha - \beta_{\alpha,\beta}$$

Equation A1.4.

Where $n\alpha = E\{X\}$, the expected value of X, and $\beta_{\alpha,\beta} > 0$, it follows that:

$$n\alpha - \beta_{\alpha,\beta} \leq X$$

Equation A1.5.

or

$$\alpha \leq \frac{X + \beta_{\alpha,\beta}}{n}$$

Equation A1.6.

and this will hold in a fraction 1-β of the cases. The right-hand side of the inequality (Equation A6) may be associated with $Y(X)_\beta$ and thus specifies a (1-β) *100% upper confidence limit for the probability α.

In the ARINC study, as well as in the 2012 Risk Collision Analysis performed by AENA, it could be assumed that k=1, and the value of α_U could be directly obtained using Equations A1 and A3, for β = 0.05, i.e:

$$Prob\{X \geq 1 | \alpha = \alpha_U\} = 1 - Prob\{X = 0 | \alpha = \alpha_U\} = 1 - \beta$$

$$1 - \binom{n}{0} \cdot \alpha^0 \cdot (1-\alpha)^n = 1 - \beta$$

$$(1-\alpha)^n = \beta \quad \rightarrow \quad \alpha = (1-\beta)^{1/n}$$

Equation A1.7.

In this case, it has been also assumed that k=1, as only one or no lateral deviations, depending on the FIR/UIR, have been reported.

Annex 2
Methods for occupancy estimate

A2.1 Definition

The occupancy concept is applicable for both vertical and lateral separation. In the case of lateral occupancy, the concept is applicable for aircraft flying in parallel routes at the same flight level, whilst in the vertical case, the concept is applicable to aircraft flying in the same route or in crossing routes at adjacent flight levels.

Same direction lateral occupancy for a parallel tracks system refers to the average number of aircraft which are, in relation to the typical aircraft:

- flying in the same direction as it;
- nominally flying on tracks one lateral separation standard away from it;
- nominally at the same flight level as it; and
- within a longitudinal segment centred on it.

The above definition has been expanded to include tracks that are separated by more than one lateral separation standard because there is a significant collision risk arising from the probability of overlap between non adjacent tracks.

A similar set of criteria can be used to define opposite direction occupancy, just replacing “flying in the same direction as it” by “flying in the opposite direction”.

The length of the longitudinal segment, $2S_x$, is considered to be the length equivalent to 20 minutes of flight at 480kts.

A2.2 Methods for occupancy estimate

There are two methods to estimate lateral occupancy, called “Steady state flow model” and “Direct estimation from time at waypoint crossing”.

The first one is the only way of achieving an estimation of the occupancy when only records of daily traffic are available or if, in the direct estimation from time at waypoint crossing there are not big amounts of hourly information. The method of direct estimation provides more precise estimations and it is, generally, preferred.

For a given system, lateral occupancy, E_y, can be expressed as:

$$E_y = \frac{2T_y}{H}$$

Equation A2.1

Where:

- Ty represents the proximity time generated in the system, i.e. the total time spent by aircraft pairs on adjacent flight paths at the same flight level and within a longitudinal distance Sx of each other.

- H represents the total number of flight hours generated in the system during the considered period of time.

A2.2.1 Steady state flow model

This section is a transcription of sections 2.3, 3.1, 3.2 y 3.3 and appendix C of Chapter 4, Section 2, part II of [Ref. B1].

The occupancy E_y will be estimated for a parallel routes system in which it will be supposed that the flow of traffic towards the flight paths and along them is statistically stable during the considered period.

For a general system, the occupancy will be obtained as a weighted sum of the occupancy of all the subsystems "in stable state", with respect to the number of flight hours generated in each one.

Tracks are numerated from 1 to t and flight levels from 1 to f. The traffic flow on track i, at flight level j (flight path ij) is m_{ij}, i.e. m_{ij} aircraft cross every point of the track every hour. The length of the track is L and it is assumed that all aircraft fly at the same speed V. T is the time during which the system is observed.

A2.2.1.1 Number of flight hours H

The time L/V is needed for an aircraft to fly through the system. So, in the flight path ij there are always $m_{ij} \cdot L/V$ aircraft and the number of aircraft in the whole system will be:

$$\sum_{i=1}^{i=t} \sum_{j=1}^{j=f} m_{ij} \frac{L}{V}$$

Equation A2.2

From this equation it is deduced that:

$$H = \frac{T \cdot L}{V} \sum_{all\ trajectories\ ij} m_{ij}$$

Equation A2.3

A2.2.1.2 Total proximity time T_y

Calculation of T_y is a little bit more complicated. Let's consider an aircraft on the flight trajectory ij: the foreseen number of proximate aircraft on the adjacent flight trajectory i-1 is given by:

$$\frac{2S_x}{V} \cdot m_{i-1,j}$$

Equation A2.4

So, during the L/V flight hours of this aircraft, the proximity time generated is:

$$\frac{2S_x}{V} \cdot m_{i-1,j} \cdot \frac{L}{V}$$

Equation A2.5

During the T hours in which the system is observed, mij*T aircraft fly on the flight path ij, and the proximity time generated between trajectory ij and trajectory i-1,j is:

$$\frac{2S_x}{V} \cdot m_{i-1,j} \cdot \frac{L}{V} m_{i,j} \cdot T$$

Equation A2.6

The total proximity time, T_y, is obtained adding all the previous pairs:

$$T_y = \sum_{i=1}^{i=t} \sum_{j=1}^{j=f} \frac{2S_x}{V} \cdot m_{i-1,j} \cdot \frac{L}{V} m_{i,j} \cdot T$$

Equation A2.7

Or (simplifying notation):

$$T_y = \sum_{all\ pairs\ of\ tracks} m_{i-1,j} \cdot m_{i,j} \cdot \frac{2 \cdot S_x \cdot L \cdot T}{V}$$

Equation A2.8

A2.2.1.3 Occupancy

Substituting Equation B3 and Equation B8 into Equation B1, occupancy is finally given by:

$$E_y = \frac{2T_y}{H} = \frac{2 \cdot \sum_{all\ pairs\ of\ tracks} m_{i-1,j} \cdot m_{i,j} \cdot \frac{2 \cdot S_x}{V}}{\sum m_{ij}}$$

Equation A2.9

For same direction lateral overlap, aircraft flying on adjacent tracks in the same direction and at the same flight level must be considered. For opposite direction lateral overlap, aircraft flying on adjacent tracks in the opposite direction and at the same flight level must be considered.

If the system is not statistically stable, as it happens in the case in which traffic flows depend on the time, the occupancy value E_y should be calculated adding all the subsystems that are in a stable state. Thus, if there are r subsystems of this type:

$$E_y = \frac{2 \cdot \sum_{p=i}^{p=r} T_y^p}{\sum_{p=i}^{p=r} H^p} = \frac{\sum_{p=i}^{p=r} H^p E_y^p}{\sum_{p=i}^{p=r} H^p}$$

Equation A2.10

Where the subindex p indicates that the value corresponds to the subsystem p. T_j^p and H^p can be obtained for every subsystem p using the method described before.

A2.2.2 Direct estimation from time at waypoint passing

This has been the method used in this report.

It is based on the daily flight progress data of aircraft in the tracks system studied. The period of time of available flight progress data should be long enough, in order to be able to detect any important variation in the traffic flow.

Basically the method consists in examining the crossing time notified by all the aircraft of the system at a given waypoint.

The points utilized as reporting points must be approximately on a plane at right angles to the track system, in order to be able to compare passing times of aircraft on one route with passing times of aircraft on another route. That is why, in this study, times in SAL2 had to be corrected (extrapolated) to obtain crossing times in points that are at right angles to the route network.

The comparison of crossing times will give the number of proximate pairs. A proximate pair, between aircraft on adjacent routes and at the same flight level, is defined as the occurrence of two aircraft passing within a given longitudinal distance $2S_x$. If both aircraft fly in the same direction it will be a proximate pair in the same direction, whilst it will be an opposite direction proximate pair if they fly in opposite directions. As far as the distance S_x is concerned, it is often given by the time T_0, being the time it takes an aircraft with an average speed of 480kts to fly that distance. In this study, S_x is 80NM and T_0, 10 minutes.

If, for each and every flight level, passing times at the reporting point of all aircraft on one route are compared with the passing times of all aircraft on another route at the homologous reporting point, the number of proximate pairs between these two routes will be given by the number of cases in which the absolute value of the difference between both times is less than 10 minutes.

The same procedure must be followed with the remaining pairs of routes.

Considering all this, occupancy can be estimated using the following equation:

$$E_y = \frac{2n_y}{n}$$

Equation A2.11

where n_y is the total number of proximate pairs of aircraft and n is the total number of aircraft in the system.

A2.3 Crossing occupancy

Crossing occupancy for a pair of routes with intersection angle θ is given by:

$$E_z = \begin{cases} \dfrac{t_{sh}(\theta)}{t_F}\dfrac{2K(\theta)}{N}; & for\ t_{sh} < t_F \\ \dfrac{2K(\theta)}{N}; & for\ t_{sh} > t_F \end{cases}$$

Equation A2.12

Where:

- N is the number of aircraft in the system during the observation period
- K(θi) is the number of aircraft pairs in the crossing routes with angle θi
- t_{sh} is the average proximity time of pairs of aircraft in the crossing routes with angle θ
- t_F is the average flight time in the crossing routes

The "direct estimation from time at waypoint passing", can also be used to estimate crossing occupancy. In this case, it is necessary to determine a time window so that the identification of the proximate pairs may be accomplished.

Lets consider two crossing routes, A and B, with angle θ, and aircraft flying at speeds V_A and V_B. This window depends on the crossing angle of the routes, the speeds of the aircraft and the horizontal distance, S_h. Pairs of aircraft for which separation is greater than S_h will not be considered as proximate events.

The time window can be obtained using the following expression:

$$\Delta t_{max} = \sqrt{\frac{(V_A^2 + V_B^2 - 2V_AV_B cos\theta)S_h^2}{V_A^2V_B^2 sen^2\theta}}$$

Equation A2.13

A2.4 References

Ref. A2.1: Air Traffic Services Planning manual. Doc 9426 OACI